INSTITUT FÜR VERFAHRENSTECHNIK DES INDUSTRIELLEN UMWELTSCHUTZES
Montanuniversität Leoben
Peter-Tunner-Straße 15
www.vtiu.com
A-8700 Leoben

Diploma thesis

Resource Recycling in Waste Management with X-ray Fluorescence

erstellt für

BT Wolfgang Binder GmbH

Vorgelegt von:
Martin Weiss, BSc.
M0435164

Betreuer/Gutachter:
Ing. Johann Felber
Ao.Univ.Prof.,Dipl.-Ing.,Dr.techn. Josef Draxler

Leoben, 22.06.2011

EIDESSTATTLICHE ERKLÄRUNG

Ich erkläre an Eides statt, dass ich diese Arbeit selbständig verfasst, andere als die angegebenen Quellen und Hilfsmittel nicht benutzt und mich auch sonst keiner unerlaubten Hilfsmittel bedient habe.

AFFIDAVIT

I declare in lieu of oath, that I wrote this thesis and performed the associated research myself, using only literature cited in this volume.

_____ _____

Datum Unterschrift

Acknowledgements

Die Diplomarbeit entstand im Zusammenhang mit der Firma BT-Wolfgang Binder GmbH, einem Anlagenbauer im Bereich der Umwelt- und Mineraltechnik. An dieser Stelle möchte ich mich beim Unternehmen, für die Möglichkeit diese Arbeit in Kooperation zu verfassen, bedanken. Speziellen Dank möchte ich an Herrn Ing. Johann Felber richten, der mich als Betreuer seitens BT-Wolfgang Binder GmbH stets tatkräftig unterstützt hat und hilfreiche Anregungen gab.

Besonderer Dank gilt ebenfalls Herrn Tom Jansen und Herrn Bradley Hubbard-Nelsen, Ph.D. von Innov-X Systems Inc., die mir bei Fragen insbesondere hinsichtlich der Röntgenfluoreszenz und der Software stets bereitwillig weitergeholfen haben.

Weiteres möchte ich mich bei Herrn Ao.Univ.Prof.,Dipl.-Ing.,Dr.techn. Josef Draxler für die Betreuung der Diplomarbeit und der Montanuniversität Leoben, insbesondere dem Institut für Verfahrenstechnik des industriellen Umweltschutzes, herzlich für jegliche Unterstützung bedanken.

Auch möchte ich mich bei meiner Freundin Maria-Luise Dunst, die mir durch ihre Unterstützung vor allem in den letzten oftmals zeitreibenden Monaten einige stressfreie und freudige Augenblicke verschafft hat, herzlich bedanken.

Der letzte, aber sicherlich allergrößte Dank geht an meine Eltern, die mich für den gesamten Zeitraum meines Studiums sowohl monetär, als auch moralisch und psychisch in größtmöglichem Ausmaß unterstützt haben und mir stets Freude bereiteten.

„Freude ist die einfachste Form der Dankbarkeit“

Karl Barth, Schweizer Theologe

Kurzfassung

Wertstoffsortierung in der Abfallwirtschaft mittels Röntgenfluoreszenz

Diese Masterarbeit beschäftigt sich mit einem Trennsystem zur Wertstoffsortierung in der Abfallwirtschaft, entwickelt durch eine Kooperation der Firmen BT-Wolfgang Binder GmbH und Innov-X Systems. REDWAVE XRF ist ein optisches Sortiersystem, bei welchem die Objekterkennung auf dem physikalischen Prinzip der Röntgenfluoreszenz basiert. Der erste Teil der Arbeit behandelt die Grundlagen der Röntgenfluoreszenz, beginnend mit einer kurzen Beschreibung der Entdeckung durch C. W. Röntgen und einer Erklärung der Röntgenfluoreszenz von Röntgenquelle über die Anregung der Objekte und Einfluss der Materie bis hin zur Entstehung der charakteristischen Röntgenstrahlung und den dabei auftretenden Einflussfaktoren. Im zweiten Teil wird auf das Sortiersystem REDWAVE XRF genau eingegangen. Es erfolgt eine Beschreibung über Aufbau und Funktionsweise sowie eine weitere Erklärung der technische Spezifikationen und eine genaue Beschreibung der Funktion der Detektion sowie deren Einflussfaktoren. Der nachfolgende, dritte Teil befasst sich mit der praktischen Anwendung der REDWAVE XRF. Bereits kommerziell genutzte, aber auch zukunftsträchtige und potentiell mögliche Applikationen werden betrachtet. Die praktische Anwendung wird anhand eines detaillierten Sortierversuches näher gebracht. Abschließend erfolgen eine Aufstellung der Ergebnisse und eine kritische Nachbetrachtung sowie ein Ausblick hinsichtlich künftiger Entwicklungen.

Abstract

Resource Recycling with X-ray Fluorescence in Waste Management

This thesis is about REDWAVE XRF, a sensor-based sorting system for resource recycling in waste management, developed in collaboration of BT-Wolfgang Binder GmbH and Innov-X Systems. The detection for that system is based on X-ray fluorescence. The first part of this work deals with the background of X-ray fluorescence, beginning with the development by C. W. Röntgen. Furthermore, the physical process is described from excitation with different X-ray sources to interaction of X-rays with matter and finally the origin of secondary X-ray radiation. The second part gives detailed information about the assembly and function of the sorting system as well as a detailed technical description of the function of detection and factors of influence. The practical use of REDWAVE XRF is described in part three. Both an example of commercial use is given and some fields with high potential of possible successful applications are presented. Additionally, the practical use is being displayed by a detailed sorting test of scrap metal. Finally all results are summarized and reviewed and future directions are given.

Contents

Page

1 Introduction

In the recent decades waste management developed away from waste disposal towards waste treatment, waste recovery as well as recycling. Material flow management aims with an economical and ecological worthwhile interaction of material flows, attempts an environmental-friendly and resource-conserving production as well as a reuse of recyclable materials, and targets to a minimization of emissions at all. Recycling economy and cleaner production make the use of secondary resources possible and hence, save primary resources, energy and prevent waste. Even though, waste collection has reached a high standard, and many different waste streams are collected separately, an after-treatment of every single waste stream is obligatory. BT-Wolfgang Binder GmbH is a general contractor specialized in mineral and environmental technology and has developed different sensor-based sorting systems with.

1.1 Background

For several years sensor-based sorting systems have taken over the recycling market. In the beginning of waste management only treatment of homogenous waste streams was possible, but based on more and more sophisticated technologies the sorting of heterogeneous waste streams became possible nowadays. Due to the extinguishing of primary resources, rising energy prices as well as increasing prices for raw materials, but also as the result of stricter getting laws, as for landfill prohibitions or recycling rates, in the coming future more and more applications for sensor-based sorting systems come up. Near Infrared Spectroscopy, Infrared-Transmission and Line Scan Cameras, but also X-ray Fluorescence are only a few examples of sophisticated sensor-based sorting-systems. Last mentioned is a new sensor-based sorting system based on X-ray fluorescence analysis. REDWAVE XRF was developed by BT-Wolfgang Binder GmbH in collaboration with Innov-X Systems.

1.2 Purpose

The main purpose of this thesis lies in the display of the X-ray fluorescence system, REDWAVE XRF. The theoretical background and the assembly of the system are explained in detail. The main focus of attention regarding theoretical background is on the physics of X-ray fluorescence and on factors of influences due to physics. The basic design of REDWAVE XRF is similar to other sensor-based sorting systems. A detailed description of the assembly and furthermore a technical description of the detection unit is given. A further focus of attention in this thesis lies on practical applications. Glass-sorting, more precisely the separation of heat resistant and leaded glass out of recyclable material stream of recovered glass, is already a commercial use of REDWAVE XRF. A detailed sorting test covered in this work is metal sorting respectively the separation of CRES (Corrosive Resistant Steel), copper, and brass out of scrap metal. Furthermore, areas of application having high potential of possible market entries are presented. Factors of influences due to physics, geometry,

assembly, software etc. are based on the given data, mentioned and discussed at the end of this thesis. Finally, possible advancements are briefly discussed.

2 Theoretical Background

This Chapter includes the basic knowledge essential for the thesis. A description about development of X-ray fluorescence from the beginning of last century to the present including the discovery of X-rays, an explanation of X-ray radiation as well as the physical principle and possible X-ray sources is given. Since REDWAVE XRF uses an X-ray tube, the main focus of attention regarding X-ray sources lies on X-ray tubes. Furthermore, this Chapter includes different factors of influence as interaction of X-rays with matter (Scattering and photoelectric effect) and the process of excitation, X-ray fluorescence and characteristic X-ray fluorescence radiation.

2.1 The Discovery of X-Rays

In the year 1885 W. C. Röntgen discovered X-ray radiation (X-rays) in his laboratory at the physics institute of Julius-Maximilians University of Würzburg, Bavaria. At this day he had studied cathode rays using a Hittorf-Crookes tube. Such tubes were to be found in much physics laboratories that time. Electrons were created by ion bombardment of a cold cathode in a high voltage gas discharge. The electrons are accelerated by the tube voltage onto the anode resulting in X-rays. The tube was shaded with black paper and the wall was hit by electrons and emitted light. W.C. Röntgen recognized a weak luminescence which radiated from a fluorescence screen located near the tube. This radiation originated from the tube. It was the first time X-rays were measured. In 1901 Röntgen awarded the very first Nobel Prize in Physics.

C. G. Barkla (Nobel Prize 1917) observed about ten years later secondary X-rays that were emitted from a target sample. In doing so he used the aluminum filter method for separation of X-rays and an ionization chamber for X-rays detection. By observing these secondary X-rays he discovered the gaps in atomic absorption 1909 and finally the distinction between continuous X-rays and characteristic X-rays in 1911.

Based on Barkla´s work von Laue, who awarded the Nobel Prize 1914, investigated the wave properties of X-rays by diffraction of continuous X-rays at lattice atoms of a single crystal 1912. Wave properties were confirmed as well as the comparability of wavelength of X-rays with the atomic distances. In the same year W. H. Bragg (Nobel Prize 1915) used a NaCl (sodium chloride) single crystal and KCl (potassium chloride) single crystal for observing X-ray reflection patterns (Bragg spectrometer). The differences in the X-ray intensity if comparing sodium and potassium was the starting point of crystal structure analysis with X-rays. H. G. Moseley discovered 1913 the relationship between characteristic X-ray, wavelength and atomic number (respectively the measured element). Due to Moseley´s law (compare Chapter 2.6.4) all known elements in the periodic table of the elements could be designated explicit as well as existing gaps could be identified.

From now on K. M. Siegbahn (Nobel Prize 1924), G. v. Hevesy and others enhanced the X-ray spectroscopy. Until the fifties of the last century X-ray spectroscopy was only used within atomic physics and molecule physics respectively for determining energy states or

modifications in energy states at chemical bonds. The considerable advantages in chemical analysis arose particularly due to developments at high performance and stable X-rays and energy dispersive detectors. [1 p. 1-4], [2, p. 2-3], [4]

2.2 X-Ray Radiation

As mentioned in 2.1, X-rays were first detected and discovered by W. C. Röntgen. X-rays are high energy, electromagnetic waves with a wavelength in the range of 0.001 nm and 80 nm, corresponding to energies between 1.2 MeV (0.001 nm) and 15 eV (80 nm). In the spectrum of electromagnetic radiation X-rays are between UV-light and Gamma-rays (compare Figure 1). [1 p. 33-36]

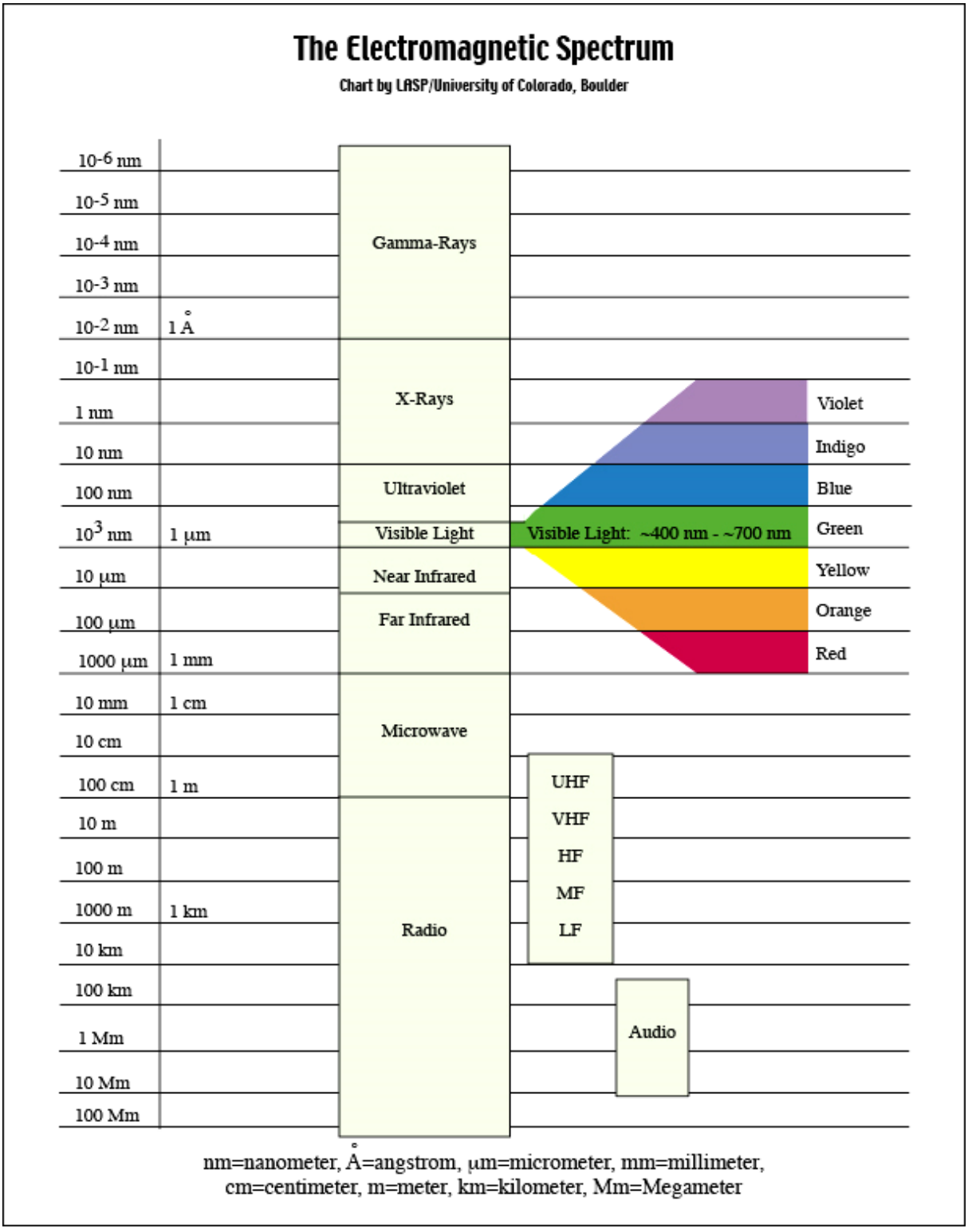

Figure 1 Electromagnetic spectrum [3]

According to quantum theory, electromagnetic waves can also be considered as a “stream” of particles (photons), which travel with the vacuum velocity of light. The particles energy is proportional to its frequency *f* with the proportionality factor *h* for Planck´s constant. The energy can be calculated from the Planck-Einstein equation (sometimes also called Einstein-Bohr equation):

$$E = hf[eV] \tag{1}$$

Since the frequency *f*, wavelength *λ*, and velocity of light *c* are correlated by $c = \lambda.f$, the relation can also be expressed as

$$E = hf = h\frac{c}{\lambda}[eV]. \tag{2}$$

[4]

The intensity of X-ray radiation (respectively radiation) relative to a distance can be described by using the inverse-square law. The inverse-square law describes not only electromagnetic waves such as X-ray radiation or light, but also gravitation (gravitational attraction force between two point masses) or electrostatics (force of attraction between two electrically charged particles).

$$I \propto \frac{1}{r^2} \rightarrow \dot{H} = \frac{A}{r^2}\Gamma_H \tag{3}$$

The intensity *I* (or power per unit) varies inversely with the square of the distance r^2 from the source. In radiation protection this law describes the equivalent dose rate H, whereby the proportional factor *A* is the activity of the radiation source [MBq] and Γ_H the absorbed dose constant. The absorbed dose constant is a physical constant calculated for various radionuclides and X-ray tubes. An increase of the distance by the factor of two will cause an intensity-drop to one fourth and similarity, by doubling the distance the equivalent dose rate will decrease by the factor of four. [5 p. 6-7]

2.3 X-Ray Sources

2.3.1 Introduction

For practical purpose mainly two different principles of X-ray radiation sources are used, **X-ray tubes** and natural or artificial **radioactive isotopes**. Despite these two, **Synchrotron Radiation** (SR) is also a possible source but not in commercial use for X-ray fluorescence. Röntgen used, when he discovered X-rays, the previous described Hittorf-Crookes-tube. Since such tubes have a short lifetime, are difficult to control and instable as well, they are out of use nowadays. An extensive development of X-ray tubes for different kind of purposes began after X-rays were developed and is still progressing. Now a wide range of X-ray tubes for various applications and from low power (a few Watt) up to very high power (tens of kW) are available, particularly W. D. Collidge´s hot cathode tube (Coolidge tube), which is nowadays the most used X-ray tube. Nevertheless, new technologies and new materials lead to new highly specialized X-ray tubes. Most recent developments deal with field electron emitters instead of thermo-electron emitters as in the hot cathode tube. By using field electrons it is possible to get rid of the clumsy hot cathode with its heating circuit that has to

run at high potential. Furthermore, there are promising results with carbon nano tubes as field electron emitters.

Radioactive isotopes are in principle convenient X-ray sources. Radioactive isotopes are not only compact and low cost, but also continuously radiating with high stability. Furthermore, radionuclides emit monochromatic radiation, which is a requirement for some applications. Besides that, radionuclides are also independent on surrounding conditions and do not need any power supply. These advantages led to the use of radioactive isotopes in many engineering applications in X-ray fluorescence devices in particular in portable instruments. Apart from these advantages the major problem is certainly their hazard potential due to their never ending and almost inexhaustible radiation leading to very strict safety conditions. Hence, these sources became unpopular but are still irreplaceable in many applications. [1 p. 33-36]

Synchrotron Radiation (SR) is the electromagnetic emission of fast charged particles moving in strong magnetic fields. It is produced by any charged particle undergoing centripetal acceleration but nowadays mostly created by electrons or positrons in storage rings or similar circular high energy particle accelerators. SR is an electromagnetic radiation with a continuous spectra beginning from infrared to gamma rays. It is emitted in very short pulses of a few ps to ns duration and repetition rate of about 10^6 pulses per second. SR sources have energies up to a few GeV for X-ray generation. Nowadays around 45 synchrotrons operate worldwide to generating SR of specific wavelength for the use in spectroscopy or photon scattering studies and in applied research in fields as chemistry, physics or biology. The so called 4^{th} generation of X-ray sources is Free electron Laser (FEL) and light sources but both are regarding the development process behind SR. [1 p. 35-36]

In XRF and especially in the application of resource recycling using X-ray fluorescence as detection technique, the use of X-ray tubes as X-ray radiation source is established and known as best and most reliable technique meeting the state of the art. Hence, the main focus at this chapter is given on X-ray tubes. [1 p. 33-36]

2.3.2 X-Ray Tubes

2.3.2.1 Basic Physical Principles

An X-ray tube is a vacuum tube where electrons are emitted from a cathode and accelerated towards an anode due to a high positive potential of the anode relative to the cathode. These electrons from the cathode collide with the anode-target material, interact with its atoms and finally lose their energy through different processes. First, about 99 % of all electrons interact with atoms of the anode resulting in a conversion into heat energy, which leads to a heating of the anode. These interactions are, however, by now not developed in detail. Secondly, electrons can undergo scattering. This scattering can be backscattering, elastic scattering (Compton scattering) and inelastic scattering (Rayleigh scattering). Depending on various factors as energy, atomic number, angle etc. all scattering takes place simultaneously but at

different probabilities. Inelastic scattering decelerates electrons resulting in a conversion of kinetic energy into electromagnetic energy. This process gives rise to the continuous spectrum and the so called “bremsstrahlung”, German for braking radiation. This bremsstrahlung is caused by just a few per mil of all incident electrons. Thirdly, remaining electrons (also only a few per mill) interact with electrons of the target material. During this interaction incoming electrons carry energy and as a consequence of this energy absorption, electrons are emitted from matter (photoelectric effect). The dominant process consists of collisions with electrons of the outermost electron orbital with small energy losses. Nevertheless, sometimes an inner electron is removed from its orbital leading to an ionized atom. Then another electron from an outer orbital fills the vacancy radiating X-rays (X-ray fluorescence radiation). This radiation is called characteristic X-ray radiation or secondary X-ray fluorescence radiation. A further description about scattering effects, bremsstrahlung and mechanism of origin of X-rays is given in Chapter 2.4. In conclusion, X-ray tubes emit continuous radiation (bremsstrahlung), characteristic radiation typically for the anode-material and Auger electrons. [1 p. 36-38], [6 p. 3-9]

In general, commercially available X-ray tubes can be roughly divided into three categories:

- Low-power X-ray tubes (< 1 kW)
- High-power X-ray tubes (1-5 kW)
- High-power X-ray tubes with rotating anode (> 5 kW)

The current developing progress of X-ray tubes leads to compact low-power tubes with small focal spots and high brilliancy and to huge power (> 30 kW) tubes with rotating anodes for medical applications or defectoscopy. [1 p. 47]

Efficiency of X-ray Excitation

The efficiency of X-ray excitation is very low. The total irradiated X-ray power can be estimated by following equation (*P* is power, *I* current and *U* voltage):

$$\eta \equiv \frac{P}{IU} \approx 10^{-6} ZU[kV] \tag{4}$$

In practice, high thermal energy dissipation occurs in anodes of X-ray tubes, which leads to an efficiency for X-ray excitation in the range of only 0.1-1 %. The maximum electric power of X-ray tubes can reach several kW for continuous operations. This makes anode cooling to a serious technical problem. [1 p.36-38]

2.3.2.2 Technology and Design of the Components

In general, X-ray tubes consist of anode and cathode mounted in high vacuum chamber (< 10^-6 Torr) within a tube envelope enclosed in a protective casing to ensure safe operation. The cathode is a heated filament often composed of tungsten and the anode is normally an elemental metal. Most common target materials for anodes are molybdenum, copper and

tungsten. The target is imbedded in a massive copper block that conducts dissipated heat away from it. Nowadays, a directly heated electron emitter is arranged in a so-called “Whenelt Cylinder”. The Whenelt Cylinder, named after A. Whenelt, a German physicist who invented the Cylinder in 1903, is an electrode used for focusing and controlling the electron beam. It is held to a slight negative voltage relative to the hot cathode. As mentioned above, emitted electrons were accelerated in an electric field between cathode and anode. Usually this field is created by applying a negative potential to the cathode while the anode is held on ground, which makes the anode´s cooling easier. X-rays are emitted from the target in all directions, but can emerge just at a special exit window at the side (side-window geometry) or the front (end-window geometry) of the tube. In spectroscopic X-rays this exit window is usually made of a thin beryllium film for minimizing X-ray absorption at lower energies. A possible arrangement of side-window geometry is shown in Figure 2 and Figure 3 shows an end-window X-ray tube for fluorescence analysis. Such end-window geometries allow realizing smaller anode-windows respectively anode-samples distances. Furthermore, in contrast to side window geometry the anode at end window tubes has a high positive potential, while the cathode is usually grounded. End-window tubes are often used for low-energy applications but are limited to a high voltage of about 60 kV due to small anode-cathode distances. [1 p. 36-42]

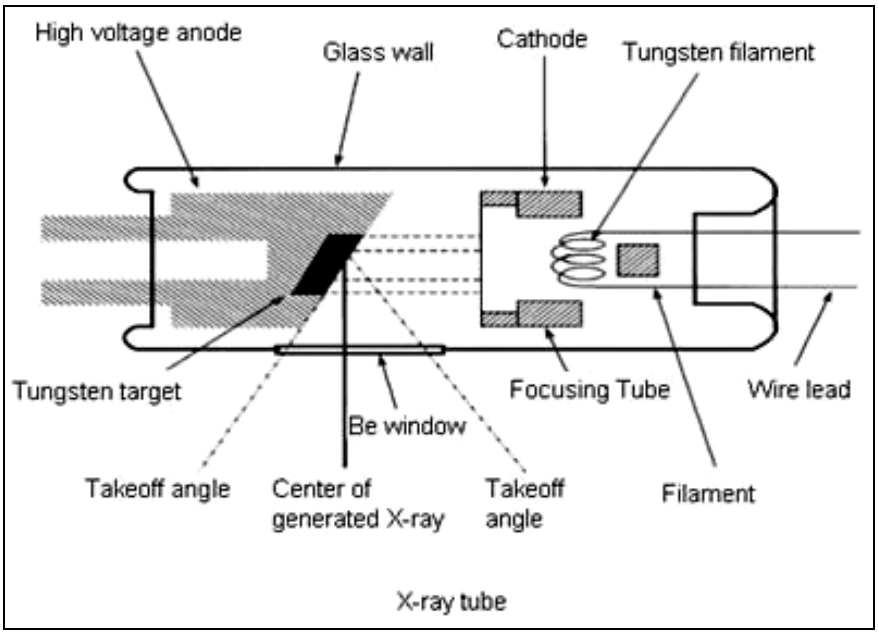

Figure 2 design of a side-window X-ray tube [7]

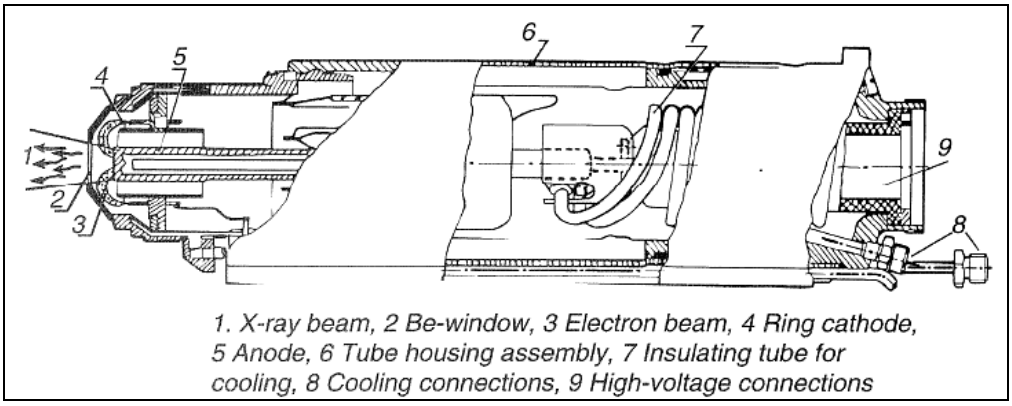

1. X-ray beam, 2 Be-window, 3 Electron beam, 4 Ring cathode, 5 Anode, 6 Tube housing assembly, 7 Insulating tube for cooling, 8 Cooling connections, 9 High-voltage connections

Figure 3 design of an end-window X-ray tube [1 p.40]

Another construction possibility of X-ray tubes are transmission-anode X-ray tubes. At transmission-anode X-rays tubes, the target is a thin layer deposited directly on the internal side of the beryllium exit window. The electron beam strikes the target at right angle and fluorescence radiation goes directly through the deposited exit window. Hence, a continuous spectrum of transmission X-ray tubes is filtered (attenuated) at certain energies due to the absorption of bremsstrahlung in the target. The greatest suppression is at low energies and above the absorption edge of the excited line. The consequence of this low contribution of the continuous spectra is a reduction of the background, resulting in an improvement of the detection limits in X-ray fluorescence analysis. X-ray tubes for transmission targets usually do not exceed 100 kV because of the thin anode foil, which cannot withstand large heat loads.

The main problem in achieving small focal spots is the immense heat dissipation on the anode. Obtaining small focal spots is only possible at the cost of power reduction. One possibility to overcome this issue is minimizing the optical spot relative to the electron beam spot. Often, only the optical spot is of primary importance. If the anode angle for instance amounts 6°, the length of the optical spot is approximately ten times smaller than the length of the electronic spot on the anode. In order to operate at higher power, it is necessary to use a rotating anode. A disk-like anode is fixed on a rotor and rotates under a space-fixed electron beam. [1 p. 40-42]

Technology and Design of the Cathode

Emission currents in X-ray tubes are controlled by the temperature of the cathode. The temperature of the cathode its turn depends on the value of the filament current. Depending on the required shape, emitters are used in different forms as shown in Figure 4. Since very low heat capacities are required for emitters due to the control of the emission current through the cathode temperature, tungsten wires and foils are mainly used. As can be seen in Figure 5, operating is only possible within certain limits. At small filament currents there is no emission and at large filament currents a saturation of the anode current occurs. [1 p. 42-43]

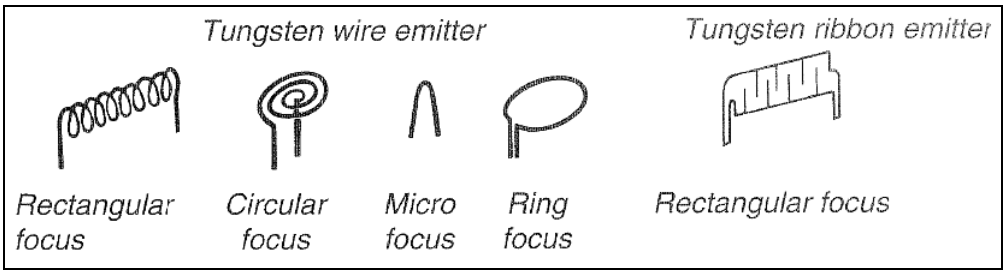

Figure 4 Different types of emitters for cathodes [1 p. 43]

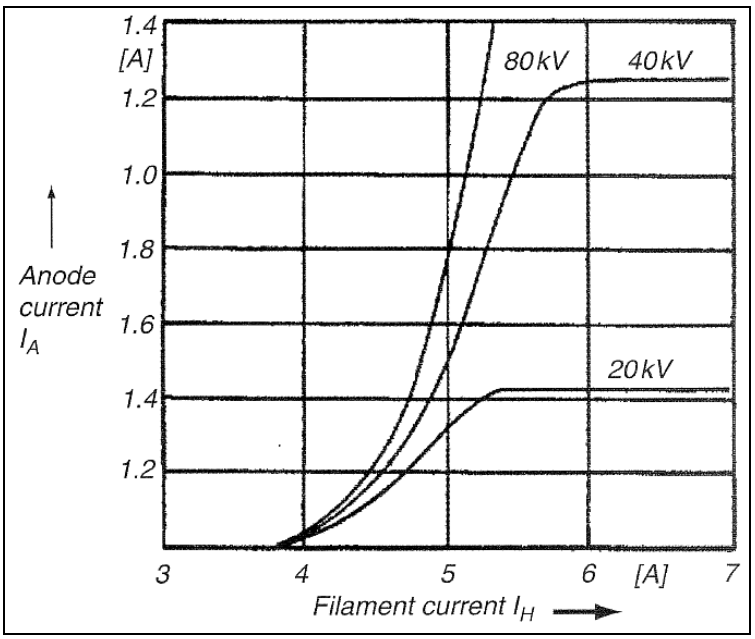

Figure 5 Anode current as a function of filament current (parameter anode voltage) [1 p. 43]

Technology and the Design of the Anode

As mentioned above, most common target materials for anodes are molybdenum, copper and tungsten, but other metals such as rhodium, palladium, titanium, silver, chromium, nickel etc. are also used. The technology for rotating anodes is more complicated than for “conventional” anodes. A disadvantage of the rotating anode is abrasion in the surface region due to high thermo-mechanical stress. This causes the absorption of radiation of deeper lying layers before it leaves the anode (so called “heel effect”). Furthermore, mechanical deformation occurs, which in the worst-case can lead to a damage of the anode. New developments are based on a Rhenium-Tungsten-Molybdenum (RTM) composite material. This improves the elastic properties and doubles the heat storage capacity of the anode. Since the rotating anode is not used in X-ray tubes for process recycling in waste management further description is not given here. [1 p. 43-45]

Vacuum Envelope and Housing Assembly

All components of an X-ray tube are positioned within a tube envelope. The housing serves with vacuum isolation high voltage insulation. Common materials used for tube envelopes

are glass and ceramics or a blend with metal, whereby glass is the most commonly used. Glass has high specific resistance, good dielectric strength and the capability to withstand temperature changes, but also a smooth and easy to clean surface, which is an important advantage for high voltage insulator. Despite glass the middle part of the glass envelope can be made of metal to establish a definite electrical potential. This metal layer extents the lifetime of the tube and avoids the negative effect of evaporated metal from anode or cathode deposited on the surface and consequently reduces the dielectric strength.

Metal-ceramic tubes have some advantages over glass tubes. At first, metal-ceramic tubes allow easier mechanical treatment resulting in more freedom in shaping. Furthermore, surface conductivity of ceramic is low, which enables short distances to insulate high voltages. Besides that, ceramic tubes are compact, robust and light but also long lasting. Apart from the vacuum envelope X-ray tubes are enclosed in a protective casing to ensure their safe operation. The casings´ main function is high voltage insulation, cooling, protection against implosion and protection against radiation. [1 p. 46-47]

2.3.2.3 The Spectrum of an X-ray tube

The intensity and distribution of continuous X-rays were dependent on the number of electrons in an atom and the characteristic X-rays were related to the electron energy configuration in the atom. Figure 6 shows typical spectra of X-ray tubes using a tungsten anode at different anode voltages. As can be seen the intensity of spectra differs with the anode voltage. Every spectrum is a superposition of bremsstrahlung and characteristic lines (secondary X-ray radiation). The form, the intensity and the maximum energy of the continuous spectrum depend on the voltage value. The position of discrete lines is characteristic for the used anode material. This is visible for Kα and Kβ principle lines for tungsten at Kα = 59.32 keV and Kβ = 67.24 keV [8]. For every characteristic line there is an excitation threshold of energy resulting in a corresponding absorption edge. A line is not present in a spectrum if the acceleration voltage does not exceed this threshold. The intensity of characteristic lines increases with the acceleration voltage. The falloff of the spectra at low voltages is due to X-ray absorption in the exit window and the air plus due to possible built-in filters for additional filtering at low energies. Such built-in filters are implemented in some applications, for instance medical utilities or special XRF applications. Common materials used for filters are aluminum and copper. For further descriptions about X-ray tubes see Chapter 3.4.6.5. [1 p. 36-38]

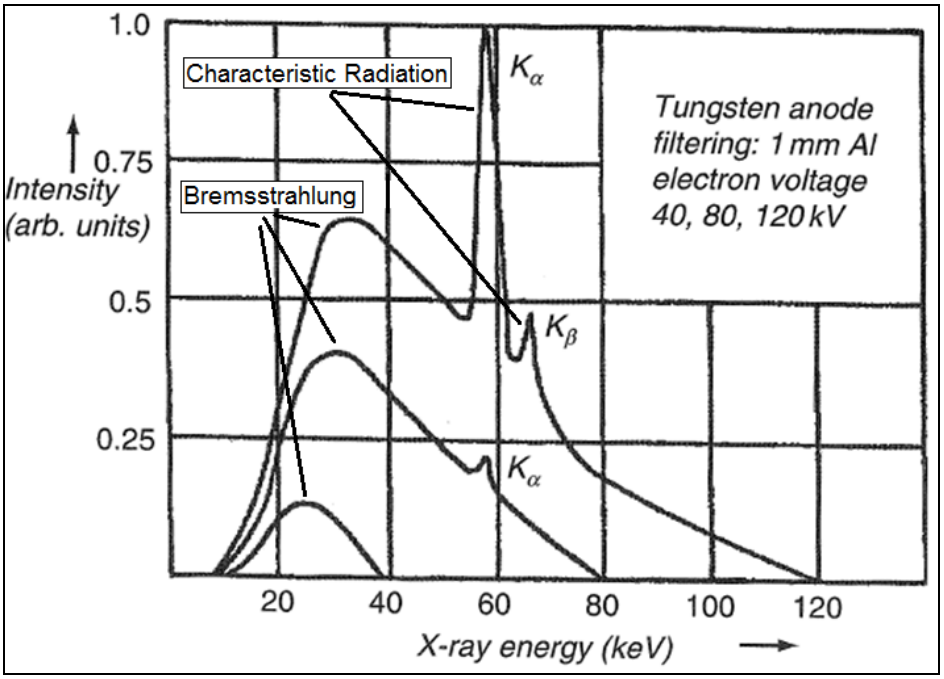

Figure 6 Typical spectra of an X-ray tube with tungsten anode [1 p. 37]

Bremsstrahlung

The X-ray radiation generated by slowing down processes of electrons (bremsstrahlung) has a continuous spectrum (compare Figure 6) since the electrons were scattered at different extents. The course of the spectrum is highly influenced by the kinetic energy $E_{kin} = e.U$ of the accelerated electrons respectively by the acceleration voltage U. Furthermore, the energy of electrons and the wavelength of X-rays are inversely related (compare Chapter 3.4). The spectrum has a sharp termination of the wavelength λ_0 depending on the acceleration voltage. Bremsstrahlung below λ_0 is not possible. W. Duane and F. Hunt investigated the so called Duane-Hunt law, which gives the minimum wavelength (maximum frequency) of X-rays that can be emitted by bremsstrahlung in an X-ray tube by accelerating electrons through an excitation (acceleration) voltage:

$$\lambda_0[nm] = \frac{c}{f} = \frac{ch}{E_{kin}} = \frac{ch}{eU} = \frac{1.24}{U[kV]} \tag{5}$$

Just a few per cent of all electrons are slowed down in one step and have λ_0 as expressed in above equation. Most electrons deliver energy step by step, which leads to the continuous spectrum and the certain range of the wavelength. The intensity distribution follows the rule of Kramer (K is Kramer´s constant):

$$I(\lambda) \propto iZ\left(\frac{\lambda}{\lambda_0}-1\right)\left(\frac{1}{\lambda^2}\right)[cm^{-2}s^{-1}] = KiZ\left(\frac{\lambda}{\lambda_0}-1\right)\left(\frac{1}{\lambda^2}\right)[photons.\sec^{-1}] \quad (6)$$

As can be seen in equation (6) electron current *i* and atomic number *Z* only influence the intensity of the spectra but not whose course, whereby both electron current and atomic number are proportional to the intensity. The integral intensity of the spectra can be estimated by following expression (proportional constant 1.5*10-9 evaluated by measurements):

$$\int I(\lambda)dI \equiv I_{ges} = \frac{1.5*10^{-9}}{V} iU^2Z \quad (7)$$

According to above equations following predications can be done (compare Figure 7):

- The increase of the voltage *U* leads by a constant current *i* to a reduction of the minimal wavelength λ_0. Furthermore, there is a quadratic correlation between the voltage and the intensity.
- There is a linear correlation between the atomic number *Z* of the anodes element and the intensity.
- There is also a linear correlation between the current *i* of the X-ray tube and the intensity.

In general, bremsstrahlung can be generated by slowing down processes of all charged particles (e.g. protons, ions, α-particles etc.) but due to the fact that intensity is inverse proportional to the square of mass of braked particles (I ~ 1/m²), it approaches zero at high mass. Protons for instance have a by the factor of 10^6 reduced intensity relative to electrons. [1 p. 33], [2 p. 3-6], [6 p. 10-11]

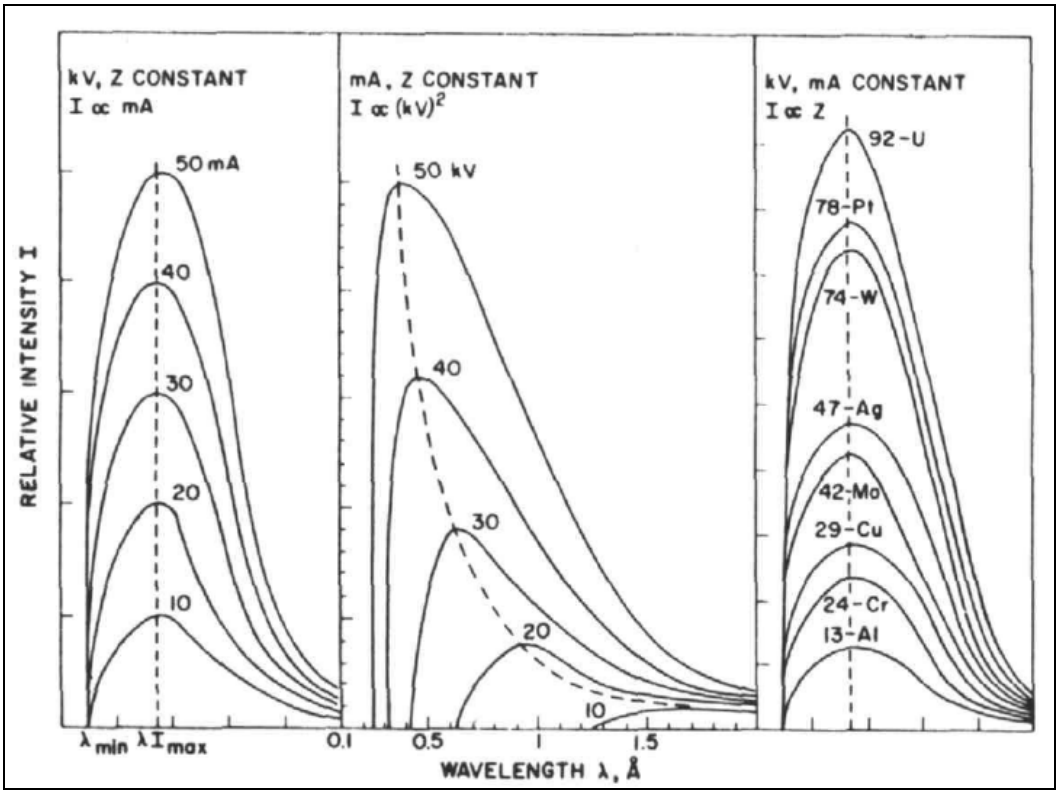

Figure 7 Correlation of intensity from tube current (left), tube voltage (middle) and atomic number (right) [6 p. 11]

Characteristic X-ray Radiation

As mentioned above characteristic X-ray radiation is generated by electron transitions of outer orbital filling the vacancy of inner orbital. This leads to the emission of secondary X-ray radiation visible by characteristic peaks in the spectrum typically for the element and electron transition. Figure 6 shows the typical peaks Kα (59.32 keV) and Kβ (67.24 keV) [8] for tungsten. Characteristic lines in the spectrum of X-ray tubes are caused by the used anode material (target). Hence, the choice of anode materials is of high interest for analysis.

In X-ray spectroscopy characteristic lines at certain energies can be correlated to elements in the excited material making quantitative and qualitative analysis of those elements possible. In Chapter 2.5 a detailed description of characteristic X-ray radiation is given including different factors of influence, transition rules, nomenclature of electron transitions etc. [1 p. 36-38]

2.4 Interaction of X-rays with Matter

2.4.1 Introduction

As mentioned in Chapter 2.3.2.1 different interactions of photons (emitted of X-rays) with matter exist, leading to the generation of heat, scattering and the emission of photons

(Photoelectric effect respectively photo effect). Scattering results in a loss of intensity and can be separated by Rayleigh scattering and Compton scattering. Photo effect and Compton effect transfer energy but Rayleigh effect does not. Figure 8 shows all possible interactions of X-rays with matter. Interaction incorporates all events in which a photon participates while absorption relates only events, where a transition of energy from a photon occurs. Absorbed energy is responsible for the creation of secondary X-ray fluorescence radiation but also for changes in the chemical state of absorbing atoms due to primary photon absorption, exposure of secondary photons and electrons originating from primary interaction. Pair production, a high energy phenomena and the creation of an elementary particle and its antiparticle (positron) from a photon, is beside mentioned interactions in general also possible. The minimum energy necessary for pair production is 1.02 MeV and follows the law of conservation of energy. Incident radiation has to exceed twice the potential energy of an electron, which amounts $E_e = m_e \cdot c^2 = 2 * 0.511\ MeV$. Since X-ray fluorescence does not exceed the low kV-range, pair production of X-rays is impossible. [1 p. 312], [10. p. 13]

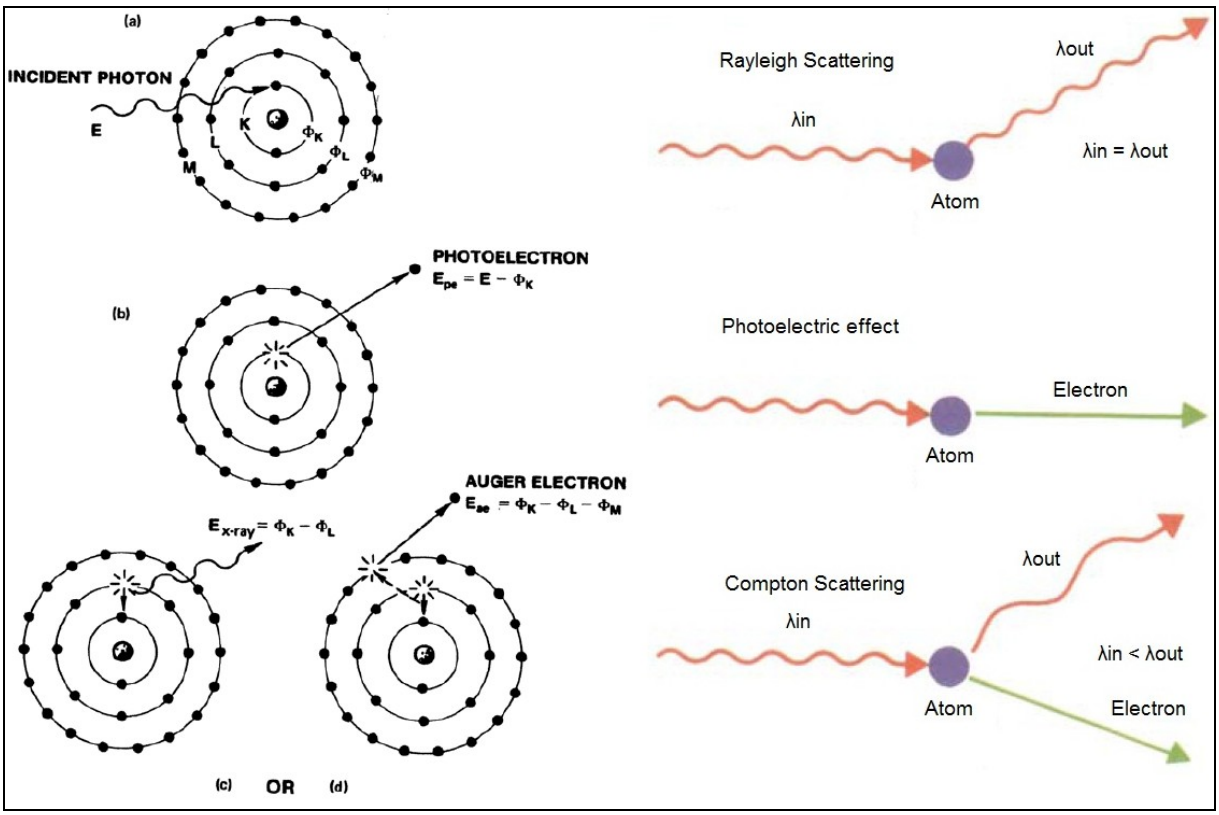

Figure 8 Interaction of X-rays with matter (Photoelectric effect and Scattering) [10 p. 8, 13]

Electromagnetic radiation is attenuated by penetrating matter. The extent of the interaction is affected by the energy and spectral composition of incoming radiation and by the chemical composition plus crystalline structure of the sample. The attenuation can be estimated with Beer-Lambert´s law following exponential:

$$I = I_0 e^{-\mu d} \tag{8}$$

I is the intensity of radiation before and I_0 after attenuation, and d the distance the radiation travels through the material. μ is the attenuation coefficient, a material constant dependent on the energy of X-rays (wavelength) and the material. By dividing the attenuation coefficient with the mass, the in the literature also well known mass attenuation coefficient μ_{mass} *[g/cm²]* is obtained. In general, in the literature three different forms of attenuation coefficients are known, linear attenuation coefficient μ_{linear} *[1/cm²]*, mass attenuation coefficient μ_{mass} *[g/cm²]* and atom attenuation coefficient μ_{Atom} *[cm²/atom]* (there are N_A/A atoms in 1 g of atoms, where N_A is Avogadro´s number and A is the atomic weight or relative atomic mass). Since the interaction of photons with matter is due to scattering and Photo effect, the attenuation coefficient is the sum of all possible factors of influence:

$$\mu_{Atom,total} = \tau_{Atom} + \sigma_{Atom,Rayleigh} + \sigma_{Atom,Compton} = 1 \tag{9}$$

For photo absorption the Greek τ is used, while for scattering σ. Symbols for μ_{Atom}, μ_{mass} and μ_{linear} are not standardized. Literature data are generally given as mass attenuation coefficients μ_{mass}. If not marked, attenuation coefficients in this work are always mass attenuation coefficients ($\mu_{mass} = \mu$). Real materials, such as chemical compounds, alloys etc. always consist of several elements. If the mass fractions are known for each element (sum of $C_j = 1$), then the total atomic attenuation coefficient of the materials is the weighted sum of all individual atomic attenuation coefficients (same applies to τ and σ):

$$\mu_{total} = \sum_j C_j \mu_j \tag{10}$$

The probability of each interaction is the mass attenuation coefficient of the interaction divided by the total mass attenuation coefficient. For instance the probability of photo absorption can be estimated by following equation:

$$w_{photo} = \frac{\tau_{Atom}}{\mu_{Atom,total}} 100\% \tag{11}$$

[1 p. 312-316], [2 p. 31-33], [9 p. 4-6]

Figure 9 shows the contribution of all possible interactions of radiation in matter for lead in the range of eV to GeV. Despite interactions of X-rays as Photo effect (τ), Compton scattering (σ_{incoh}) and Rayleigh scattering (σ_{coh}), also visible in this figure pair production (κ_n - nuclear field, κ_e-electron field) and photonuclear absorption (σ_{ph} –usually followed by emission of a neutron or other particle). [11p. 3-1- 3-4]

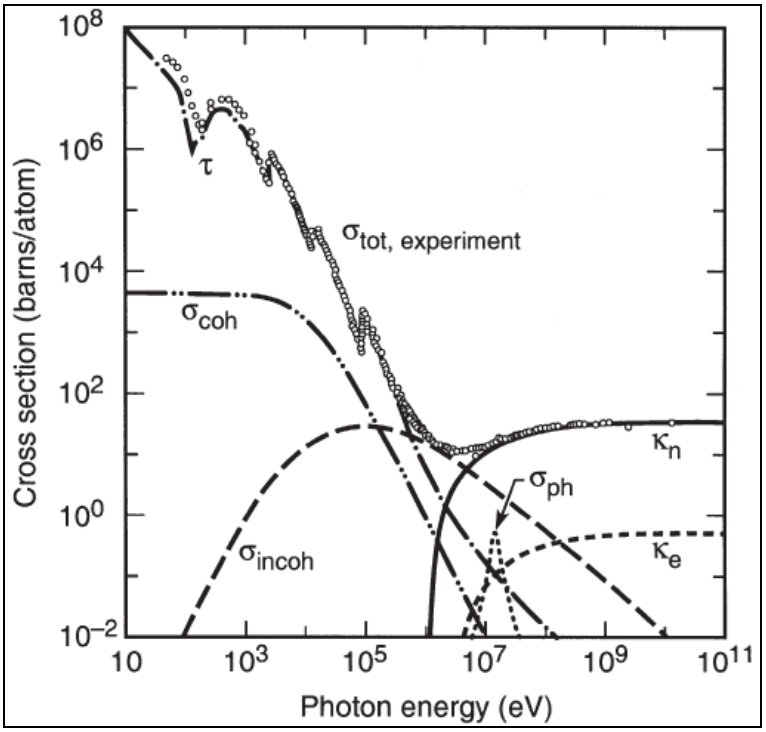

Figure 9 Mass attenuation of possible interactions of X-rays in matter [11p. 3-4]

2.4.2 Scattering

2.4.2.1 Compton Scattering

Compton scattering also referred to as incoherent or inelastic scattering is the interaction of photons with weakly bounded electrons of the outer orbital. A part of the energy of X-rays is transferred to the electron resulting in its ejection. Hence, the atom becomes ionized and the remaining energy is taken by the scattered photon. The wavelength of the scattered photon is thus longer (has less energy) than the wavelength of the incident photon. Compton estimated the relationship between the wavelength and the scattering angle by following expression:

$$\Delta\lambda = \lambda_{scat} - \lambda_0 = \frac{h}{m_e c}(1-\cos\psi) \cong 0.00243.(1-\cos\psi), \qquad (12)$$

whereby h is the Planck´s constant, m_e is the remaining mass of the electron and c is the velocity of light in vacuum. The angle ψ is the angle between the original direction and the direction of the photon after scattering. If the wavelength is calculated in nm, the expression $h/(m_e c)$, the Compton wavelength of the electron, evaluates 0.00243 nm.

Compton scattering is significant at radiation absorption for energies >100 keV and increases with degreasing angle ψ. Despite that, Compton scattering is strongly related to the mean atomic number of the sample and increases with a falling atomic number. Furthermore, most

of the photons are scattered by large angles from the trajectories of primary photons. [1 p. 204, 363-369], [2 p. 33], [6 p. 5], [12 p. 254]

2.4.2.2 Rayleigh Scattering

Rayleigh scattering also referred to as coherent or elastic scattering results from the interaction of radiation with strongly bounded inner orbital electrons. The wavelength of incident photons is equal to the wavelength of the scattered photons, which means no energy is transferred. The intensity of Rayleigh scattering is inverse proportional to the fourth power of the wavelength, leading to a significant higher scattering of shorter wavelength. Since the amount of strongly bounded electrons increases with the atomic number, Rayleigh scattering rises with the atomic number. Rayleigh scattering significantly occurs only at small energies. At the measuring range of conventional X-ray fluorescence spectrometer, Rayleigh scattering does usually not exceed 10-20 % of the total absorption probability. Photons scattered in elastic process are dominant in the forward direction resulting in a very small angle from the trajectories of primary photons. [1 p. 204, 363-369, 769], [2 p. 33], [12 p. 254]

2.4.3 Photoelectric Effect

If X-ray radiation (e.g. from X-ray tubes) incidents matter and is not scattered and if the energy of this incident radiation is high enough, more precisely exceeds the bond energy of electrons on the orbital (ionization energy), emission of electrons due to the photoelectric effect takes place. Hence, in photoelectric effect electrons are emitted from matter as the consequence of their absorption of energy from photons, whereby this photon is annihilated. The quantity of absorbed energy is equal to the bond energy of the emitted electron. The remaining energy $E_{kin,Photo\text{-}electron} = E_{Photon} - E_{Binding}$ is carried by the emitted (photo-) electron. This mechanism is certainly only possible if the energy of incident radiation is greater than the ionization energy of the electron. The dominant process consists of collisions with electrons from the outermost electron orbital and small bond energies, but nevertheless, sometimes an inner electron is removed from its orbital. This causes the occurring of vacancies and the atom gets ionized. Then within ps the excited atom relaxes (ground state) by refilling the vacancy from an outer shell. This effect favors interactions with electronic shells for which E_{kin} is small but $E_{Photon} > E_{Binding}$. Absorption of energies just above the absorption edge is most effective and probable (compare Figure 11).

Since the bond energy of outer orbital electrons is always higher than inner ones, energy is obtained during the electron transition. Then, this energy can either be emitted as secondary fluorescence radiation or as so called Auger-electron. Which mechanism (X-ray fluorescence or Auger-electron) is more likely to take place, depends on the atomic number and the electron transition. In general, the fraction of fluorescence radiation increases with rising atomic number but is also different for various principle lines (Kα, Kβ, Lα etc.) at the same element. Transitions are governed by quantum-mechanical selection rules (compare Figure 14). For further details see Chapter 2.5. [2 p. 31-32], [6 p. 6-9]

2.4.3.1 X-ray fluorescence

X-ray fluorescence is the emission of characteristic (secondary) X-rays (photon emission) from atoms that have been excited by X-rays. This secondary X-ray radiation is characteristic for each element and characteristic for each electron transition. By measuring this radiation with special detectors (Si-PIN, Si-Drift etc. compare Chapter 2.6.6), it is possible to determine the elemental composition for the targeted object material. Hence, it is used as sorting criterion in resource recycling. X-ray fluorescence and Auger effect are always competing interactions. The fluorescence yield for heavy elements amounts 0.5-0.9 (around 50 % for Z = 32) but drops for very light elements up to the range of 0.001 (e.g. Carbon). Carbon has therefore an Auger yield of 0.999. Auger probability p_{Auger} and probability of photon emission (fluorescent yield) ω complement each other $p_{Auger} + \omega = 1$. Figure 42 gives an overview of probabilities for X-ray fluorescence and Auger effect at different elements and ionization of K and L-orbital. [1 p. 316-317], [2 p. 6-7], [14 p. 14]

2.4.3.2 Auger-electron

Apart from the emission of secondary X-ray radiation during relaxing of the atom to ground state, a transfer of the energy to another electron is also possible. This Auger-electron from an outer electron shell absorbs the originated energy. Hence, it is emitted from the atom, while the atom gets double ionized. This mechanism is radiationless and named Auger effect. The energy of Auger-electrons is $E_{kin,Auger} = \Delta E - E_{Binding}$. As secondary X-ray radiation is characteristic, also the energy of Auger-electrons is both characteristic for the specific transfer and characteristic for each element. Thus, quantitative and qualitative analysis is also possible by detecting Auger-electrons. The probability an Auger-electron is emitted decreases with rising atomic numbers. This is a result of stronger bond energies for outer electrons at higher atomic numbers. Therefore, the Auger-electron spectroscopy is only for very low atomic numbers of interest for analysis (e.g. Carbon 0.999). A special case of the Auger effect is the Coster-Kronig transition. In the Coster-Kronig transition the vacancy is filled by an electron from a higher subshell of the same shell (instead of a higher shell like at the Auger effect). Auger-electron energies for the elements $3 \leq Z \leq 92$ are shown in Figure 10. Points indicate the electron energies of the principal Auger peaks for each element, whereby larger points represent the most intense peaks. The strongest Auger peaks for most elements ($3 < Z < 90$) are below 3 keV. This leads to a very low possibility of generated Auger-electrons at higher energies. [1 p. 316-317], [6 p. 8-9], [14 p. 13-15]

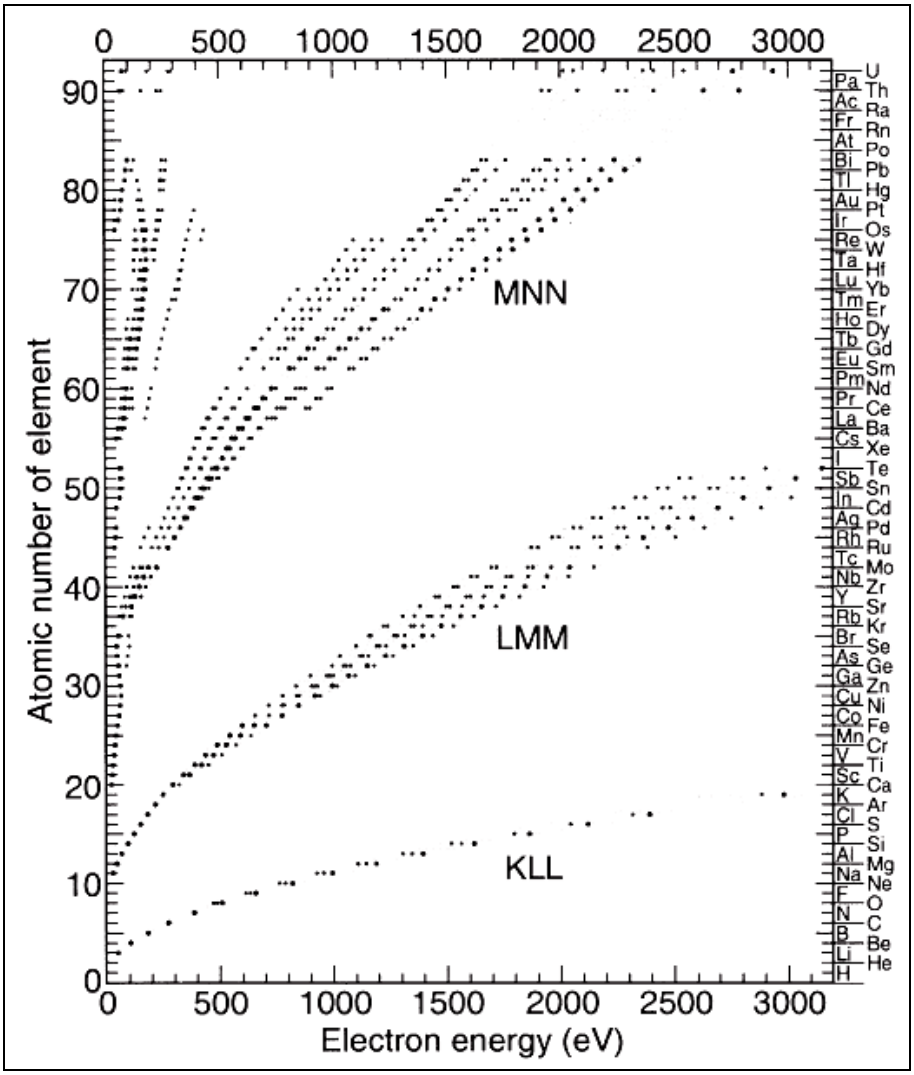

Figure 10 Auger electron energies [11 p. 1-31]

2.4.4 Fractions of Interaction

Figure 11 shows the relative contribution of total mass attenuation coefficients for Photoelectric, Compton and Rayleigh effect versus the photon energy for the elements argon (Z = 18), silicon (Z = 14) and germanium (Z = 32). Argon for instance, has principle lines at about 3 keV, which is visible at the absorption edge at exactly this energy (for other absorption edge energies see Appendix II). The photoelectric effect has, therefore, the highest peak (respectively intensity of the secondary fluorescence radiation) at energies of 3 keV or little higher. For energies lower than the energy of the absorption edge no excitation can take place, while the higher the energy differs from the energy of the absorption edge, the lower will be the mass attenuation (and accordingly intensity). Compton scattering is dominant over Rayleigh in the range of 20-50 kV for very low Z elements. Good to see in Figure 11 is the different scattering fraction of Compton and Rayleigh at a given energy (say 20 kV) and different Z. The Compton scattering is roughly constant (more precisely it slightly increases with falling atomic number- a little bit less than 10^{-1} cm²/g for germanium but a little bit above 10^{-1} cm²/g for silicon). In contrary, Rayleigh contribution at a given energy of 20 kV

is much lower for low Z. Silicon has a mass attenuation coefficient of approx. 0.25 cm²/g, while the mass attenuation coefficient for germanium for the same energy amounts approx. 0.8 cm²/g (The log-log plot makes this a bit difficult to see) [27]

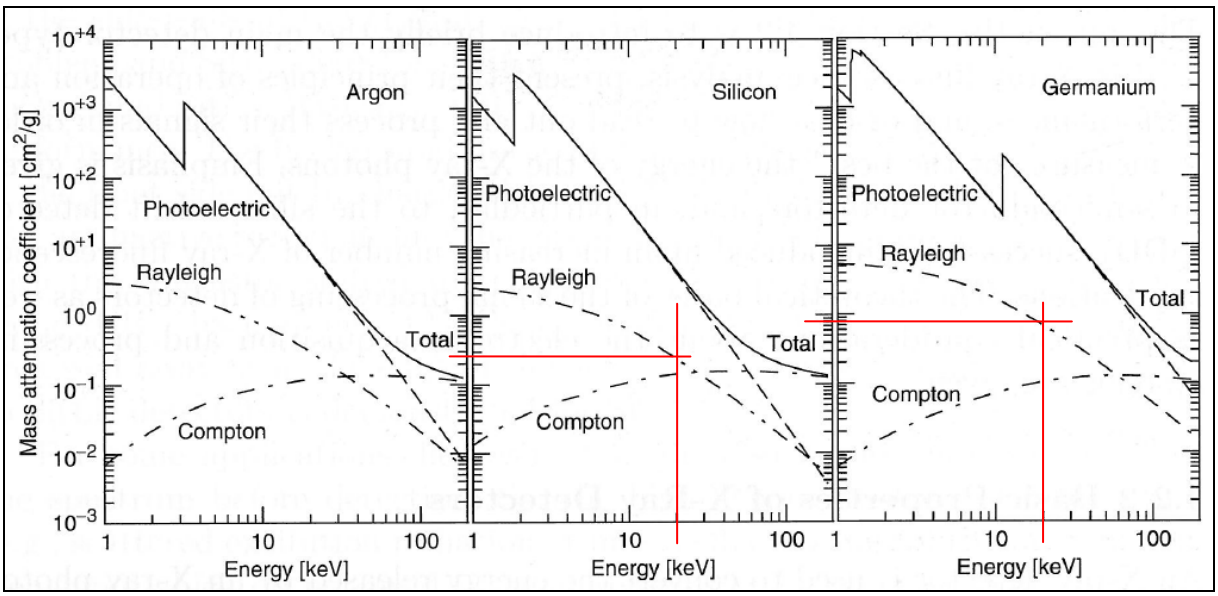

Figure 11 Different mass attenuation coefficient (Note: double logarithmic scale) [1 p. 204]

2.5 Excitation

In the excitation of matter by X-rays a differentiation has to be done depending on the origin of the excitation radiation. Primary or direct excitation is excitation of (primary) fluorescent photons by primary (external) X-ray radiation e.g. emitted by X-ray tubes. If these primary fluorescence photons have sufficient energy to excite further atoms in the sample, then this interaction is called secondary excitation (indirect excitation).

The photon counts *N* after attenuation is a function of penetrated thickness *x*, or mass thickness *m* (m equals mass per area) and given by the attenuation (absorption) law

$$N(x) = N_0 e^{-\mu linear * x} \qquad N(m) = N_0 e^{-\mu m} \tag{13}$$

and the integral attenuation (absorption) law

$$dN = -N * \mu linear * dx \qquad dN = -N * \mu * dm \tag{14}$$

The photo absorption coefficient τ (compare (9)) in a specific shell (or subshell) is composed of the absorption coefficients of the individual shells: $\tau = \tau_K + \tau_{L1} + \tau_{L2} + \tau_{L3} + \tau_{M1} + \ldots$ These coefficients are not known but the ratios (τ_K/τ, τ_{L1}/τ etc.) can be estimated from tabulated values of absorption edge jump ratios, S_K, S_{L1}, S_{L2} etc. Absorption edge jump ratios are defined as the ratio of the photo-absorption coefficients at higher and lower energy sides of an edge. The K-edge for instance, is

$$S_K = \frac{\tau}{\tau - \tau_K} \Rightarrow \tau_K = \frac{S_K - 1}{S_K}\tau \tag{15}$$

and the L_2-edge

$$S_{L2} = \frac{\tau - \tau_K - \tau_{L1}}{\tau - \tau_K - \tau_{L1} - \tau_{L2}} \Rightarrow \tau_{L2} = \frac{S_{L2} - 1}{S_K S_{L1} S_{L2}}\tau. \tag{16}$$

Above equations are valid for $E_{K\text{-edge}} < E_{Photon}$. For cases where $E_{L1\text{-edge}} < E_{Photon} < E_{K\text{-edge}}$ set $\tau_K = 0$ and $S_K = 1$, for $E_{L2\text{-edge}} < E_{Photon} < E_{L1\text{-edge}}$ set $\tau_K = \tau_{L1} = 0$ and $S_K = S_{L1} = 1$ etc.

The calculation of the amount of excited atoms is a very complex subject. Specimens are always heterogeneous and consist of several different elements influencing the radiation by scattering, attenuation, fluorescence etc. A simplified derivation of the number of excited photons of mixed atoms (thick stack of layers) for the differential thickness *dx* in the layer *x* is given for direct excitation. The derivation of indirect excitation is similar to described direct excitation but more complex and complicated. Hence, this work does not address the derivation of indirect excitation. [1 p. 313-316]

2.5.1 Direct Excitation

As mentioned above direct excitation is a process where primary photons by X-ray tubes, radioactive sources or synchrotron beam excite atoms resulting in the emission of (primary) fluorescent photons.

The following derivation shows the amount of fluorescent radiation excited by polychromatic sources of bulk material, beginning with monochromatic sources and a small number of incident atoms, going to fluorescent radiation from a large number of mixed atoms and finally to the fluorescent radiation of bulk material excited by polychromatic sources:

Note: The following derivation was done to give an overview about the complexity of such calculations. On further calculations about excitation has not given any thought.

Based on (14) arises for N_{Prim} monochromatic primary photons hitting a small number Δn [atoms/ cm²]

$$\Delta N = N_{\mathrm{Pr}im}\mu_{Atom}\Delta n \tag{17}$$

With the inclusion of following factors for the electron transition KL_3

- the probability for photo-absorption is $\tau_{Atom}/\mu_{Atom,}$
- the corresponding probability for the K-shell is $\tau_{KAtom}/\tau_{Atom,}$
- relaxation by the transition KL_3 takes place with the probability $p_{K\alpha 1,}$
- the fluorescent yield for the emission of photons is $\omega_{K,}$

- the absorption edge jump ratio S_K and τ_K, respectively is given with (15),

the number of emitted $K_{\alpha 1}$-photons is

$$\Delta N_{K\alpha 1} = N_{\mathrm{Prim}} \frac{S_K - 1}{S_K} \Delta n \tau_{Atom} p_{K\alpha 1} \omega_K = N_{\mathrm{Prim}} \frac{S_K - 1}{S_K} \Delta m \tau p_{K\alpha 1} \omega_K . \quad (18)$$

In general for a mixed atom and only a certain fraction of interacting atoms of element *i,* the amount of photons absorbed by *i* is as follows (relative amount of *i*-atoms must be known)

$$\Delta N_i = N_{\mathrm{Prim}} \frac{S_i - 1}{S_i} C_i \Delta m \tau_i p_i \omega_i \quad (19)$$

For the derivation of the equation for a larger number of mixed atoms two further steps have to be considered. First, the layer from which the secondary fluorescent photons are emitted is shielded by a stack of atoms with thickness *x* (compare Figure 12). The second step includes the adding of all layers which emit fluorescent radiation.

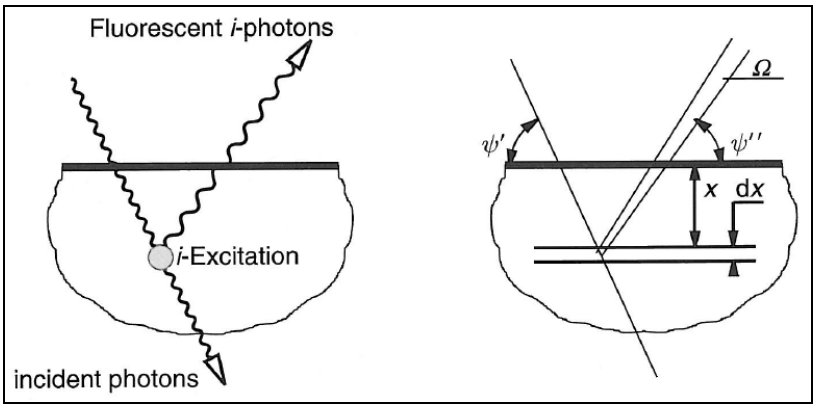

Figure 12 Direct excitation, geometry [1 p. 319]

The number of emitted photons at layer $\Delta N_{i,em}$ *x* can be estimated by using previous equation and μ_{linear} as well as the amount of observed atoms $\Delta N_{i,ob}$ (see Figure 12 for definitions)

$$\Delta N_{i,em} = N_{prim} \exp\left(-\frac{x}{\sin\psi'} \mu_{linear,E} \right) \frac{S_i - 1}{S_i} C_i \frac{\Delta x}{\sin\psi'} \frac{\rho}{\rho_i} \tau_{i,linear} p_i \omega_i \quad (20)$$

$$\Delta N_{i,ob} = N_{i,em} \exp\left(-\frac{x}{\sin\psi''} \mu_{linear,i} \right) \frac{\Omega}{4\pi} \quad (21)$$

By integration over *x* (with the thickness *T*) and mass attenuation coefficient instead of linear coefficient (bulk materials: T → ∞ or m → ∞) follows

$$N_{i,ob} = \int_{x=0}^{x=T} dN_{i,ob} = \ldots = N_{prim} \frac{S_i - 1}{S_i} p_i \omega_i \frac{\Omega}{4\pi \sin\psi'} C_i \tau_i \frac{1}{\frac{\mu_{linear,E}}{\sin\psi'} + \frac{\mu_{linear,i}}{\sin\psi''}} \tag{22}$$

For polychromatic sources, the sum of photons excited by all primary photons of energies within $E_{edge,i}$ and E_{max} (respectively $\lambda_{edge,i}$ and λ_{max}) must be computed by integration of previous equation

$$N_{i,ob} = \frac{S_i - 1}{S_i} p_i \omega_i \frac{\Omega}{4\pi \sin\psi'} C_i \int_{E=Eedge}^{E=E\max} \tau_i N_0(E) \frac{1}{\frac{\mu_{linear,E}}{\sin\psi'} + \frac{\mu_{linear,i}}{\sin\psi''}} dE \tag{23}$$

[1 p. 312-321]

2.5.2 Indirect Excitation

Direct (primary) excitation results in the emission of (primary) fluorescent photons. If these fluorescent photons have sufficient energy to excite atoms of her part, then this process is called secondary excitation (compare Figure 13). Furthermore, it can be observed that emitted secondary fluorescence photons have also sufficient energy for exciting further fluorescent radiation, which is then named tertiary excitation. Higher levels of interactions (tertiary, quaternary etc. excitation) are possible but have no practical importance. Indirect excitation is the umbrella term for secondary, tertiary etc. excitation.

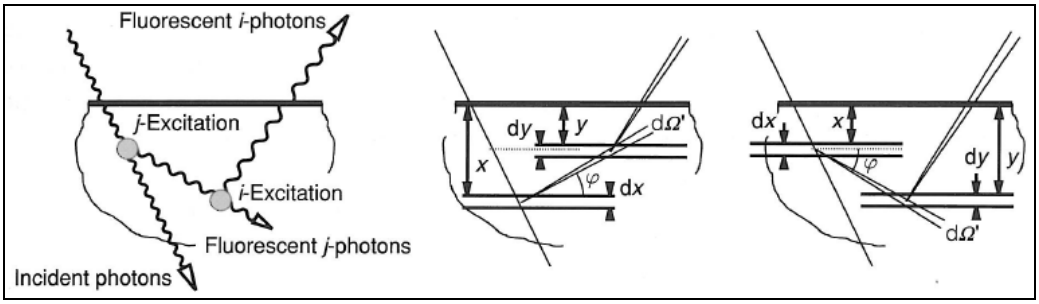

Figure 13 Indirect excitation, geometry [1 p. 323]

At transition elements secondary excitation is particularly strong for elements differing by two in the atomic number. Stainless steel (Cr-Fe-Ni, Cr=Chromium, Fe=Iron, Ni=Nickel) is a typical example. Contributions amount up to 30 % from secondary excitation (Fe → Cr, Ni → Cr and Ni → Fe) and up to 2.5 % from tertiary excitation (Ni → Fe → Cr). This means in stainless steel Cr has always a higher relative count rate as Ni, which is essential for detection.

Another possibility of indirect excitation is the cascade effect. The cascade effect describes indirect excitation within the same atom. If an atom is ionized in the K-shell, it radiates a Kα1-photon, whereby an L_3 hole is generated in the same atom. This is virtually same as after direct L_3 excitation by an incident photon. The contribution of cascade effect at the application of X-ray fluorescence in resource recycling is only slight and can be neglected. [1 p. 322-325, p. 382-384], [15]

2.6 Characteristic X-rays

2.6.1 Introduction

As mentioned above, characteristic X-ray radiation is emitted when electrons fill the vacancies of inner orbital by electron transitions from outer orbital. This radiation can also be called secondary X-ray radiation and is specific for each element and each electron transition. The fluorescence yield ω for heavy elements amounts up to 0.9 and is around 0.5 for Z = 32 (germanium) but drops at very light elements down to the range of 0.001 (p_{Auger} = 0.999), for Z = 6 (carbon). The emission of characteristic X-ray radiation is only possible for elements having a completed electron orbital and furthermore another electron on the L-orbital that is able of filling the vacancy. Hydrogen and helium do not comply with this requirement, for lithium and beryllium the electron transition from L-2s onto K-1s-orbital is of remote likelihood.

2.6.2 Transition Level

Depending on the energy of incident radiation, vacancies at different orbital are generated- the higher the electron orbital, the higher will be the bond energy. The excitation energy has to be at least the bond energy of the emitted electron. Therefore, for high excitation energies the possibility of the remove of an N-electron is indeed unlikely but possible. If the innermost electron (K-orbital) is removed, the vacancy can be filled by electron transitions from different outer electron orbital (L, M, N or O-orbital.), but however, the most likely electron transition is from L to K-orbital. By assuming an electron transition from the L-orbital, the generated vacancy from this transition can either be filled by an M, N, O or P-electron. Again by assuming the following electron transition is from the next orbital M, the generated vacancy by this can be filled from N, O or P-orbital- continuative for all further transitions. If shells (K, L, M, N O, P) are divided into its subshells, a lot more different electron transitions can origin, but as can be seen in Figure 14 only a few electron transitions are of importance. The most important and likely electron transitions are represented with thick solid line. A detailed description about possibilities of electron transitions is given later in this chapter. Appendix I shows bond energies of elements with $1 \leq Z \leq 92$ for every single subshell. Appendix II gives characteristic X-ray line energies for the strongest and most likely transitions (Kα1, Kα2, Kα3, Lα1, Lα2, Lβ1, Lβ2, Lγ1 and Mα1) for elements with $3 \leq Z \geq 95$. [2 p. 6-13], [4]

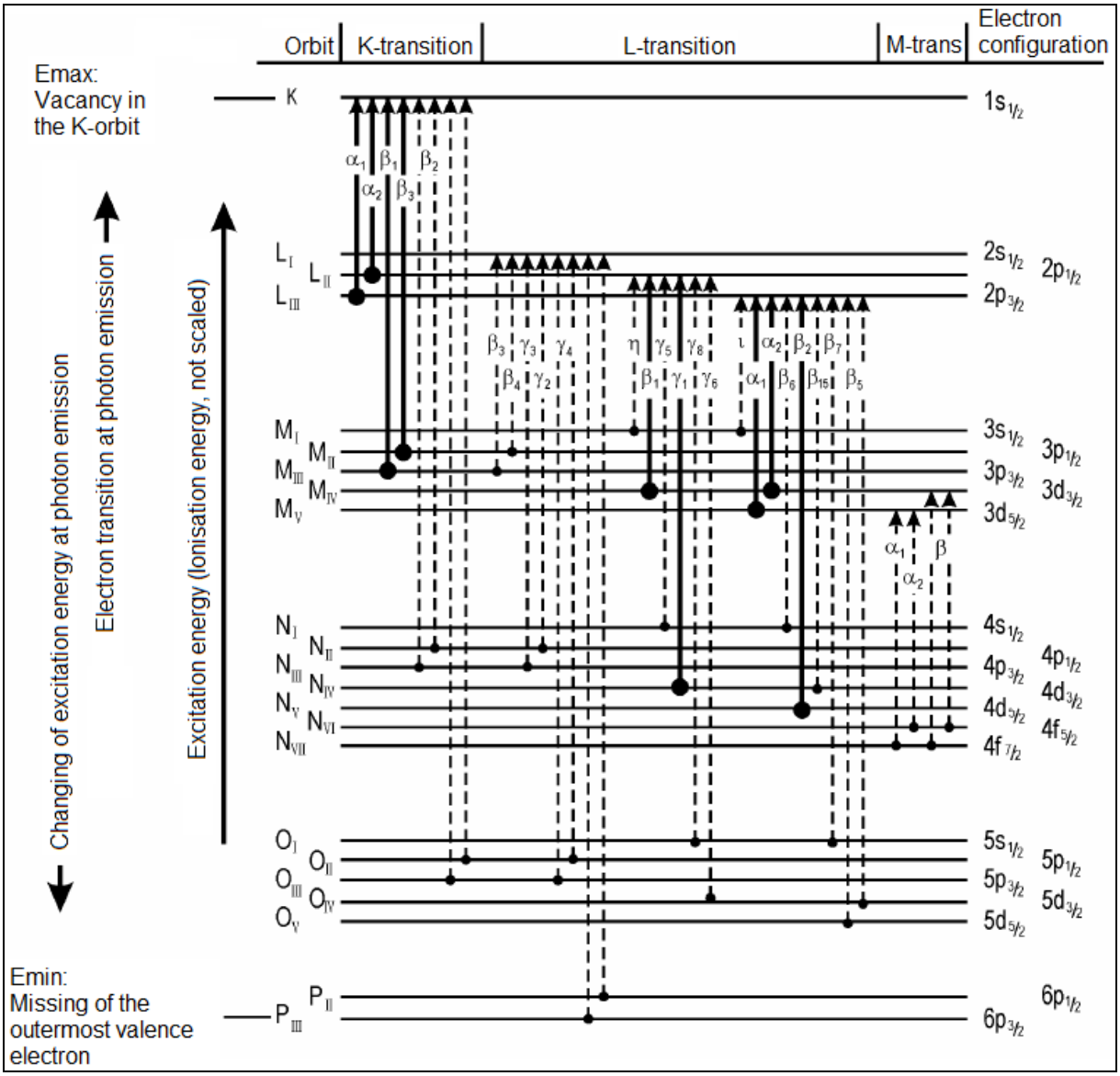

Figure 14 X-ray energy transmission [2 p. 8]

2.6.3 Nomenclature

The nomenclature, used for X-ray spectroscopy, was introduced in the 1920´s by M. Siegbahn. It is based on the relative intensities of lines from different series but does not give information about the origin of these lines. A number of lines have been observed afterwards and are therefore not classified. Also Siegbahn´s nomenclature is difficult to learn. Hence, a new and more systematic nomenclature for X-ray emission spectra was introduced by IUPAC (International Union for Pure and Applied Chemistry). That IUPAC Notation is based on energy-level designation, simple and easy to extend to any kind of transition. Table 1 shows the correspondence between X-ray level and electron configuration. In Table 2 Siegbahn nomenclature as well as IUPAC Notation is given. In Appendix I electron binding energies [eV] for $1 \leq Z \leq 92$ are listed, Appendix II shows the most important characteristic X-ray energy lines for $3 \leq Z \leq 95$. [4], [16]

Sometimes instead of exactly notations as Kα1 and Kα2 respectively K-L3 and K-L2 only Kα respectively K-L is given in the literature. This is in most cases accurate enough since α1 and α2 values respectively L2 and L3 do not differ with reasonable extents. For zink the electron transition Kα1 has for instance, the energy of 8,638.86 eV, whereby Kα2 amounts 8,615.78 eV resulting in the difference of only 0.27 % or 23.08 eV (compare Appendix II).

Table 1 Electron configuration vs. X-ray diagram levels [14 p. 5]

level	electron Configuration	level	electron Configuration	level	electron Configuration
K	$1s^{-1}$	N_1	$4s^{-1}$	O_1	$5s^{-1}$
L_1	$2s^{-1}$	N_2	$4p1/2^{-1}$	O_2	$5p1/2^{-1}$
L_2	$2p1/2^{-1}$	N_3	$4p3/2^{-1}$	O_3	$5p3/2^{-1}$
L_3	$2p3/2^{-1}$	N_4	$4d3/2^{-1}$	O_4	$5d3/2^{-1}$
M_1	$3s^{-1}$	N_5	$4d5/2^{-1}$	O_5	$5d5/2^{-1}$
M_2	$3p1/2^{-1}$	N_6	$4f5/2^{-1}$	O_6	$5f5/2^{-1}$
M_3	$3p3/2^{-1}$	N_7	$4f7/2^{-1}$	O_7	$5f7/2^{-1}$
M_4	$3d3/2^{-1}$				
M_5	$3d5/2^{-1}$				

Table 2 Correspondence between the Siegbahn and IUPAC notations [14 p. 8]

Siegbahn	IUPAC	Siegbahn	IUPAC	Siegbahn	IUPAC	Siegbahn	IUPAC
$Kα_1$	$K-L_3$	$Lα_1$	L_3-M_5	$Lγ_1$	L_2-N_4	$Mα_1$	M_5-N_7
$Kα_2$	$K-L_2$	$Lα_2$	L_3-M_4	$Lγ_2$	L_1-N_2	$Mα_2$	M_5-N_6
$Kβ_1$	$K-M_3$	$Lβ_1$	L_2-M_4	$Lγ_3$	L_1-N_3	Mβ	M_4-N_6
$K^{I}β_2$	$K-N_3$	$Lβ_2$	L_3-N_5	$Lγ_4$	L_1-O_3	Mγ	M_3-N_5
$K^{II}β_2$	$K-N_2$	$Lβ_3$	L_1-M_3	$Lγ_4'$	L_1-O_2	Mζ	$M_{4,5}-N_{2,3}$
$Kβ_3$	$K-M_2$	$Lβ_4$	L_1-M_2	$Lγ_5$	L_2-N_1		
$K^{I}β_4$	$K-N_5$	$Lβ_5$	$L_3-O_{4,5}$	$Lγ_6$	L_2-O_4		
$K^{II}β_4$	$K-N_4$	$Lβ_6$	L_3-N_1	$Lγ_8$	L_2-O_1		
$Kβ_{4x}$	$K-N_4$	$Lβ_7$	L_3-O_1	$Lγ_8'$	$L_2-N_{6(7)}$		
$K^{I}β_5$	$K-M_5$	$Lβ_7'$	$L_3-N_{6,7}$	Lη	L_2-M_1		
$K^{II}β_5$	$K-M_4$	$Lβ_9$	L_1-M_5	Ll	L_3-M_1		
		$Lβ_{10}$	L_1-M_4	Ls	L_3-M_3		
		$Lβ_{15}$	L_3-N_4	Lt	L_3-M_2		
		$Lβ_{17}$	L_2-M_3	Lu	$L_3-N_{6,7}$		
				Lv	$L_2-N_{6(7)}$		

2.6.4 Moseley´s Law

H. Moseley invented and published in 1913 an empirical law showing that the frequency of certain characteristic X-rays emitted from chemical elements is proportional to the square of the atomic number (the term "Z – σ" equals the actual atomic number, σ is a screening constant). This is historical important since until Moseley´s work the atomic number was only an element´s place in the periodic table of the elements and not known to be associated by physical measurements. Following equation shows Moseley´s law and consequential the proportional of reciprocal root of wavelength to atomic number, whereby *R* is Rydberg constant and *n* is main quantum number:

$$hf = Rhc(Z-\sigma)^2\left(\frac{1}{n_1^2}-\frac{1}{n_2^2}\right) \Rightarrow \sqrt{\frac{1}{\lambda}} = c_1(Z-c_2) \Rightarrow \sqrt{\frac{1}{\lambda}} \propto Z \qquad (24)$$

Figure 15 shows the approximate linear relationship between the reciprocal root of wavelength and atomic number. Deviation from linearity applies only at high atomic numbers. [6 p. 6], [4]

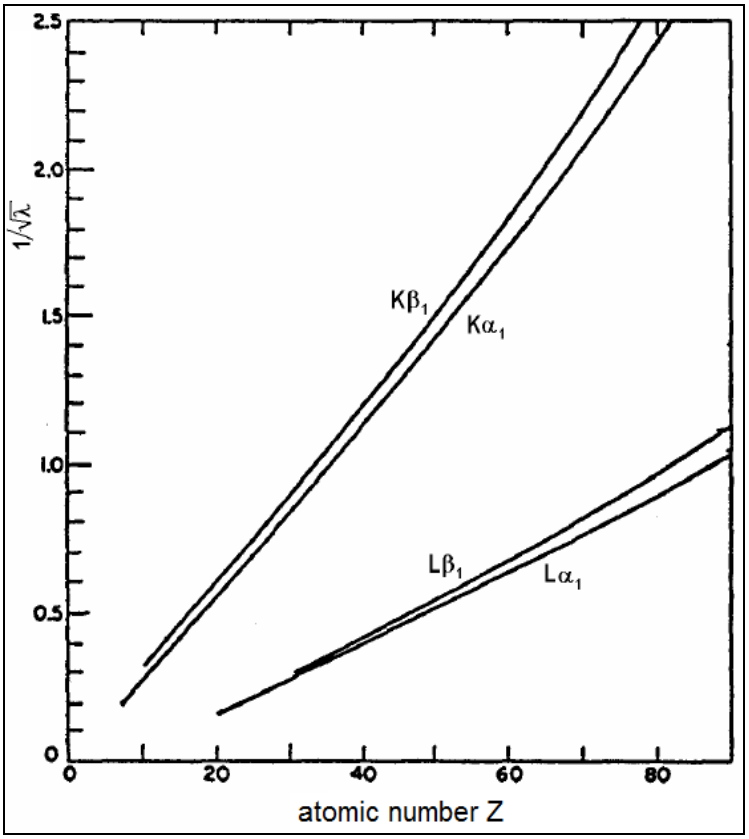

Figure 15 Relationship of wavelength and atomic number [2 p. 11]

2.6.5 Intensities

XRF spectroscopy has very less intensive characteristic lines that can be used for qualitative analysis. This is due to following reasons:

- For analytic (quantitative and/or qualitative) only a very few electron transitions can be used, mainly the strong K and L-lines (compare Figure 14).
- Within one level relative intensities drop rapidly resulting in only one or two intensive lines, strong enough for the purpose of detection. Remaining rarely consists of intensities greater than five per cent of the most intensive line in the level.
- Due to measurement conditions, it is often impossible detecting K as well as L-levels.

In general, following rules give a good overview for intensities at different lines (compare Figure 14):

- K-level: most intensive lines are Kα1/3 and Kβ1/3
- K-level intensities: Kα1 : Kα2: Kβ1 ≈ 100 : 50 : 10
- L-level: Lα1, Lβ1 respectively Lβ2 and Lγ1-lines are most intensive ones
- L-level: Lα1 : Lβ1 : Lβ2 : Lγ1 ≈ 100 : 60 : 30 : 10 [2 p. 12]

2.6.6 Detectors

For detection of secondary X-ray fluorescence radiation two main principles are used, energy dispersive analysis and wavelength dispersive analysis. In energy dispersive spectrometer (EDS or EDX) X-ray fluorescence radiation emitted by the excited material is directed into a solid-state detector. Detectors are based on silicon semiconductors in the form of lithium-drifted crystals or high purity silicon wafers. This produces constantly pulses, whereby the voltage is proportional to the incoming photon energies. Then, this signal is processed by a multichannel analyzer (MCA) that produces a digital spectrum used for quantitative and qualitative analysis (see Figure 16). In contrary, wavelength dispersive spectrometer (WDS or WDX) uses diffraction grating monochromator (usually a single crystal) for the separation of incoming photons before analysis (compare Figure 17). Different wavelength can be detected by varying the angle (incidence and take-off). Wavelength and angle are related by the Bragg Equation (whereby n is the integer and d is the spacing between the planes in the atomic lattice):

$$n\lambda = 2d\sin(\Theta) \tag{25}$$

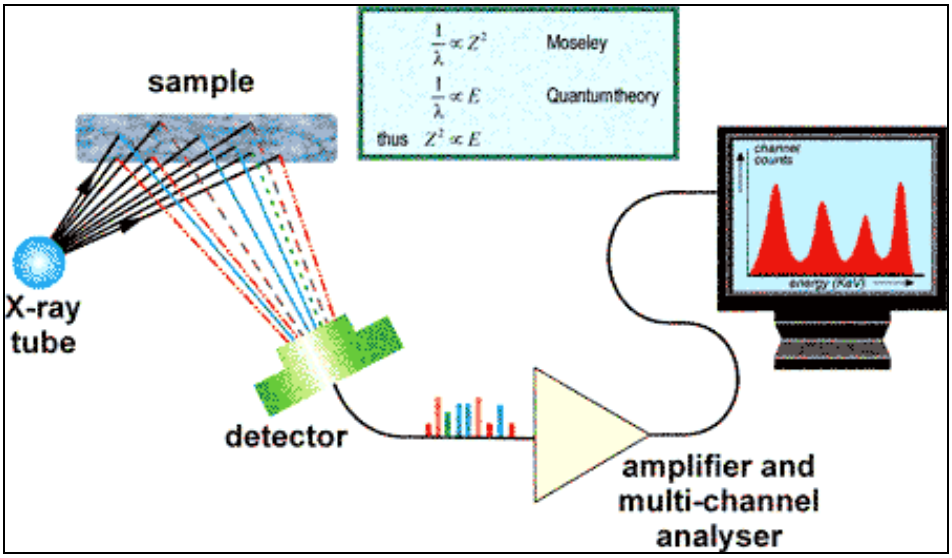

Figure 16 Function of energy dispersive spectrometer [18]

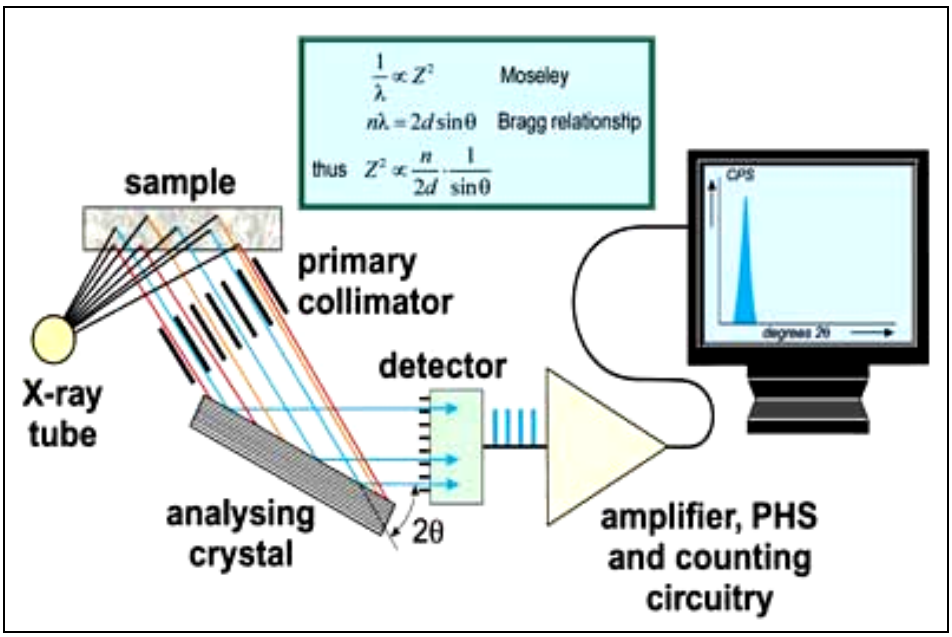

Figure 17 Function of wavelength dispersive spectrometer [18]

In REDWAVE XRF and in the application of resource recycling using X-ray fluorescence in general, the use WDS for detection is for several reasons not possible. Hence, the main focus of this chapter is given on EDS.

Energy dispersive spectrometers have all the same detection principle. A captured photon (secondary X-ray fluorescence radiation) ionizes a certain number of detector atoms. When an X-ray photon passes through the crystal it causes a swarm of electron-hole pairs to form, which then causes a voltage pulse. The amount of charge produced is proportional to the energy of the incoming photon. The cause of one electron-hole pair requires the energy of

3.6 eV. One X-ray quantum with the energy of 30 kV creates approximately $1.4*10^4$ electron-hole pairs. The created charge is analyzes and the process repeats itself for further incoming photons. By measuring the charge, the spectrum can be built by dividing the energy spectrum into discrete bins and counting the number of pulses registered within each energy bin. As a matter of fact, detector speed is critical because all charge carriers measured have to come from the same photon. Otherwise, the photon energy would not be measured correctly. EDS detector types nowadays in commercial use vary in resolution, speed and the way of cooling. Ordered by resolution following EDS detector types are available:

- Proportional counter- resolution of several hundred eV
- PIN diode detector
- Si(Li) detector
- Ge(Li) detector (no longer used in recent years)
- Silicon drift detector- high end of performance scale

Proportional counter have been used for almost 100 years and are still in use since they are cheap and easy to operate but have compared to further mentioned detectors a low density. This results in a low efficiency for X-ray detection. Much higher detection efficiency for high energy photons provide scintillation detectors. State of the art scintillation detectors use for detection of fluorescence light different scintillating material. The scintillated material is coupled either to photo multipliers, photodiodes or CCDs (charge-couple device). Scintillating detectors offer high efficiency but the disadvantage is their poor energy resolution. In the 1960s first detectors using ionization chambers with a high-density material were produced. These Ge(Li) or Si(Li) detector were possible, since high-purity germanium and silicon became available and offered a much higher resolution than gas detectors and scintillators. A schematic design of the main parts of a Si(Li) detector is visible in Figure 18. The mean energy needed for creating electron-hole pairs is about 20-30 eV for gases while only a few eV for semiconductors. The main disadvantage of last mentioned detector is the need of liquid nitrogen cooling. The reason for the cooling is the high leakage current at room temperature and the rather high read-out capacitance. The high capacitance then results in a high contribution of the noise part, which requires long shaping times. For long shaping time though, the noise contribution from the leakage current increases. Hence, Ge(Li) and Si(Li) are not of use for high-resolution applications.

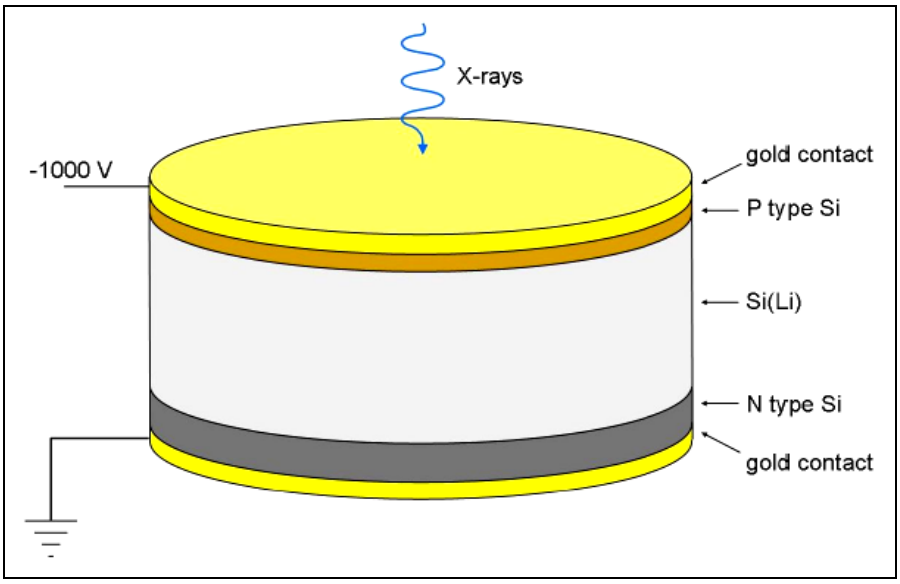

Figure 18 Schematic design of the main part for a Si(Li)-detector [19 p. 5]

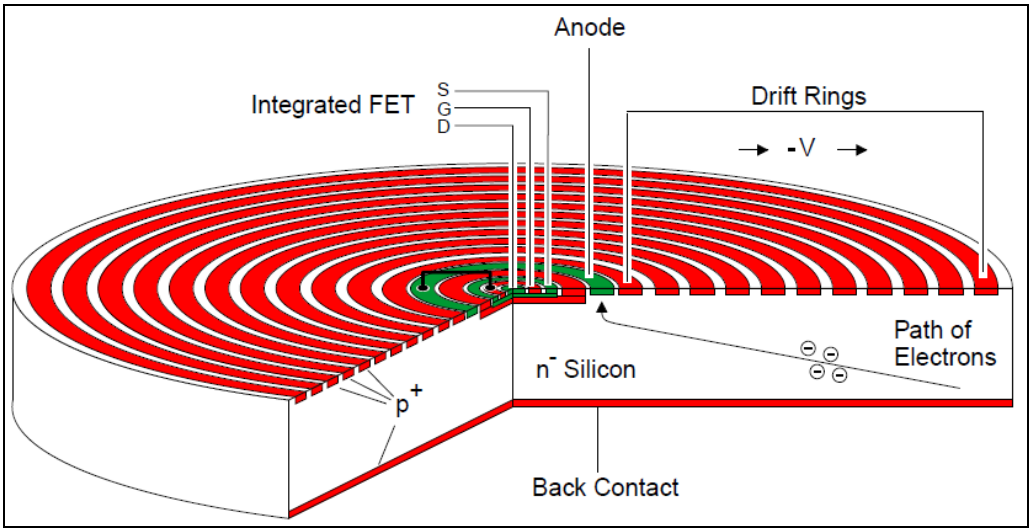

Figure 19 Schematic design of a SDD [6 p. 14]

In SDD (compare Figure 19) however, the charge drifts from a large area into a smaller read-out node with low capacitance. Hence, noise decreases and shorter shaping times can be achieved. This results in two advantages, faster counting is enabled and at the same time, higher leakage current can be accepted. This, its turn drastically reduces the need for cooling. The process of photon capture and charge allocation of a SDD can be seen in Figure 20. The thin solid line in this figure represents the barrier between both depletion layers. Three photon quantums strike the detector at the same time at different spots. This causes the creation of electron-hole pairs that are separated due to the electric field. Positive charged holes (red dots) move towards electrode and electrons (blue dots) towards anode. This produces pulses, whereby the voltage is proportional to the incoming photon energies.

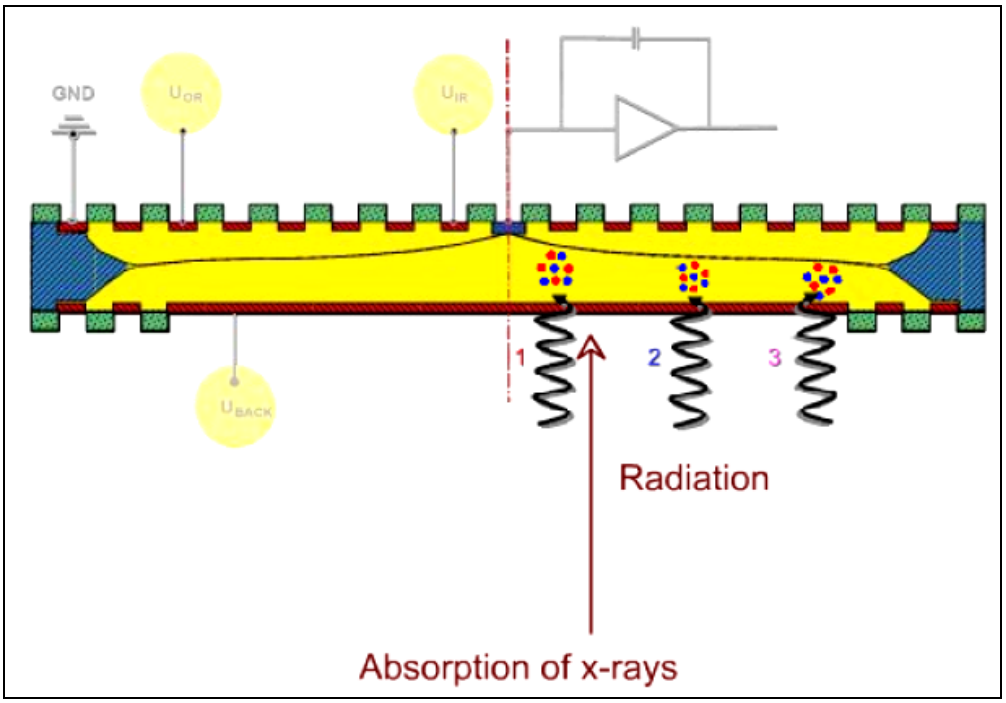

Figure 20 Photon capture and charge allocation in a SDD [19 p. 6]

[1 p. 199-203] [2 p. 14-22] [6 p. 14-20] [19 p. 4-6]

3 REDWAVE XRF- X-ray Fluorescence Sorting Machine

This Chapter deals with the sorting machine REDWAVE XRF, developed by BT-Wolfgang Binder in collaboration with Innov-X Systems. At the beginning of this Chapter the assembly and function of a sensor-based sorting system are described by following the material stream from vibratory feeder via detection unit towards the point of ejection. This explanation follows a detailed description of the detection unit. Furthermore, the function of detection including standardization, calibration and operation sequence of measurement is mentioned. Chapter 3 concludes with various factors of influence about detection and separation.

3.1 Assembly of REDWAVE XRF

REDWAVE XRF is a sensor-based sorting system working with X-ray fluorescence. As every sensor-based sorting system REDWAVE XRF consists in general of four main assemblies, vibratory feeder and conveyer belt, detection system, control and evaluation unit and ejection unit. Figure 21 shows a cross section of a schematic drawing of REDWAVE XRF including following units:

1 Vibratory Feeder
2 Conveyer Belt
3 Detectors
4 X-rays
5 Control Cabinet
6 Control Unit
7 Cooling Unit
8 Ejection Unit with Valves
9 Pressurized Air Service Unit
10 Ejection Chute
11 Throughout Chute
12 Signal Lamp
13 Air Box

Sorting material is constantly fed with a certain throughput over the entire sorting width of a conveyer belt by a vibratory feeder. The conveyer belt conveys the material its turn with a certain speed towards detection area, where it is excited by X-rays. Detectors capture secondary X-ray radiation emitted by the material. A signal is constantly evaluated by the control and evaluation unit and if it meets the set ejection criteria a further signal is sent to the ejection unit. High speed valves and air jets operated by compressed air then reject those materials.

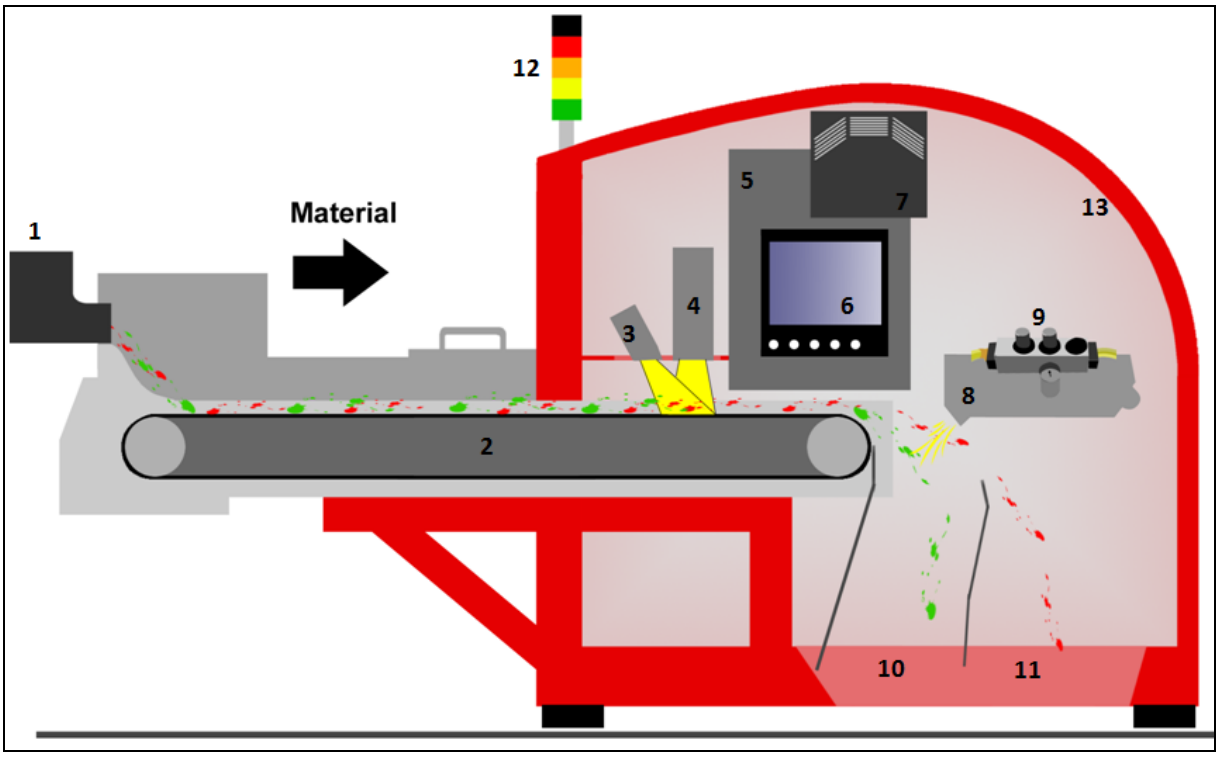

Figure 21 schematic drawing REDWAVE XRF

3.1.1 Vibratory Feeder

The in-feed material to be sorted is transferred with a vibratory feeder towards a conveyer belt. The main purpose of the vibratory feeder is the separation of the material in order to avoid groups or composites and to homogenize the layer. Ideally all samples are thin layered on the conveyer belt. The vibratory feeder has to meet a certain throughput but also separate the material for ensuring a reliable detection.

3.1.2 Conveyer Belt

By using a certain frequency of the vibratory feeder and speed of the conveyer belt, the material samples were accelerated, separated and transferred towards detection area. Frequency and speed of vibratory feeder and conveyer belt are always correlated to each other. To guarantee optimal sorting, it is necessary to ensure small gaps between samples. This separation is done by a difference in speed of vibratory feeder and conveyer belt. An increased speed of the conveyer belt relative to the feeder lengthens this gap and leads to a higher throughput. Furthermore, it is essential to ensure no speed difference of material and conveyer after passing the detection area which requires a certain conveyer length. A difference in speed while or after passing the detection area would cause a miss-shot of detected material since the delay time is then incorrect.

3.1.3 Detection Unit

The detection is as above mentioned based on X-ray fluorescence and consists of two main parts, X-ray source and detector. As X-ray source is the X-ray tube Varian VF-50J used in REDWAVE XRF (see Appendix IV for technical description). The X-ray tube generates the primary X-ray radiation that excites the material, which then emits secondary X-rays. This secondary radiation is captured by Si-PIN detectors, Amptek XR-100CR (see Appendix V for technical description). A further and detailed description about procedural method of detection process is given in Chapter 3.3.5 and basic information can be looked-up in Chapter 2. The cooling unit generates a constant temperature within the detection unit.

3.1.4 Control and Evaluation Unit

The detector signal is constantly evaluated and compared with a set threshold. If there is conformity of this information with a pre-set ejection category, a temporary delay signal is sent to the ejection unit. The delay time between detection and ejection can either be estimated by time distance or calculated internal by using a rotary encoder connected to the conveyer belt. All electrical devices are arranged in the control cabinet. The machine is operated and set at the operating unit via touch screen. Various settings e.g. recipes, acquisition parameter, thresholds, general settings etc. can be changed at this unit.

The signal lamp show the current machine status. Several illuminating or flashing colors (green, yellow, orange, red) indicate different status.

3.1.5 Ejection Unit

In the ejection unit the nozzle manifolds and valves are located. Compressed air out of valves separates the ejection material from the passing material by a systematic blow. The ejection of each detecting line (respectively detector) is driven by one valve with its correlated four nozzles. These nozzles are arranged above the material stream. Each nozzle has an exit window of 2 mm (0.079 in) (compare Figure 22).

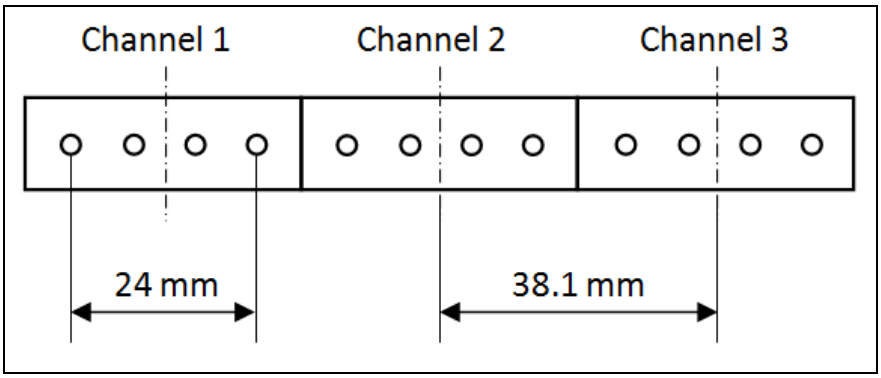

Figure 22 Design of Ejection Unit

Additionally, pressure measuring equipment monitors the actual pressure. For how long each valve respectively which valve is activated is given by the length of the measured signal and the detector number. The ejected material is due to the air blast diverted into the ejection chute and to another conveyer, whereby the remaining material follows its trajectory parabola into the passing chute and again to conveying equipment.

The air service unit cleans by filter cartridge the compressed air, regulates the pressure and services with automatic valves the system with compressed air during operation.

3.2 System Structure

The REDWAVE XRF system is divided into several levels, which communicating with a PLC-control. Table 3 shows all different levels including its subsystem.

Table 3 REDWAVE XRF System Structure

System Levels	Subsystems	Remarks
Detection Unit	• High voltage power supply • Detectors • X-ray tubes	This unit is for signal acquisition
Electronic Unit	• DCM (Detector Channel Module) • LPM (Local Processor Module) • PLC (Programmable Logic Controller)	Electronic components are processing the signals given by the detectors
Control Panel **UI (User Interface)**	• Data management system • Control of all electric components and X-ray system • UI (User Interface)	
PLC (Programmable Logic Controller) & low-voltage system	• Safety control • Drive control • Valve control • Connection to main plant	
Vibratory Feeder		Distributes and separates the in-feed material onto the conveyer belt
Conveyer	• Speed encoder for speed control (controlled by frequency converter)	Conveyer belt accelerates and transports the in-feed material towards detection area and discharge
Discharge System	• Valves	Ejects identified material

3.3 Assembly and technical description of Detection Unit

3.3.1 Basic Design

The optical stage as shown in Figure 23 houses all optical components of the system. The subassembly of the detection unit (compare Figure 27) includes, depending on the machine type and size, a various number of high-voltage power supplies, X-ray tubes and detectors. Furthermore, a special Kapton window at the bottom of the detection unit is implemented for protection against contamination. Kapton is used due to its high radiation transmission properties. Detachable maintenance openings secured with safety switches are provided at the top and rear side. The distance between Kapton window and conveyer belt is adjustable and influenced by the grain size of the material to be sorted. A photograph of a commercially used REDWAVE-system shows Figure 24.

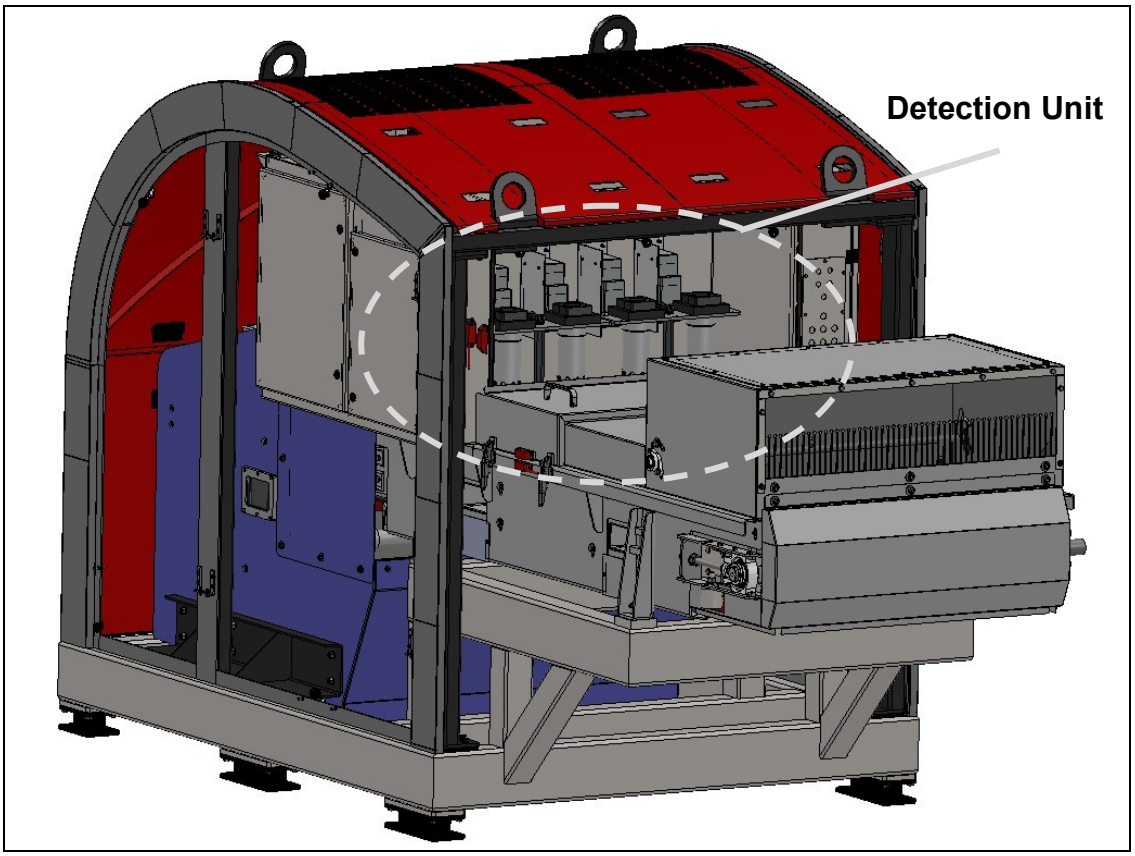

Figure 23 REDWAVE XRF housing

Figure 24 Commercial used REDWAVE XRF-system (without vibratory feeder)

X-ray tubes are adjusted perpendicular to the axis of the conveyer belt. The detectors axis is, however, positioned at a certain angle relative to the axis of the X-ray tube. The vertical centre line of X-ray tube and detector enclose an angle of approximately 25° in sorting direction. Hence, the extended axis of both X-ray tube and detector meets somewhere close to the top of the conveyer belt, but the exactly meeting point is certainly dependent on the variable gap between conveyer belt and detection unit (compare Figure 25.

Immediately underneath the conveyer belt and below X-ray tubes and detectors a special **alloy-plate** with known composition is installed. This is since the elemental composition of all parts below detection unit has to be known. X-ray radiation penetrates matter up to a certain extent and causes the emission of secondary X-ray fluorescence radiation of elements in this matter (alloy-plate) which then are certainly detected as well. Furthermore, the alloy more precisely the molybdenum in the alloy is used for standardization.

A detailed description about the standardization process is given in Chapter 3.4.1.

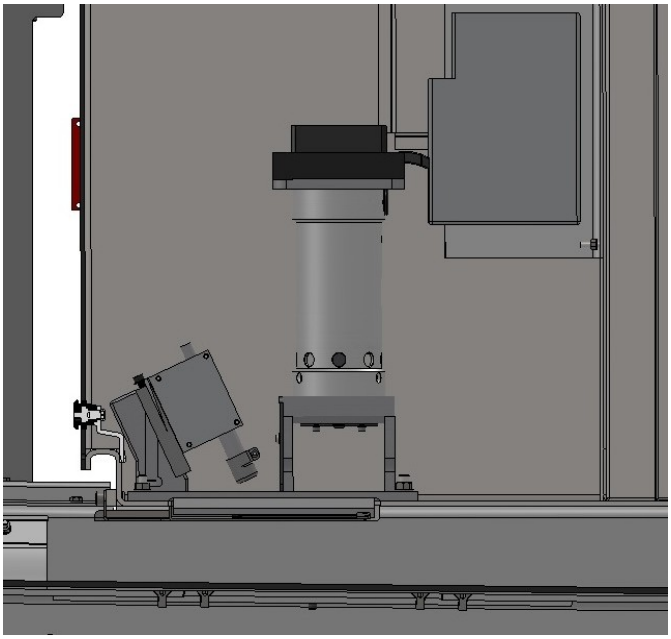

Figure 25 Section of detection area

3.3.2 Fundamental Information to Detection Area

All detection tests were done by using a square plate of pure zirconium with a size of 1 cm² (0.16 in²). The plate was moved 5 mm (0.19 in) in longitudinal respectively cross direction (length and width) for every measurement. By noting the count rate of each measurement point, the detection area could thus be estimated. The count rate for an element is the amount of detected counts per time period within the energy range for the particular element. Following further assumption were done:

Gap_Max is the highest possible gap between conveyer belt and detection unit with the distance of 65 mm (2.56 in) at beginning of detection unit. Furthermore, **Gap_Min** is the lowest adjustable gap between conveyer belt and detection unit with a distances of 43 mm (1.69 in). Hence, the difference of Gap_Min and Gap_Max amounts 22 mm (0.87 in) at the detection unit. Figure 26-left image shows an overview of the applied procedure. The right image indicates the used Zr-plate.

Specifications of Gap_Max:

- Distance: 65 mm (2.56 in)
- Distance in sorting direction: 220 mm (8.66 in)
- Tube voltage: 50 kV
- Tube current: 1000 µA
- Calibration time: 30 s
- Material: Zr, 1 cm² (0.16 in²)

Specifications of Gap_Min:

- Distance: 43 mm (1.69 in)

- Distance in sorting direction: 220 mm (8.66 in)
- Tube voltage: 50 kV
- Tube current: 1000 µA
- Calibration time: 30 s
- Material: Zr, 1 cm² (0.16 in²)

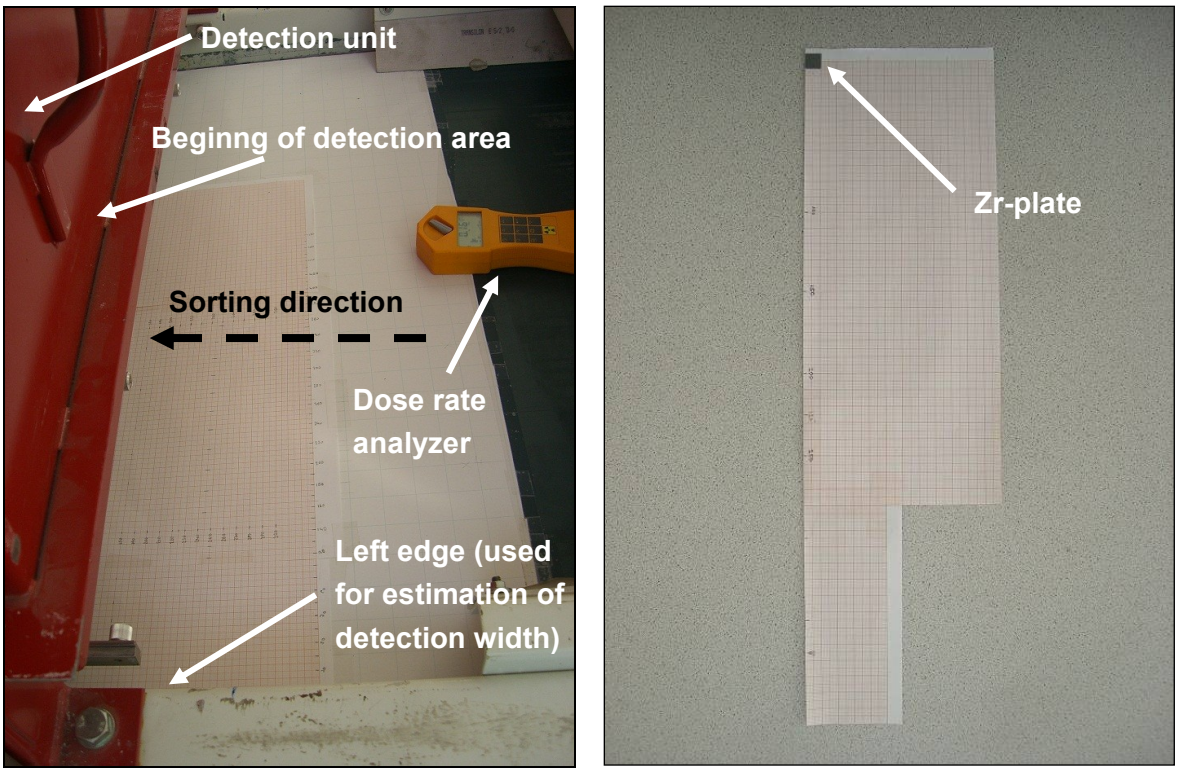

Figure 26 Procedure of detection area estimation

The estimation of irradiated area per X-ray tube was done with a 10 mm (2.54 in) Zr-stripe covering the whole detection width at the point of maximum count rate evaluated with area of detection tests.

Specifications of tube test:

- Gap setting: Gap_Min
- Distance in sorting direction: 220 mm (8.66 in)
- Tube voltage: 50 kV
- Tube current: 1000 µA
- Calibration time: 30 s
- Material: Zr, 1 cm (0.39 in) x conveyer belt width

3.3.3 X-ray source

As X-ray source the system uses Varian VF-50J X-ray tube with following main specifications (further description and Data Sheet see Appendix IV):

- Manufacture: Varian
- Tube type: VF-50J

- Power: 50 W
- Anode material: tungsten
- Maximum anode potential: 50 kV (current 1 mA)
- Envelope: ceramic
- Exit window: beryllium, 0.076 mm
- Focal spot: 1 mm x 1 mm square

Depending on the machine width, a different number of X-ray tubes is implemented. For a sorting width of 915 mm (36 in), for instance, four X-ray tubes and for a sorting width of 1372 mm (54 in) six X-ray tubes were needed. An illustration of a detection unit having a sorting width of 915 mm shows Figure 27. The irradiation test below was done with a system having a sorting width of 762 mm (30 in), three X-ray tubes and 20 detectors.

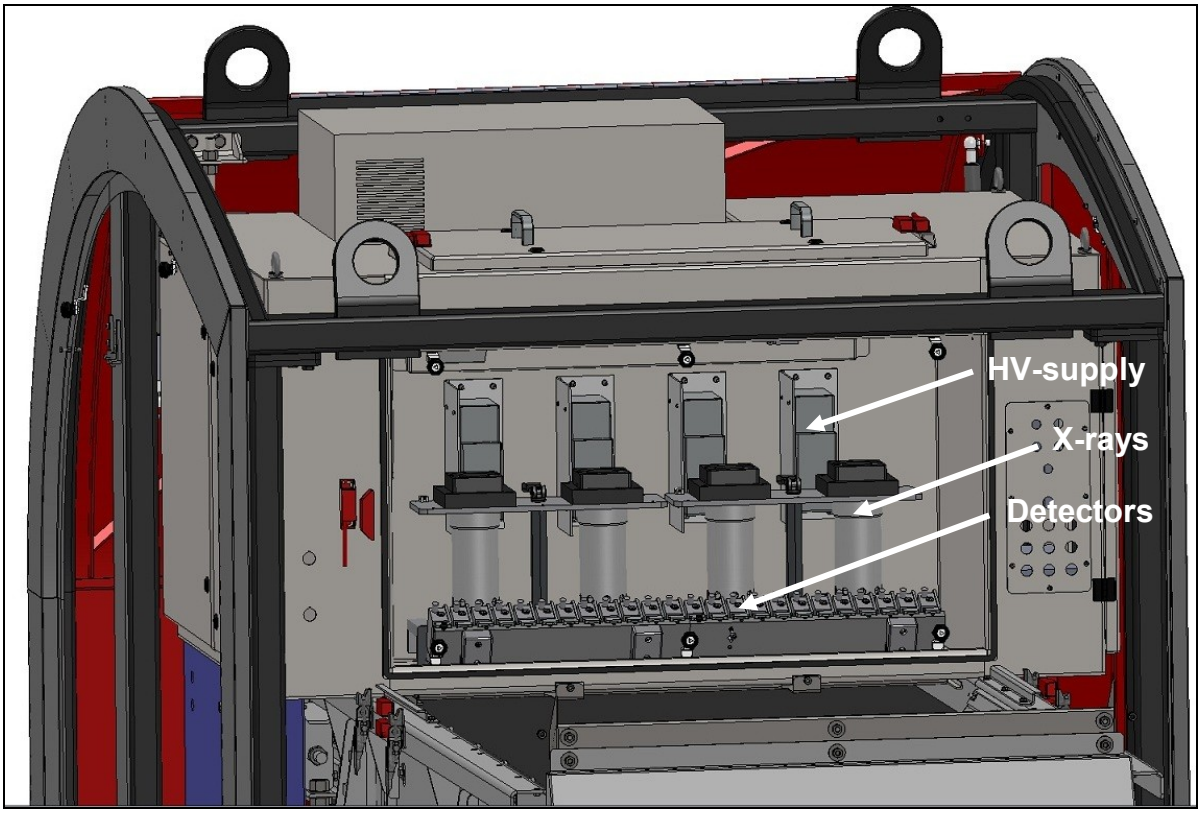

Figure 27 Detection unit of REDWAVE XRF

The irradiated area of each X-ray tube is limited by geometry and dependent on the gap between Kapton window and conveyer belt. For minimum gap the width approximately amounts 340 mm (compare Figure 28), which leads to an overlap of around 75 mm. Also obvious in the figure is a significantly lower count rate (OCR) immediately underneath the tube axis and a strong increase towards outer areas (see Appendix VII Table 18 for data). This is due to a too high current (compare Chapter 3.3.4and 3.4.6.2).

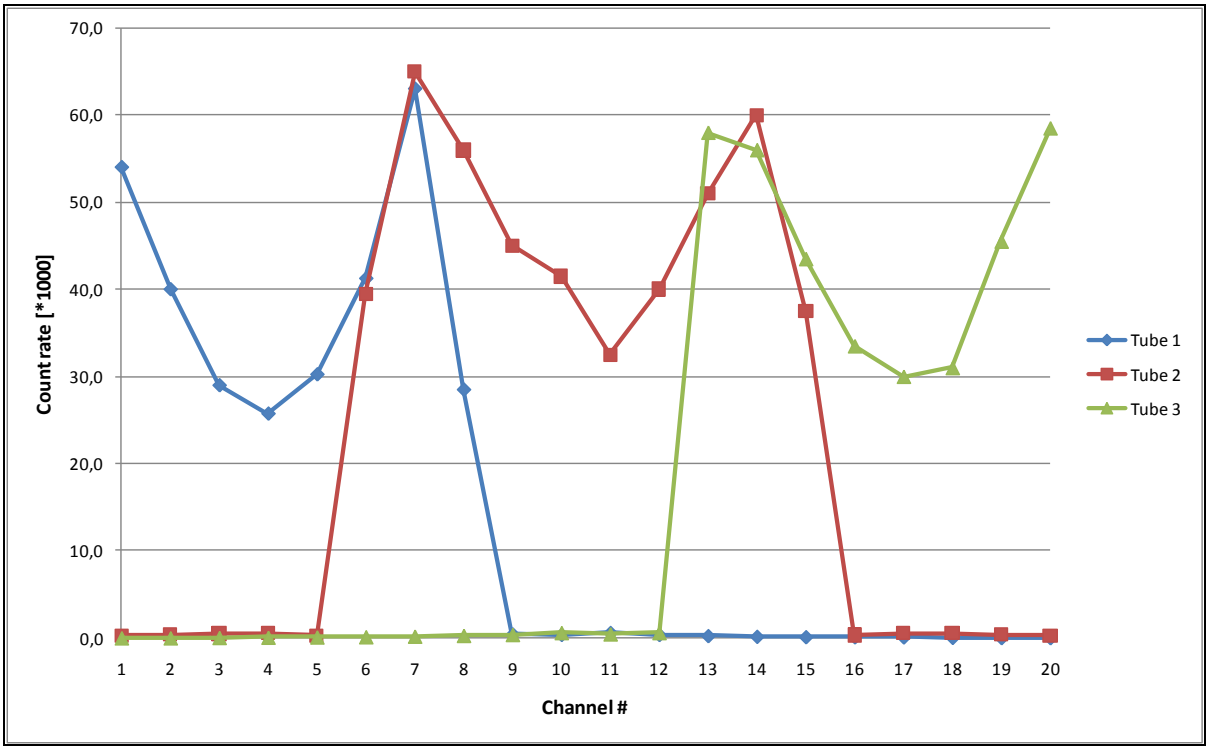

Figure 28 Irradiation width of an X-ray tube (minimum gap)

Depending on the material to be sorted, more precisely the elements in the material to be identified for ejection, various filters can be attached in-between X-ray tube exit window and detection area. An already used material is aluminum. Aluminum filter minimizes unnecessary and unwanted low energy regions in the spectra.

The maximum possible energy emission of the tube is 50 keV. In general, energy between 30-50 keV is used, depending on the elements to be detected respectively the material composition (compare 3.4.6.1). The minimal possible wavelength λ_0 for 50 keV is by estimation with equation (5) 0.0248 nm. Below this value no bremsstrahlung is possible. The spectrum of bremsstrahlung is continuous (wavelength > 0.0248 nm) since electrons were scattered at different extents. For 30 keV the minimal wavelength amounts 0.0413 nm (also compare (1)). The electromagnetic spectrum for wavelength of 10^{-6} nm for γ-rays to 100 Mm for radio waves is given in Figure 1.

3.3.4 Detector

In REDWAVE XRF a channel is specified as one detector and its associated DCM. The decision divert or not-divert is created in the DCM and passed onto the LPM for action. DCM´s are slotted on subracks, which contain up to 12 DCM in a row and furthermore one LPM. One LPM includes an ethernet switch, a fan rack and a power distribution. Every DCM and its corresponding detector can handle one “virtual lane” and are described as one channel.

The number of used detectors (Si-PIN Amptek XR-100CR) is dependent on the sorting width. The distance between each channel respectively detector amounts 38.1 mm (1.5 in). Hence,

above mentioned sorting width of 762 mm (30 in) with three X-ray tubes requires 20 detectors. Main specifications for the used detector type are (see Appendix V for further description):

- Manufacture Amptek
- Detector Type: Si-PIN XR-100CR
- Detector Power: < 1 W
- Detector Size: 25 mm² (0.0387 in²)
- Silicon Thickness: 500 µm
- Exit Window: beryllium, 100 µm (4.0 mil)
- Peaking Time: adjustable 3-5 µs
- Background Counts: < 3 x 10^{-3}/s
- Temperature in Detector: -55 °C (-131 °F)

The difference in radiation of X-ray tubes results in an unequal detected count rate, whereby detectors immediately underneath the axis of X-ray tubes are always weaker than surroundings (compare detector 4 and 11 in Figure 29 for Gap_Min). This causes a maximum deviation of 33 % between detector 4 and 7. In Appendix VII Table 16 all data for Figure 29 are given. Having a larger gap (Gap_Max) gives similar results but a lower maximum deviation of only 25 % between weakest and strongest detector and certainly a weaker count rate at all.

All data for Gap_Max are given in Appendix VII Table 17. A larger gap between conveyer belt and detection unit is always a compromise between needed distance due to material size and expected count rate.

The weakness is due to a longer dead time fraction for detectors immediately underneath the axis of X-ray tubes. As explained in Chapter 3.4.6.2 the input count rate is linear correlated to the intensity of the spectra. An increase of the tubes current also leads to an increase of the incoming count rate but at a certain point the dead time rises at a higher extent relative to the input count rate. Hence, even though the input count rate gets higher the output count rate (on the y-axis- measured to make the figures) is lower at contiguous Channels. As a result it can be said, the current for this calibration was set too high.

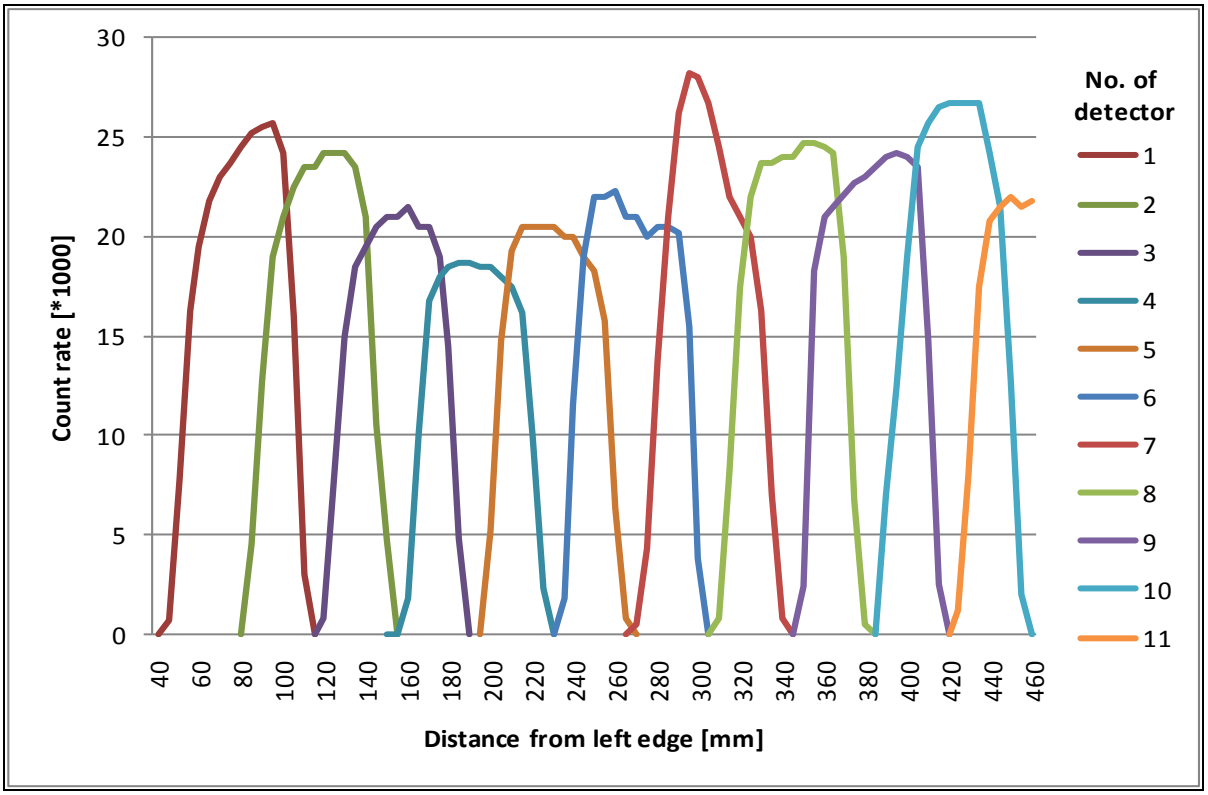

Figure 29 Detector count rate over sorting width (Gap_Min) as a result of different positions of the sample material

3.3.5 Area of Detection

Following two assumptions were done: A value of 10 % of maximum value is assumed to be a value high enough to have detection at all, whereby a value of 50 % of the maximum value is assumed to be a value high enough to have reliable and adequate detection. The area of detection is dependent on the gap between conveyer belt and detection unit (Gap_Min and Gap_Max). For Gap_Min the detection length amounts 50 mm (1.97 in) for 50 % value and 65 mm (2.56 in) for 10 % value. The detection length for Gap_Max is certainly longer and amounts 62.5 mm (2.46 in) for 50 % value and 75 mm (2.95 in) for 10 % value (compare Table 4 and Figure 30 and see Appendix VII Table 19 for data).

Table 4 Area of detection- length

10 % value	Detector	min [mm]	max [mm]	detection lenght [mm]	
Gap_Min	4	205	270	65	65
	7	210	275	65	
Gap_Max	4	200	275	75	75
	7	200	275	75	
50 % value	Detector	min [mm]	max [mm]	detection length [mm]	
Gap_Min	4	210	260	50	50
	7	215	265	50	
Gap_Max	4	205	265	60	62,5
	7	205	270	65	

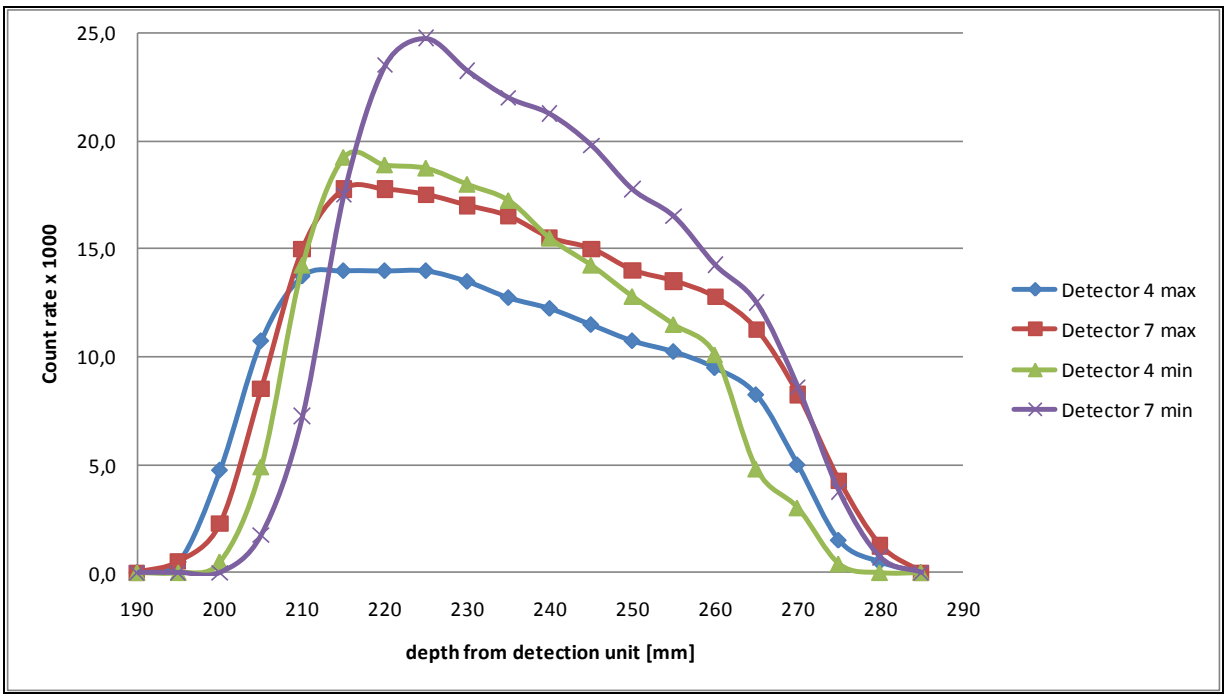

Figure 30 Area of detection- length

The estimation of detection width ensures a similar result. With a minimum gap (Gap_Min) the detection width amounts for 50 % value 53 mm (2.08 in) and 62 mm (2.44 in) for 10 % value. By having Gap_Max the detection width increases to 57 mm (2.24 in) for 50 % value and 73 mm (2.87 in) for 10 % value. Both data are given in Table 5 and were estimated by an average of each case of three different detectors (compare and see Appendix VII, Table 16 and Table 17 for data). The detection widths of all detectors for Gap_Min and one subrack are visible in Figure 29. As can be seen all detectors have approximately the same sorting width.

Table 5 Area of detection- width

10 % value	Detector	min [mm]	max [mm]	detection width [mm]	
Gap_Min	4	165	225	60	62
	7	275	335	60	
	9	350	415	65	
Gap_Max	4	155	235	80	73
	7	275	345	70	
	9	345	415	70	
50 % value	Detector	min [mm]	max [mm]	detection width [mm]	
Gap_Min	4	165	220	55	53
	7	280	330	50	
	9	355	410	55	
Gap_Max	4	165	225	60	57
	7	275	325	50	
	9	355	415	60	

A 3-dimensional display of the area of detection using Detector 4 and Gap_Max is shown in Figure 31. The count rate in sorting direction increases rapidly towards peak value, drops constantly with less rate and finally falls to zero. Additionally, there is a symmetric rise and stagnation of the count rate at detection width. All areas with none count rate are points not measured. Due to geometry and physically reason it can be assumed that the detection area is similar to a rectangle with dimensions of measured length times measured width. Hence, the detection are amounts approximately 3425 mm² (5.31 in²) for 50 % value and Gap_Max. Further results see Table 6.

Table 6 Detection area

	Detector	width 10 % value [mm]	length 10 % value [mm]	Detection area [mm²]	width 50 % value [mm]	length 50 % value [mm]	Detection area [mm²]
Gap_Min	4	60	65	**3900**	55	50	**2750**
	7	60	65	**3900**	50	50	**2500**
Gap_Max	4	80	75	**6000**	60	60	**3600**
	7	70	75	**5250**	50	65	**3250**

Since radiation is directed, it can be assumed a further in- or decrease in the gap would result in a linear rise or fall of detection area. Differences in count rates between detectors at same gap result in significantly lower count rate immediately underneath the tube axis (see Chapter 3.3.3).

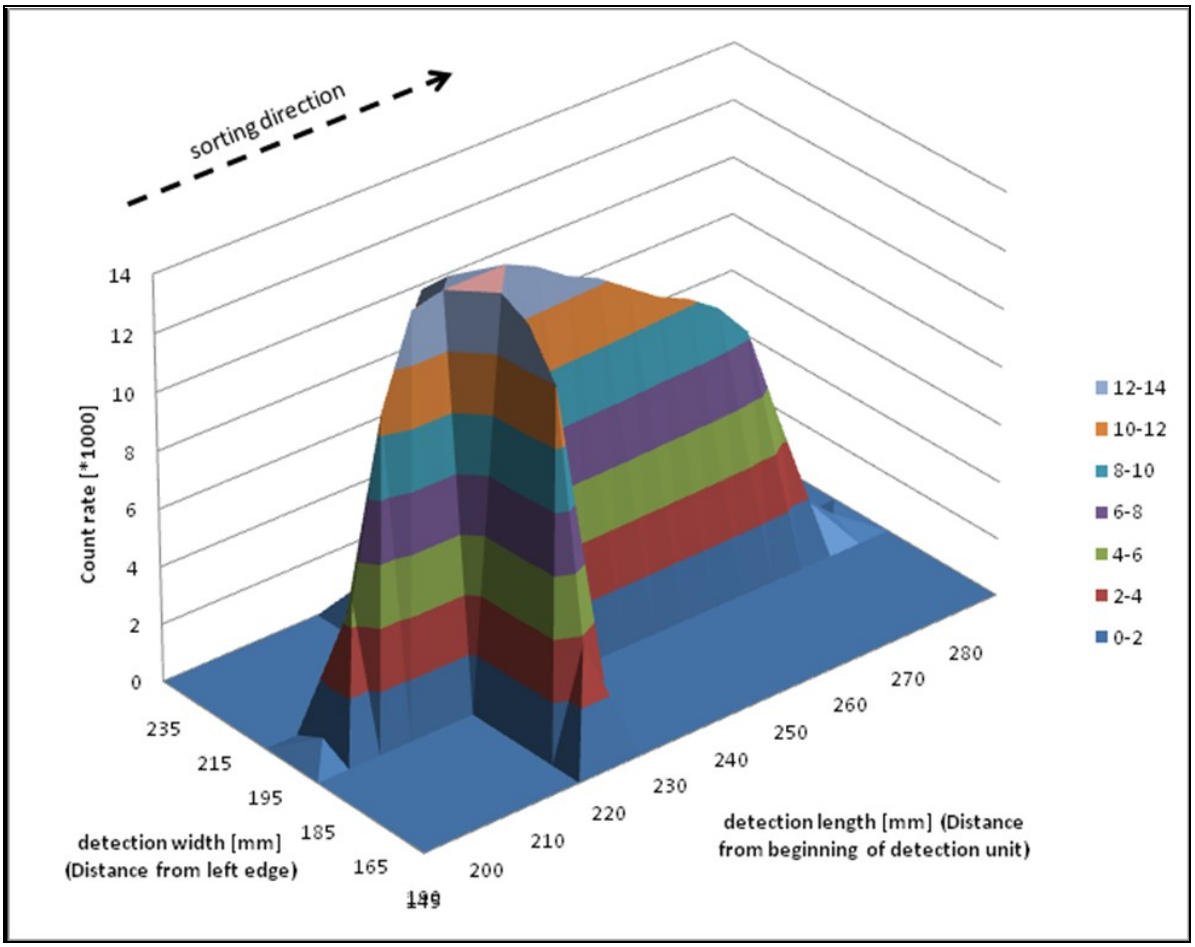

Figure 31 Area of detection 3d for detector 4

3.4 Function of Detection

3.4.1 Standardization

Before any measurement can take place a standardization of the system is required. This means the energy of principal lines has to be correlated to the internal Bin-number. This Bin-number relates the measured signals with its energies in 1000 units, whereby the system is able to detect signals within the energy range of 0 to 40 keV. Hence, 1000 units correlate to 40 keV. The standardization can be based on any element having strong principle lines. REDWAVE XRF uses the element molybdenum, more precisely its Kα1-peak with energy of 17.48 keV. Molybdenum is composited by the alloy assembled immediately underneath the conveyer belt below detection area. This alloy (Material Code: 2.4665) has a Mo-content of 8.97 %. Figure 32 shows the result of a standardization, also good to see is the Kα1 peak. The peaks energy of 17.48 keV is known and then related to a Bin-number of 435 by the software. By doing so, every energy value is correlated to its Bin-number. Hence, all principle lines of elements have its correlated Bin-number and thus can be attributed to its element. This allocation is done separately for each detector and is not exactly the same for each detector. A variation of 1-2 % is common. In Figure 32 despite two characteristic Mo-peaks

also a wide, flattened peak and furthermore some small bumps are visible. The flattened peak is a superposition of some detected elements in the background (alloy, conveyer belt, miscellaneous contaminations etc.), Compton scattering from the belt and the continuous spectrum generated by slowing down processes of electrons. This continuous spectrum is called bremsstrahlung and originates due to different extents of scattering (compare Chapter 2.3.2.3). Little bumps on the left hand side are Compton scattered background elements.

After done standardization the characteristic molybdenum line should be at a Bin-number of around 435. A deviation of ± 1-2 % is tolerable but higher deviations make adjustments necessary. Adjustments are done by an in- or decrease of the gain parameter. A rule of thumb for adjusting is an increase of the gain by two at Bin-numbers < 420 and an increase by one for Bin-numbers < 430 and vice versa.

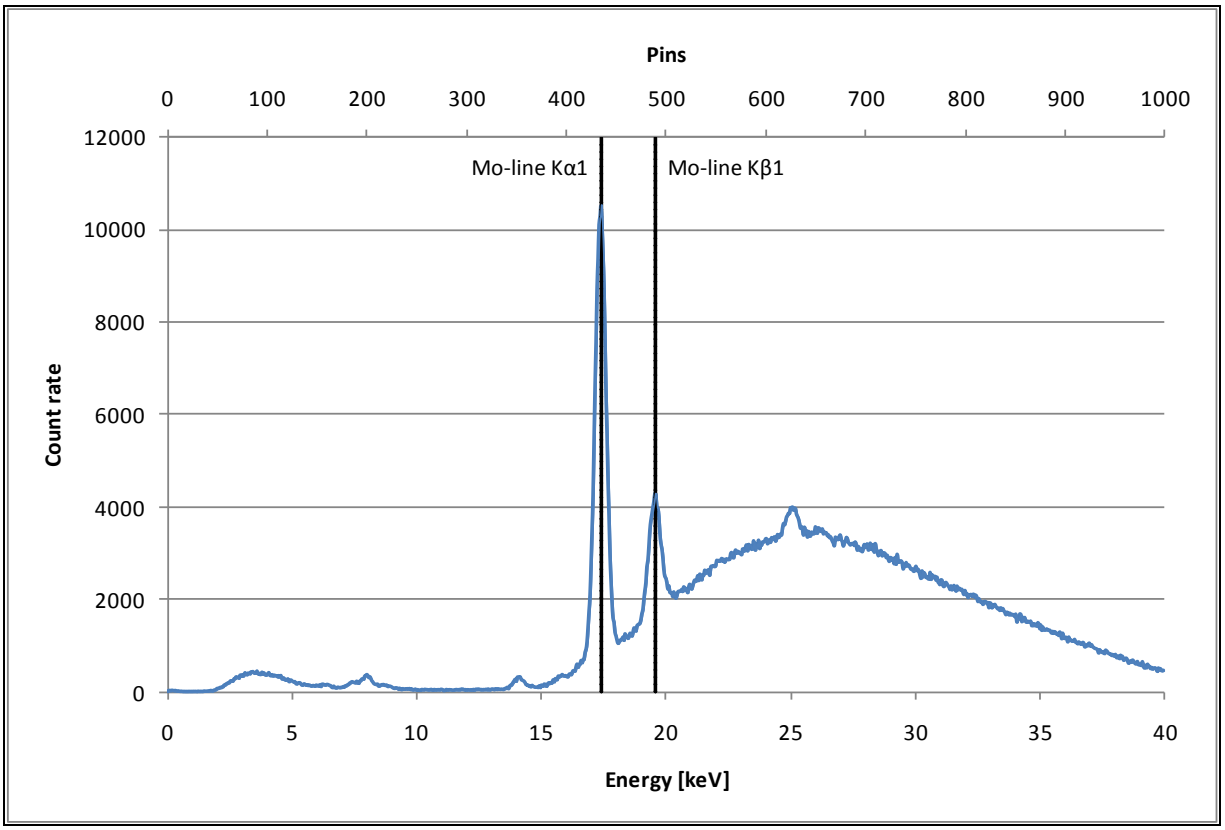

Figure 32 Spectra of standardization

3.4.2 Calibration

After standardization a calibration of all elements of desired detection is obligatory. This calibration is done by detection of principle lines of all elements desired for detection and consequently sorting. For calibration, pure element plates with a size of 1 cm² (0.156 in²) are used. These plates are fixed on a sheet enclosing a distance of 38.1 mm. For the calibration process this sheet is positioned underneath detection unit respectively detectors. This means each detector ensures its own element plate for calibration. Furthermore, a calibration of the

background using the empty belt is necessary. Depending on several factors such as calibration time, detector position, thickness and purity of element plates etc. the detected count rate varies. The detected count rate is the ratio of detected counts of one integration interval divided by the life time (compare Chapter 3.4.5 and Chapter 3.4.6.13). Figure 33 shows a calibration for various elements (energy range enhanced) used for the experiment described in Chapter 4.3. Each element possesses its visible peak with certain energy and correlated Bin-number.

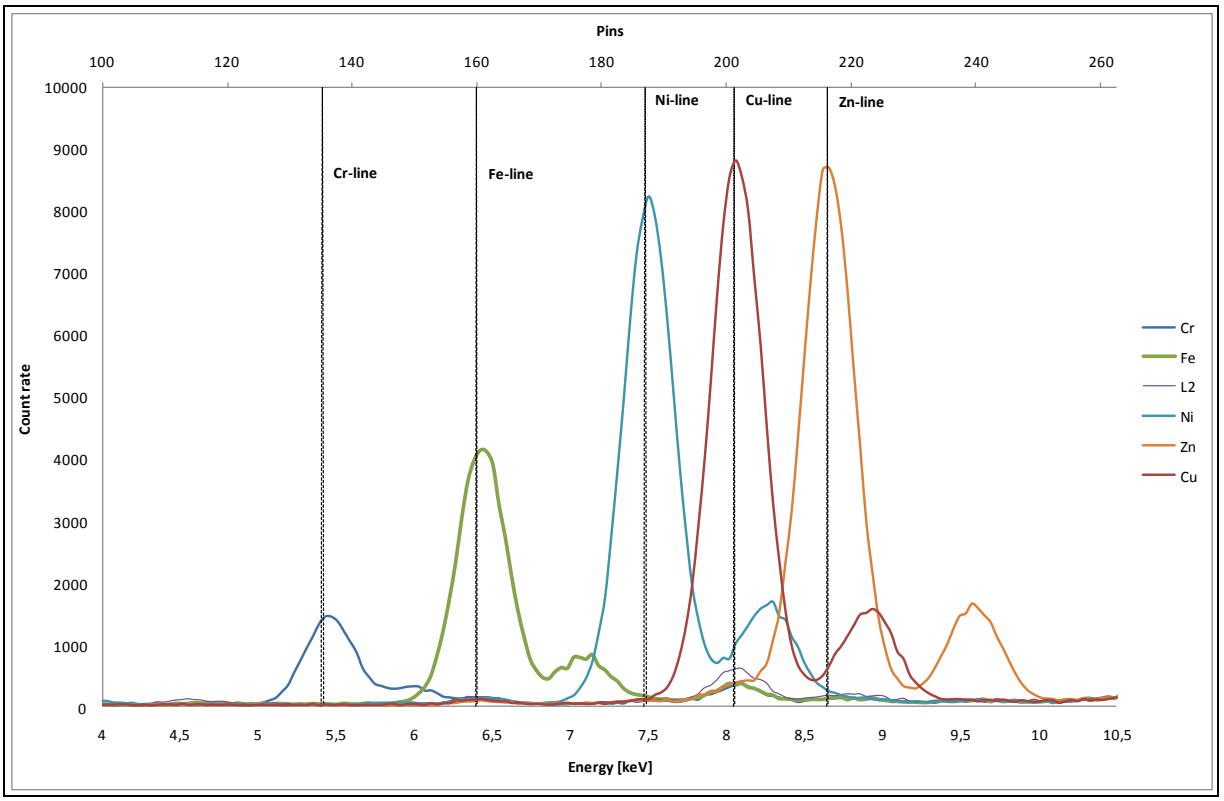

Figure 33 Spectra of a calibration- enhanced

3.4.3 Operation Sequence of Measurement

During operation detectors are continuously in operation, which means every detector captures steadily photons in the range of microseconds. The detection speed depends on the type of used detectors (Si-PIN, SDD etc.). The used Si-PIN XR-100CR has a peaking time of 3-5 µs. The actual operation and the task whether a detected signal meets a sorting criterion, is done by the software. By calibration each element data is “implemented” into the software database and allows the sorting of this element. More precisely, a detector only detects and relays. The relayed signal is internally processed and then compared with the data base calibration data and setup data. Has this value reached a specific and adjustable threshold this means it has met the sorting criterion. Hence, a signal is activated and sent towards ejection unit and the specific valve correlated to its detector. Since the distance between detection and valve is known, a delay time can be set and the detected sample can be ejected at the very right moment. The valve is open as long as the threshold is exceeded

respectively the detector captures a certain amount of photons with specific energy. Depending on material size, sorting parameter, desired quality etc. this time period can be extended for increased likelihood of ejection.

Following commentary gives a more detailed description about the question, how a sorting criterion can be set. First, the element has to be calibrated with calibration sheets using plates composited with the pure element. Secondly, this element has to be set up as sorting criterion, which means letting the software know that this element respectively material including this element has to be ejected. More precisely, the software needs to know where to look for the adjusted principle line with its energy characteristic for this element. During calibration each element is correlated to its characteristic peak with specific energy used for detection. These peaks are not only at different energies but also ensure various count rates and hence various peak heights (compare Figure 33). Finally, the threshold has to be set depending on the extent of background noise (counts) in the energy region as well as the expected content of the element in the material to be sorted. The threshold is an adjustable value based on the count rate or the counts of the calibration and needs to be set for each element to be detected. It is the minimum count rate a detected signal needs to be in order to be identified as signal to be ejected.

The threshold value is a comparison of detected counts during operation with detected counts from calibration. Hence, an in- or decrease of the threshold affects the sensitivity. Despite that, also the particle size and content of detectable elements influence the sensitivity. For instance, a small sample with high content of element x and a big sample with low content of the element x have altogether the same amount of element x. Hence, both samples cause the same amount of detected counts. A further and more detailed description about factors of influence is given in Chapter 3.4.6.7.

3.4.4 Description of detection

The detection is based on the photons captured by detectors. These photons are then gained and analyzed and calculated into a count rate (counts per time), which is then related to a calibrated count rate at the same energy. The energy resolution is expressed as full-width-at-half-maximum (FWHM) of the measured distribution (compare Figure 34). The larger FWHM, the more difficult will be the identification of peaks corresponding to photons of close energies.

The measured count rate is always the count rate for the whole area of detection of a detector (3600 mm² for Gap_Max and detector 4). Furthermore, it is an online measurement within split seconds (exactly time frame depends on the measurement time settings). The background, in this case the conveyer belt plus the material below detection unit, is known due to calibration. If then a material, containing one or more elements of detection, is below the detection unit, it gets excited by X-rays of the X-ray tube. Hence, the material emits secondary X-ray fluorescence radiation at specific energies correlated to its elemental composition. These photons (secondary X-ray fluorescence radiation) are then captured by

the detector and analyzed as describes above. Due to a continuously detection of the whole detection area, the system is only capable of qualitative analysis but not of reliable quantitative analysis. In other words, there is no object recognition. The detected count rate for a given system (tube data, assembly, etc.) is dependent on material size and content of detected element. A small object with high content of element x and a big object with low content of element x have in relation to the count rate the same content of element x. A reliable quantitative analysis with the existing system was only possible for material having the same particle size. This is neither in glass separation nor metal sorting or most other applications possible. By combination of the existing detection system used in REDWAVE XRF with object recognition by camera, and furthermore, the implementation of a calculation algorithm that correlates the material size to the elemental content quantitative analysis would be possible (see Chapter 5).

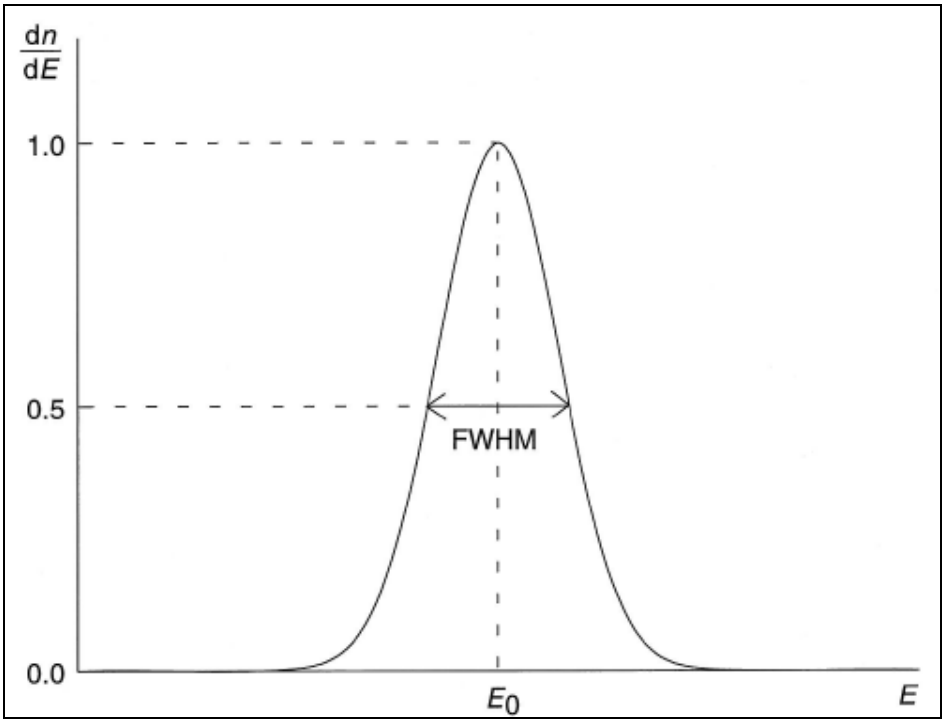

Figure 34 Statistic broadening of the energy peak [1 p. 211]

3.4.5 Measurement Time Settings

As described above the detection speed of the used Si-PIN XR 100CR detector is in the range of microseconds. This means each detector captures and receives counts every few microseconds. Depending on the conveyer belt speed, it takes a certain amount of time for a objects to pass through the detection length. During this time, data is acquired by integrating counts taken by multiple snapshots (slices). These detections are then summed-up to a count rate. How many counts are being considered for one detection signal is dependent on two parameters, time slice and integration interval. In other words, one analysis is being built up of several snapshots or slices. These slices are then summarized to one Integration Interval (compare Figure 35), which is then the signal used for comparison with the set

threshold and the sorting decision, whether the measured count rate is above or below the adjusted threshold. [21] [22 p. 5-6]

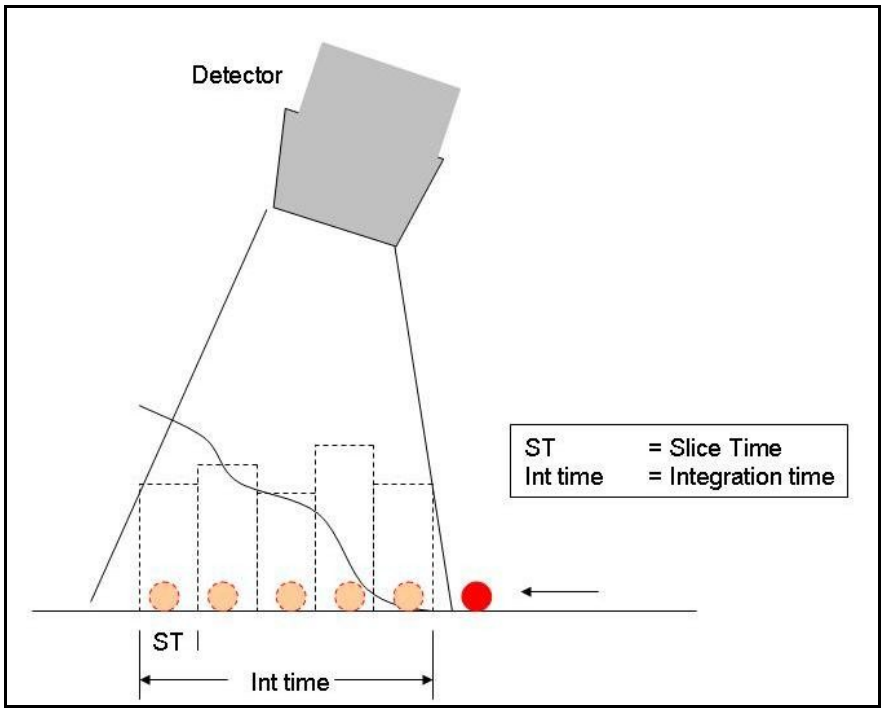

Figure 35 Data Acquisition process [22 p. 6]

3.4.6 Factors of influence

3.4.6.1 Tube Voltage

As described in Chapter 2.3.2.3, the intensity of a spectrum differs with the tube voltage. The shape, the intensity and the maximum energy of the continuous spectrum depend on the value of the voltage. Furthermore, bremsstrahlung is generated by slowing down processes of electrons. In this slowing down processes electrons were scattered at different extents, which means X-rays between 0 ≤ keV ≤ maximum voltage originate. The course of the spectrum is highly influenced by the kinetic energy of the accelerated electrons. Since the energy is proportional to the voltage, the intensity increases with rising voltage. In Figure 6 spectra of a tungsten anode at three different voltages are shown.

In contrast to the intensity, absorption of energies (X-rays) is most effective and probable just above the absorption edges of elements (compare Chapter 2.4.3 and Figure 11). For each characteristic line there is an excitation threshold of energy resulting in a corresponding absorption edge. Hence, a principle line is not present in a spectrum, if the acceleration voltage does not exceed the energy of the absorption edge. For instance, copper has its Kα-peak at an energy of 8.05 keV and the minimal energy necessary for exciting copper at this energy principle line would be right above this value. Therefore, X-ray radiation with an energy right above 8.05 keV is most effective for exciting the Kα-peak of copper.

Taking both above mentioned facts into account, the intensity rises with higher voltage, but absorption is most efficient with X-ray close to the energy of the absorption edge. This is especially for lighter elements contrary. By using an acceleration voltage of 10 keV (which means an energy right above the absorption edge of copper) no significant excitation would be possible. X-rays able of exciting copper were only X-rays between the absorption edge and the used voltage. These are only X-rays between 9.05 keV and 10 keV. By using a voltage of 30 kV in contrast, X-rays between 8.05 keV and 30 keV are able to excite copper. The amount of X-rays right above the absorption edge is higher for an energy of 10 keV rather than 30 keV, which would result in a more effective excitation for the energy of 10 keV. But since for 30 keV X-rays in the range of $0 \leq keV \leq 30$ occur and for 10 keV X-rays only in the range of $0 \leq keV \leq 10$ originate, with 30 kV much more X-rays are able of exciting copper. Hence, the efficiency of exciting copper rises with an increasing voltage but stagnates at a certain point. In general, the higher the voltage the less X-rays closer the absorption edge originate. A rule of thumb estimated with practical applications at different voltages is the use of a voltage approximately three times higher than the absorption edge of the element to be excited. [24]

The most effective excitation would occur by the use of monochromatic radiation. Monochromatic radiation of X-ray tubes is not possible, since bremsstrahlung always originates at slowing down processes at different extents but monochromatic radiation is being emitted by radionuclides. Different radionuclides radiating at different energies are commercially available for several applications. For process recycling radionuclides are for various mentioned reasons no option. Furthermore, by the use of radionuclides due to monochromatic radiation only an effective excitation of a few elements would be possible. [25 p. 20-21]

The range for tube voltage adjusting at REDWAVE XRF is quite small. The maximum possible voltage of the used X-ray tubes is 50 kV (Figure 36). A reasonable high count rate occurs above 30 kV. For light elements a voltage of 30 kV (empirical value) is used (e.g. for chromium, iron copper etc.). For glass-sorting (elements to be detected zinc, lead, zirconium) a voltage of 50 kV is used. Long time experiences for life times of X-ray tubes and a shortening due to constantly used maximum voltage are not known so far.

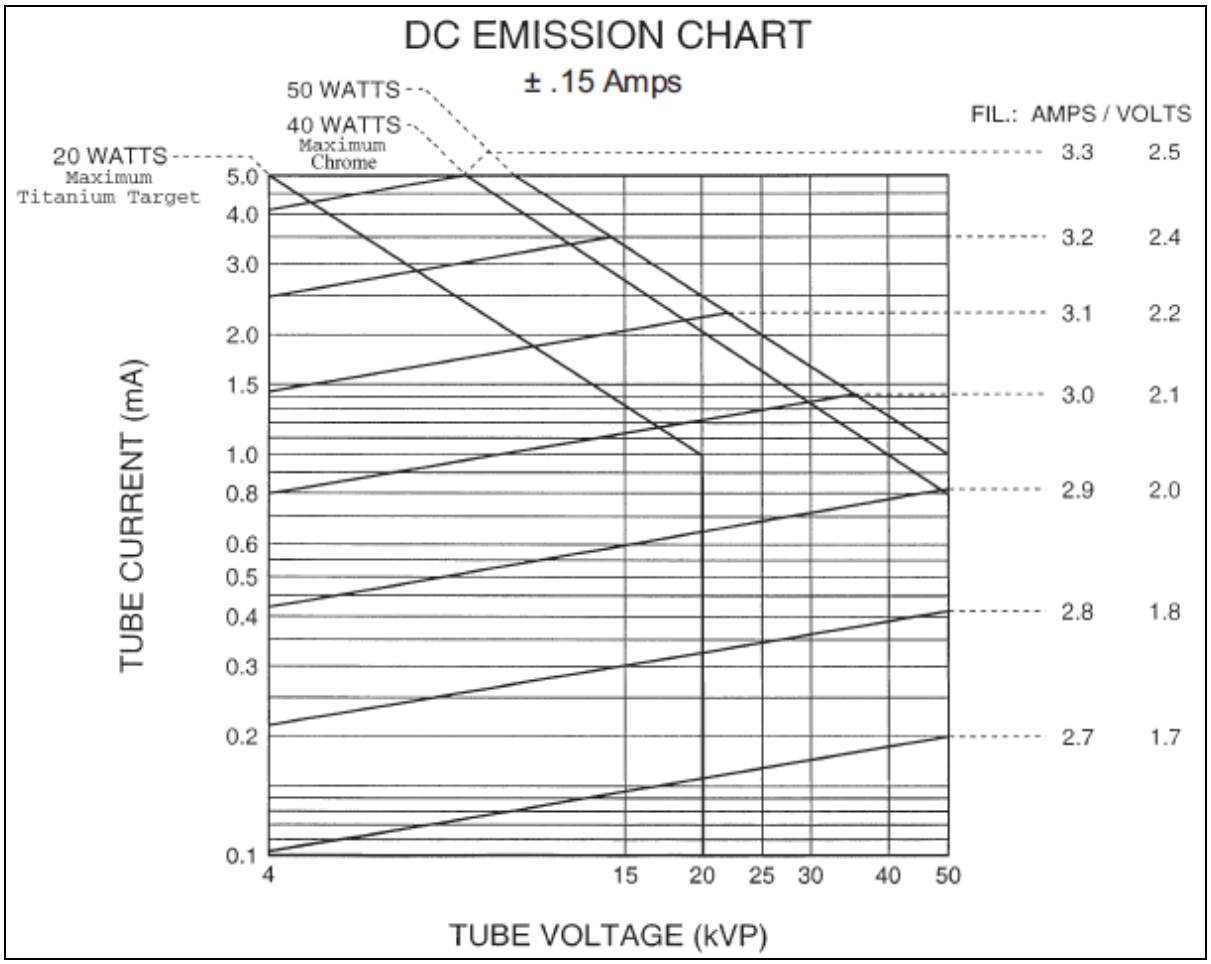

Figure 36 Tube current in relation to tube voltage and tube current [29]

3.4.6.2 Tube Current

The current is linear correlated to the intensity of the spectra (compare Chapter 2.3.2.3). Figure 7 shows relative intensities at different currents (constant voltage and same anode material). In general, a decrease of the voltage requires an increase of the current. Furthermore, the intensity influences the acquisition of data, whereby the count rate is proportional to the tube current. The Output Count Rate (OCR) can be estimated by the Input Count Rate (ICR) accounting the dead time:

$$OCR = ICR.e^{-(ICR.deadtime)}. \quad (26)$$

The ICR is the ratio of detected counts and life time, whereby the OCR is the ratio of detected counts and acquisition time. In other words OCR is the measured count rate including life time and dead time and ICR the true number of photons per second. A reasonable dead time amounts in the range of 10 µs. In crude terms can be said OCR equals about one half to one third of ICR. For a count rate of 60000 (which is reasonable for

REDWAVE XRF at given adjustments and assembly) and a dead time of 10 µs OCR amounts 32929 counts per second.

$$OCR = ICR.e^{-(ICR.deadtime)} = 60000.e^{-(6000010.10\text{^}-6)} = 32928.7C/s \quad (27)$$

Hence, with the current the recorded data respectively the statistics can be adjusted. By using a higher current, more data is being recorded because of the rising count rate. This happens non linear. An increase of the current by the factor of two does not result in recording twice as much data. This is due to the correlated increase of the dead time. In general, by adjusting the tube current a maximization of the count rate is possible.

Following two diagrams (Figure 37 and Figure 38) show the dependency of resolution vs. ICR for different peaking times as well as the OCR in relation to the ICR. Compare above calculated OCR with Figure 38. Used peaking time for REDWAVE XRF is 3-5 µs.

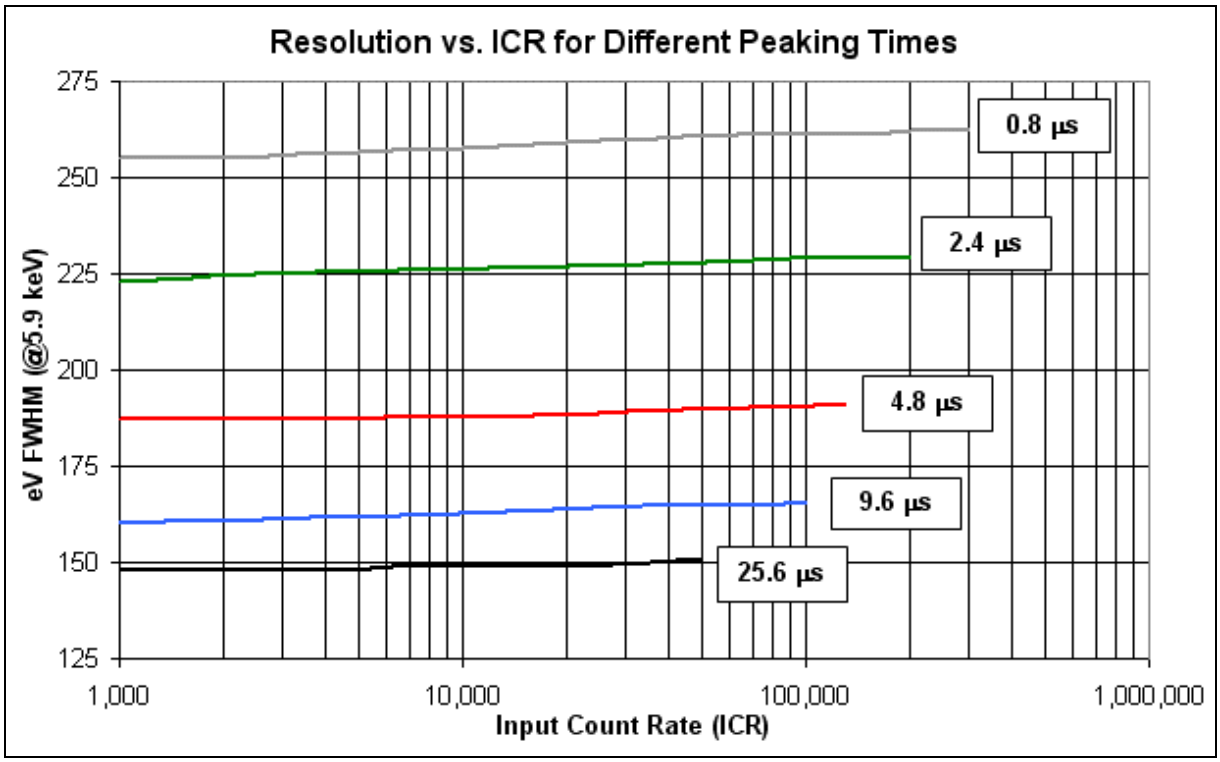

Figure 37 Resolution vs. ICR

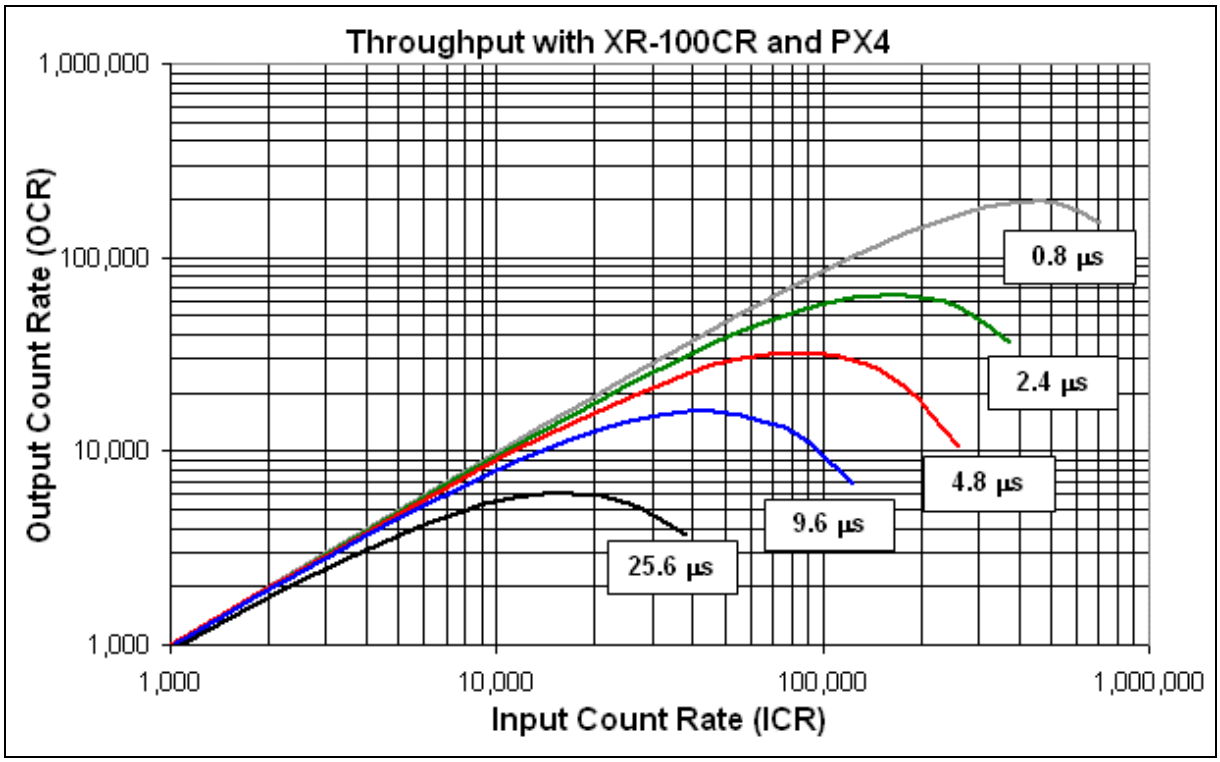

Figure 38 Throughtput (OCR) for various peaking times

In REDWAVE XRF currents in the range of 1000 µA to 1600 µA are used (compare Figure 36). With a voltage of 50 kV a current of 1000 µA or less is used, whereby up to 1600 µA are used for a lower voltage of 30 kV. Compare calculated OCR of (27) with diagram value.

3.4.6.3 Filament Current

The filament current determines the amount of electrons emitted from the cathode. Its value is correlated to tube voltage and tube current. At given conditions (tube voltage between 30-50 kV and tube current between 1000-1600 µA) the filament current varies between 2.9 A and 3.0 A.

3.4.6.4 Material of the Anode

Each spectrum is a superposition of bremsstrahlung and characteristic lines. Bremsstrahlung causes a continuous spectrum whereby characteristic lines are typically for the element and electron transition. Characteristic lines originate due to excitation of material, and can be correlated to elements in the excited material. Furthermore, characteristic lines are caused by the anode material (target). Therefore, the choice of anode materials is of high interest for analysis. Often it is necessary to avoid those lines, since detected photons of characteristic lines can distort the result. This elimination is done by filters positioned between the X-ray tube and the sample material. The filter material implemented for elimination is always composed of the element having an atomic number one or two protons less than the anode

material. For a molybdenum anode (Z = 42) the filter is composed of either zirconium (Z = 40) or niobium (Z = 41). [1 p. 36-38]

3.4.6.5 Filters

The use of filters is common in X-ray fluorescence analysis. Often filters are positioned between detector and sample but an implementation right after the X-ray tube is also popular. In order to remove the contribution of low energy, an aluminum filter is used. Hence, unnecessary and unwanted low energy regions are removed. X-rays right above the absorption edge are absorbed at high extent, while X-rays below the absorption edge almost go through. This results in higher specific count rate (less count rate at all) and therefore more efficient detection. For heavier element detection a common used filter material is copper.Filters are positioned if it is necessary to getting rid of characteristic peaks originated by the anode material. This filter is always composed of the element with atomic number one or two protons less than the anode material. [1 p. 202, 481], [24]

3.4.6.6 Distance

The distance between X-ray tube respectively detector and samples is crucial at X-ray fluorescence analysis. The intensity of X-ray radiation is described by the inverse-square law (3). An increase of the distance by the factor of two causes an intensity-drop to one fourth. Hence, the closest possible gap needs to be achieved for ensuring intensities at reliable extents. Unfortunately, this is complicated for several applications. Often material to be separated is composed of objects in a wide range of particle size. The distance is certainly always adjusted based on the largest particle size causing a significant loss of the intensity at smaller objects. Sieving definitely improves this issue, but also after sieving the material has a certain range of size. Furthermore, also sieved material may include longer objects causing problems. Such longer objects can lead to damages at the bottom side of detection unit (Kapton window) and cause machine downtimes. In concluding, the adjusted distance is always a compromise between needed gap due to material size and intensity loss. [5 p. 6-7]

3.4.6.7 Material Size and Content of Detectable Elements

As mentioned above the intensity follows the inverse square law. Hence, the gap between X-ray tube/ detector and excited material needs to be as close as possible. This is often a challenge and makes the largest particle size crucial. Despite that, the material size and the content of detectable elements are of high interest for detection. REDWAVE XRF has no object recognition. Detection process is a continuously detection of all photons emitted from the whole detection area. As described in Chapter 3.3.5 detection area is adjustable and for the given system in the range of 3600 mm² (Gap_Max, Detector 4). Hence, only qualitative analysis is possible. A small object having a high content of element x and a big object with low content of element x have relative to the count rate the same content of element x.

Quantitative analysis is possible at same particle size but this is for a material stream in waste recycling almost impossible.

3.4.6.8 Surface Contamination

Detection of REDWAVE XRF is based on captured photons emitted by the excited material. The excitation with X-ray fluorescence radiation is independent of the surface color of the material. The measurement depth depends beside energy and intensity of incoming radiation mainly on the energy of principle lines of detectable elements (compare Chapter 3.4.6.9). Hence, a general measurement depth cannot be given but is in the rage of micrometer to a few millimeters. Therefore, surface contamination and coatings influence the level of detection due to attenuation. Attenuation of both, the incoming X-ray fluorescence radiation emitted by the tube but also the re-emitted characteristic X-ray radiation by the excited material, takes place. Furthermore, attenuation but also reinforcements as a consequence of matrix effects may occur. For a detailed description of last mentioned effects see Chapter 2.4 and Chapter 2.5. In addition to attenuation, surface contaminations or coatings can also lead to false detections if non wanted objects are coated or contaminated with an element set as sorting criterion (e.g. chromium coating).

3.4.6.9 Measurement Depth

Measurement depth depends beside incoming X-ray radiation emitted by X-ray tubes mainly on the energy of re-emitted secondary X-ray fluorescence radiation and the material matrix of the embedded element of detection. Depending on the type of electron transition and the element (atomic number Z), the energy of X-ray fluorescence radiation varies between 0.05 keV for Li Kα-line and 117.15 for Pu Kβ-line [28]. For REDWAVE XRF the principal line with the lowest energy reliably detected so far was chromium with its Kα principle line with 5.41 keV. Is a light element embedded in a heavy matrix, measurement depth is limited to nanometers. But in contrary, if a heavy element is embedded in a light matrix, measurement depth rises up to a few millimeters. This is since emitted photons as secondary fluorescence radiation of light elements are only able of travelling such small distances, and furthermore, in matrices attenuation of that radiation takes place as well. This attenuation is certainly of higher extent in heavy matrices. Lead in leaded glass has for instance a measurement depth in the range of 1-2 millimeter. Alloys, in general, have a measurement depth in the range of nanometers or micrometers. The depth of the interaction most strongly depends on the average atomic number of the material. For glass or aluminum it will be a couple of mm, where for steel or copper it will be < 100 µm. Exact values of measurement depth were not figured out and cannot be given. Compare Chapter 4.3.3 for measurement depth of Handheld. [28]

3.4.6.10 Type of Principle Lines

The type of principle line used for detection is dependent on the energy range provided by the X-ray tube and the probability of principle lines of elements. The applied X-ray tube in REDEAVE XRF is limited to 50 kV, which means that elements having principle lines in the range of 0-30 keV can be excited and detected. As mentioned in Chapter 2.6 most elements have a various number of possible electron transitions but at different likelihoods. A nomenclature of possible electron transitions was introduced by IUPAC (see Chapter 2.6.3). For practical use only a few electron transitions are of importance since only these are likely enough to be used as criterion of detection. Figure 14 shows all possible electron transitions, important transitions are represented by thick solid lines. Appendix II gives characteristic X-ray line energies for strongest and most likely transitions for elements with $3 \leq Z \leq 95$. In general, XRF spectroscopy has very less intensive principle lines, strong enough to be used for qualitative analysis. Within one level relative intensities drop rapidly resulting in only one or two intensive lines. Due to measurement conditions (tube voltage) it is often impossible detecting K as well as L-levels. Following rules give a good overview for intensities at different lines (compare Figure 14):

- K-level: most intensive lines are Kα1/3 and Kβ1/3
- K-level intensities: Kα1 : Kα2: Kβ1 ≈ 100 : 50 : 10
- L-level: Lα1, Lβ1 respectively Lβ2 and Lγ1-lines are most intensive ones
- L-level: Lα1 : Lβ1 : Lβ2 : Lγ1 ≈ 100 : 60 : 30 : 10 [2 p. 12]

Summarized, it can be said that elements having a Kα principle line of less than roughly 30 keV this line is used for detection. In contrary, for heavier elements Kα principle line is close to 50 keV or exceeds that detection limit. Hence, for heavy elements L-level respectively Lα principle line is applied as sorting criterion. Lead for instance, has its Kα principle line at 74.97 keV, thus Lα principle line with 10.56 keV is used for detection. For elements having principle lines above 30 keV, it needs to be tested whether Kα principle line or Lα principle line is more intense. Following Table 7 shows implemented elements with its corresponding principle lines. For detection a range of 0.4-0.8 keV is used. A range of 0.8 keV is applied for element detection without contiguous elements, but needs to be reduced for detection of contiguous elements in the same material (see Chapter 3.4.6.12).

Table 7 Implemented Elements [keV]

Atomic Number	Short Symbol	Name	Principle Line	Energy Line	Line width	Energy_Min	Energy_Max
22	Ti	Titanium	Kα	4,51	0,50	4,26	4,76
24	Cr	Chromium	Kα	5,41	0,60	5,10	5,70
25	Mn	Manganese	Kα	5,9	0,60	5,60	6,20
26	Fe	Iron	Kα	6,4	0,60	6,10	6,70
28	Ni	Nickel	Kα	7,48	0,60	7,10	7,70
29	Cu	Copper	Kα	8,05	0,60	7,75	8,35
30	Zn	Zinc	Kα	8,64	0,40	8,40	8,80
35	Br	Bromine	Kα	11,92	0,80	11,52	12,32
40	Zr	Zirconium	Kα	15,78	0,80	15,35	16,15
42	Mo	Molybdenum	Kα	17,48	0,38	17,25	17,63
45	Rh	Rhodium	Kα	20,22	0,40	20,00	20,40
80	Hg	Mercury	Lβ	11,92	0,80	11,52	12,32
82	Pb	Lead	Lα	10,5	0,80	10,10	10,90
-	LE	Light Elements_1	-	35	10,00	30,00	40,00
-	L2	Light Elements_2	-	21,5	2,00	20,50	22,50

Note: For mercury calibration of bromine was used.

3.4.6.11 Similarities of Principle Lines

In some cases it may happen that principle lines of various elements are similar. This causes issues if both elements are constituents in the material to be analyzed. For instance bromine (Kα principle line 11.92 keV) and mercury with its corresponding principle line Lβ with 11.82 keV have very same energies. Even though Lβ of mercury is not as intense as Kα of bromine the detected signal is being distorted and always a superposition of both principle lines. Additionally, arsenic and lead have principle lines differing only 0.01 keV. In practical use, similarities of principle lines for REDWAVE XRF are unlikely. First, only a few elements of the periodic table of elements are being analyzed at the same time in waste management. Secondly, an overlapping always requires both a light but also a heavy element. Both elements in the same material is not common. At portable XRF Analyzer (compare 4.3.3.1) such similarities may cause problems, since plenty of elements need to be analyzed (qualitative and quantitative) simultaneously with the same device.

3.4.6.12 Overlapping of Principle Lines

Overlapping of principle lines contiguous elements takes place. This is in particular a problem for elements such as chromium, manganese, iron, nickel, copper and zinc. Often alloys consist of several of those elements and need to be separated. As can be seen in Table 7 Kα principle lines are for mentioned elements very close. Hence, the range for detection (black bars) needs to be reduced to 0.6 keV or 0.4 keV for zinc. This may cause further problems with the allocation of the energy to its correlated Bin-number. As mentioned in Chapter 3.4.1 this correlation differs from detector to detector within a range of 1-2 %. Thus, not every Bin-number is correlated to the very same energy, which causes dislocations

visible in Figure 39 for zinc. The characteristic peak of zinc is excentric and consequently a certain amount of counts is lost at every measurement which ends up in a decrease of the detection limit.

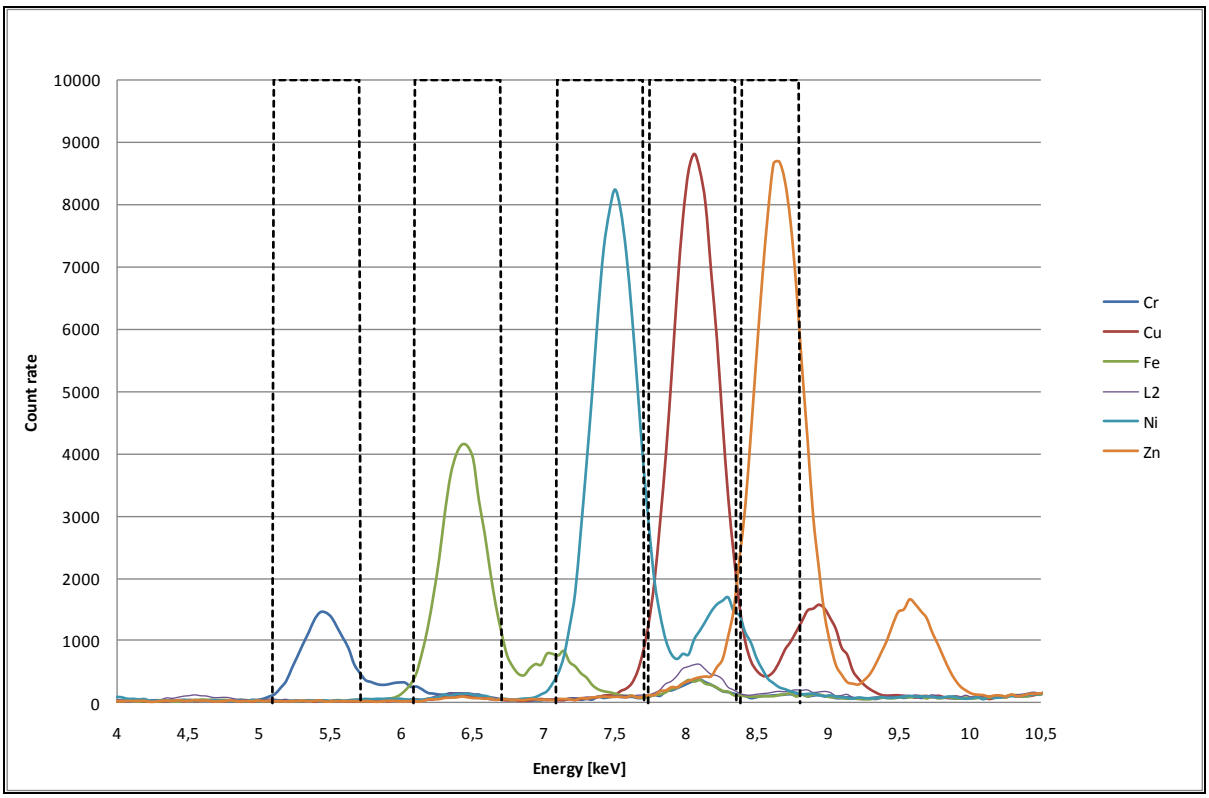

Figure 39 Energy Range of Contiguous Elements

3.4.6.13 Measurement Time

Detectors capture and receive photons every few microseconds. These detections are then summed-up and a count rate is calculated, which is dependent on the measurement time, more precisely on two parameters, Slice Time and Integration Interval. How many counts are being considered for one detection is dependent on these two settings. Depending on conveyer belt speed it takes a certain amount of time for an object to pass the detection area. Data is constantly acquired by integrating counts taken by multiple snapshots (slices). Thus, one measurement is built up of several slices. Slice Time is variable but in general set with 10 ms for standard applications. Slices are then summarized to one measurement (Integration Interval). In other words, the Integration Interval is a sum-up of a certain amount of slices. This summarized signal is constantly compared by the software with the adjusted threshold. An increase of the Integration Interval results in a more flattened detection, since more slices are averaged. A high Slice Time minimizes the influence of background radiation but causes a less sensitive detection. One or two slices with many counts disappear in the whole Integration Interval, respectively in several Slice Times with fewer counts. In contrary, a low Integration Interval leads to a more sensitive detection but outlier may cause false detections. In general, the measurement time respectively all to an Integration Interval

summed-up slices should be close to the average particle size of the material to be sorted. An Integration Interval of 3 leads at a conveyer belt speed of 1.65 m/s to a length of 50 mm.

3.4.6.14 Conveyer Belt Speed

The conveyer belt accelerates and separates the material fed by the vibratory feeder. Frequency and speed of vibratory feeder and conveyer belt are correlated to each other. The separation is done by a relative difference in speed of both. The conveyer belt speed also influences the measurement time. For instance, a higher belt speed leads to a decrease of measurement time since the material is conveyed faster through detection area (compare 3.4.6.13). Furthermore, despite material properties the conveyer belt speed defines the trajectory parabola of the material. The position of the divider is adjusted according the trajectory parabola of the throughput.

3.4.6.15 Blow Out Time

The blow out time is the minimum time interval each valve respectively its correlated nozzles open for the compressed air blow. Assuming the blow out time was set 50 ms, this means the valve opens at least 50 ms irrespective of the material size. But if the material size exceeds 50 ms (at a conveyer belt speed of 1.65 m/s this would be > 82.5 mm, 3.25 in), then the valve is open as long as the threshold is exceeded and a signal is triggered. Trigger time is an internal parameter and amounts 20 ms. The sequence can be seen in Figure 43. Solid line represents the first trigger respectively its correlated blow out time interval. This interval is extended if at the next trigger (represented with dashed line) also detection occurs. Thus, after two trigger the total blow out time equals one blow out time plus one trigger time. For instance, for a blow out time of 50 ms the total blow out time amounts 70 ms. In addition, after a third trigger (dotted line) the total blow out time amounts 90 ms (50 ms + 20 ms + 20 ms). The minimal adjustable blow out time is internally set with 30 ms. An increasing of the blow out time results in a minor increase of the efficiency but then again affect the purity negatively, and furthermore, cause higher energy consumption. In general, the adjusted blow out time should be approximately equal the minimal material length. In case of high wanted purity of the throughput or an efficient separation it can be set higher.

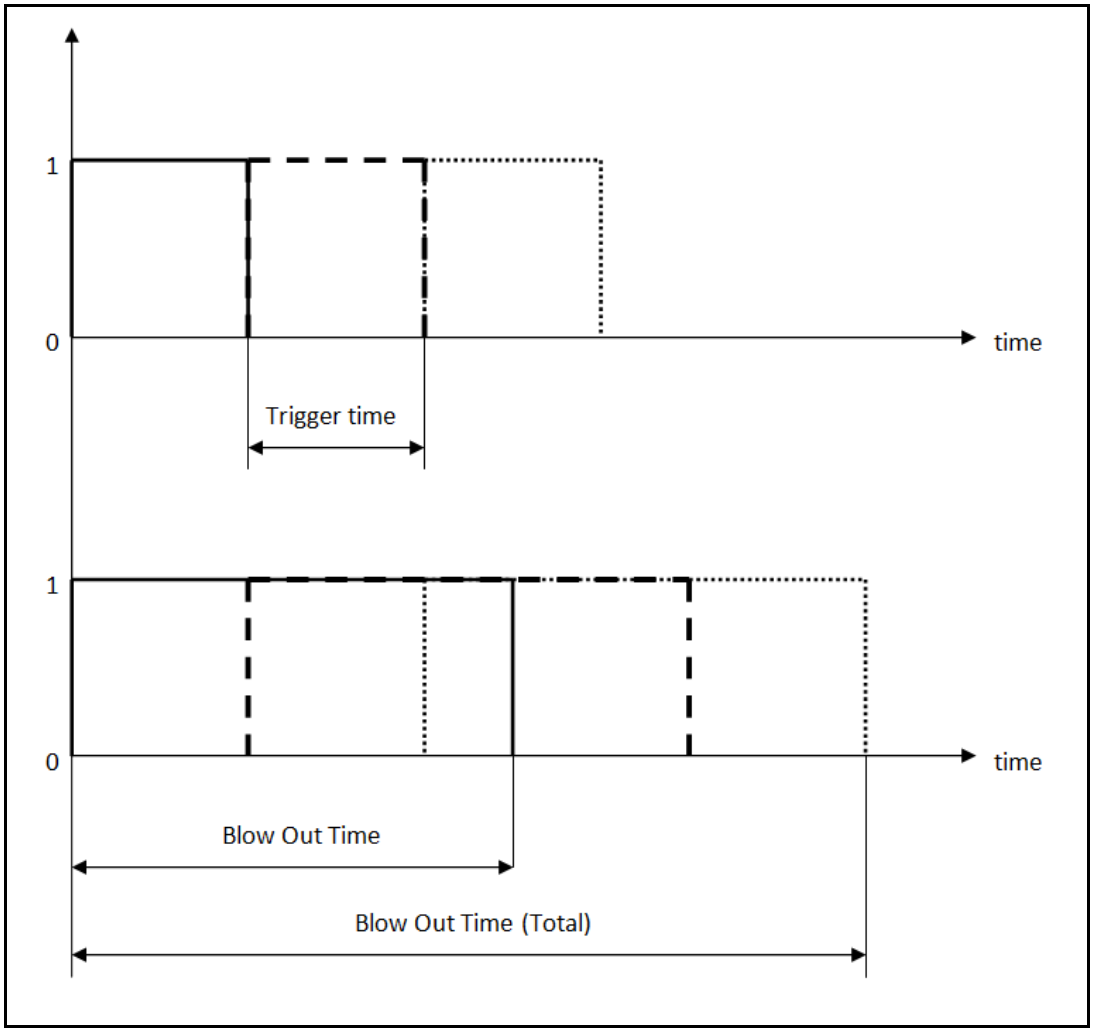

Figure 40 Blow Out Time

3.4.6.16 Alloy- Background Material

In the presence of X-ray radiation all materials respectively its constituent elements are excited. This is despite the material to be sorted also the whole background (alloy, conveyer belt, shielding etc.) and may cause problems if the element to be detected is also part of the background. Hence, the choice of background material is of high interest to ensure a reliable detection. Furthermore, traces especially in the conveyer belt or impurities on the conveyer belt cause problems. Such traces of elements to be detected increase the background radiation, which leads to a raised threshold and furthermore, to an increase of the detection limit (less sensitive). This is in particular of problem if the material to be separated has its turn a very low fraction of the detected element.

3.4.6.17 Interaction of X-rays with Matter- Scattering

Every electromagnetic radiation is attenuated while penetrating matter. The extent of interaction is affected by the energy and spectral composition of incoming radiation and by the chemical composition and crystalline structure of the penetrated material. Attenuation

can be estimated with Beer-Lambert´s law (8). The constant μ is the attenuation coefficient and the sum of all possible factors of influence, Rayleigh scattering, Compton scattering and Photo effect (Photoelectric effect). Photo effect is the umbrella term for X-ray fluorescence and Auger electron (compare Chapter 2.4).

Interesting at scattering for X-ray fluorescence is how much signal is being emitted by the sample and how much background is created by the belt.

At **Compton scattering** energy is transferred towards the scattered atom. It is the interaction of photons with weakly bounded electrons of the outer orbital, resulting in its ejection. The wavelength of the scattered photon is thus longer (has less energy) than the wavelength of the incident photon. Compton scattering decreases the closer the incoming radiation is relative to the right angle and is strongly correlated to the atomic number of excited elements. It increases with falling atomic number. In REDWAVE XRF incoming X-ray radiation and material enclose an angle of 90 ° or close to 90 °. Compton scattering from the belt is a major part of the spectrum. The belt mainly consists of elements with low Z. The factor of Compton scattering of material depends on the matrices. If the matrices is very low, Compton scattering is dominant but if scattered off dense material (high Z) like alloys Rayleigh scattering is dominant. [28]

Rayleigh scattering is the interaction of radiation with strongly bounded electrons of inner orbital. The wavelength of the scattered photon is equal to the wavelength of the incoming photon. Thus, no energy is being transferred. The intensity of Rayleigh rises with the inverse fourth power of the wavelength leading to a greater extent of Rayleigh scattering for radiation with small wavelengths and high Z (compare Figure 1). Related to Compton scattering, Rayleigh scattering is not dominant except for dense materials like alloys. [28]

The continuum part of an X-ray spectrum using an X-ray tube (non-ferrous system) with Ruthenium anode can be seen in Figure 41. That tube besides emitting the continuum radiation emits two strong principle lines at the Rh K-α and Rh K-β energies. When Rayleigh scattering appears the lines come back to the detector at the original energy, but if they Compton scatter they come back to the detector about 1.5 keV lower energy. By comparing the size of the Rayleigh peaks and Compton peaks it can be seen that the Compton scattering is significantly higher for the used belt material (rubber). For K-α principle lines the Compton peak is about 5 times higher than the Rayleigh peak. If the same thing is done for a metal belt, there would be very little scattering (mostly fluorescence) but the Rayleigh peak would be much higher than the Compton peak.

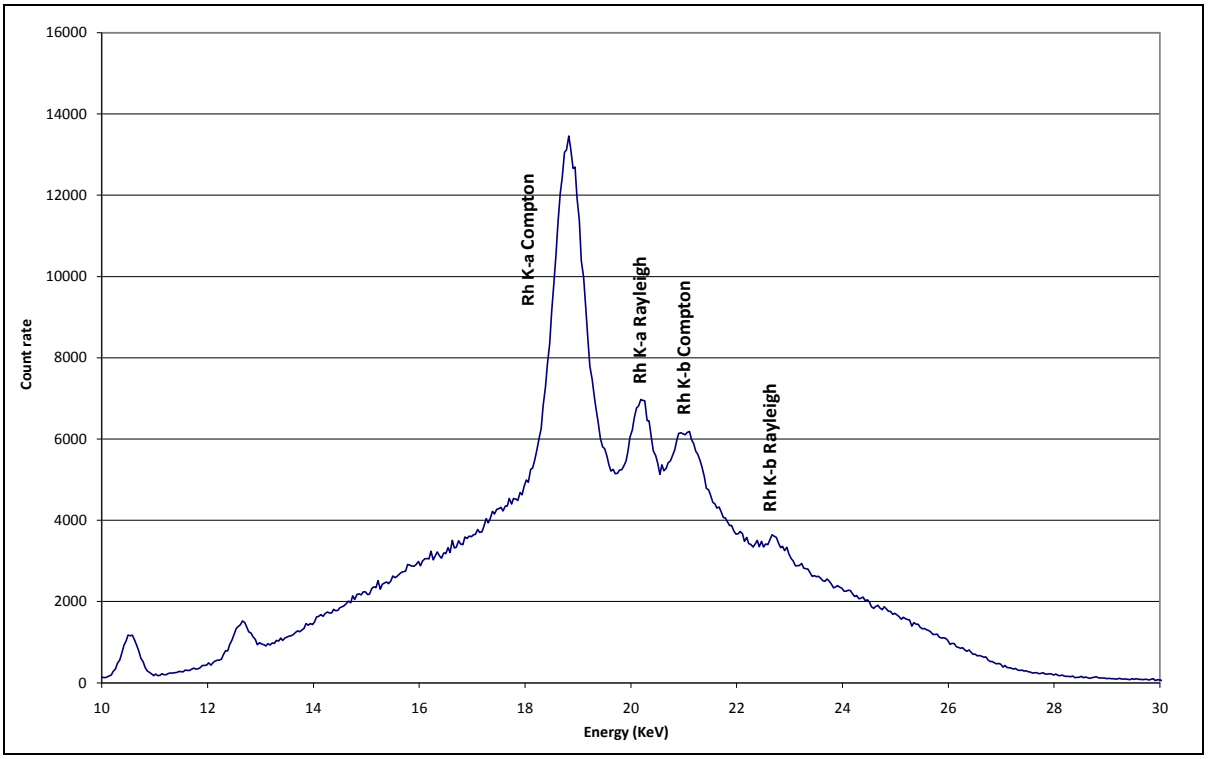

Figure 41 Continuum part of X-ray Spectrum for Rh-anode

3.4.6.18 Interaction of X-rays with Matter- Photoelectric Effect

Photoelectric effect may take place if X-ray radiation is not scattered and furthermore the energy of the incident radiation exceeds the bond energy of electrons on the orbital. At photoelectric effect electrons are emitted from matter as a consequence of energy absorption provided from incoming photons. These photons are then annihilated. The quantity of absorbed energy is equal to the bond energy of the emitted electron, whereby energy remains. This remaining energy ($E_{kin,Photo\text{-}electron} = E_{Photon} - E_{Binding}$) is then carried by the emitted photo-electron. This effect causes the occurring of vacancies on the orbital and an ionization of the atom. These vacancies, however, are refilled within ps by energy transitions from outer orbital. In general, various different energy transitions may take place, but only a few are of high likelihood. Absorption of energies just above the absorption edge (small remaining E_{kin}) is most effective and probable. The bond energy of outer orbital electrons is always higher than the energy of inner ones. Thus, energy is obtained during electron transitions. This energy can either be emitted as Auger-electron or secondary X-ray fluorescence radiation (compare Chapter 2.4).

While relaxing of the atom to ground state, a transfer of the energy to another electron is possible. This **Auger-electron** is then emitted from an outer orbital while absorbing the originated energy. Hence, the atom gets double ionized. This mechanism is radiationless and named Auger effect. The obtained energy of emitted Auger-electrons is $E_{kin,Auger} = \Delta E - E_{Binding}$. Secondary X-ray fluorescence radiation and Auger-electrons is both characteristic for

the specific transfer and characteristic for each element. Thus, qualitative and quantitative analysis is also possible by detecting emitted Auger-electrons.

In contrary to Auger-electrons, the emission of **X-ray fluorescence radiation** is also possible when electrons fill the vacancies of inner orbital by electron transition from outer orbital. The emission of characteristic X-ray fluorescence radiation is only possible for elements having a completed electron orbital and at least another electron on the L-orbital. X-ray fluorescence radiation is for elements with low atomic numbers very unlikely, and furthermore, has the emitted radiation very low energies difficult to detect reliable. X-ray fluorescence and Auger effect are always competing interactions. Auger probability and probability of fluorescent radiation complement each other ($p_{Auger} + \omega = 1$). Elements with high fraction of Auger-electrons have low fluorescence yields. Carbon for instance, has a fluorescence yield of only 0.001 by an Auger yield of 0.999. The probability of Auger effect respectively fluorescence radiation is highly dependent on the atomic number. As visible in Figure 42 both effects have a similar yield for germanium with the atomic number 32. For elements $3 \leq Z \leq 32$ the emission of Auger-electrons is more likely, and for elements $Z > 32$ fluorescent radiation is more likely.

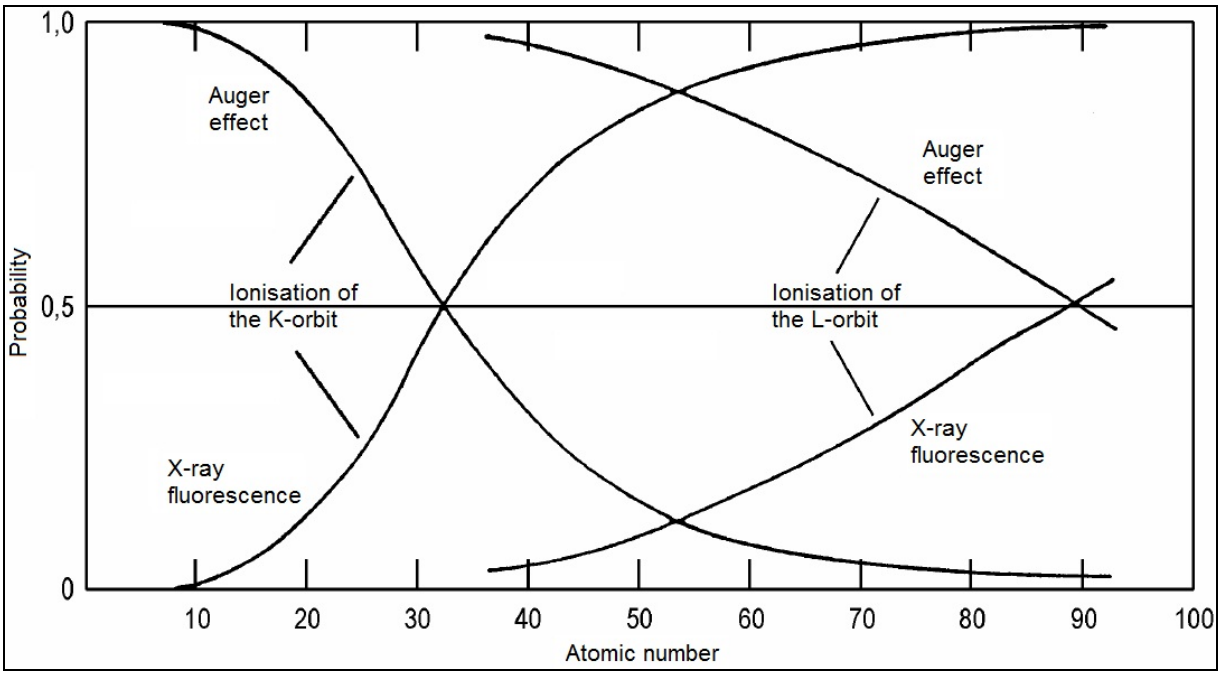

Figure 42 Probability of X-ray fluorescence radiation and Auger effect [13 p. 1]

REDWAVE XRF uses only X-ray fluorescence radiation for detection, even though Auger-electrons are more likely for light elements. Auger effect is surface sensitive due to the fact that emitted electrons usually have energies ranging from 50 eV to 3 keV. At these values electrons have a very short mean free path in a solid. Hence, escape depth of electrons is limited to a few nanometers of the target surface. Auger-effect spectroscopy therefore ofte takes place under ultra-high vacuum. Such conditions prevent electrons scattering with gas electrons and increase the range. As a result Auger-electron spectroscopy is not an option

for resource recycling in waste management. Neither is the reached mean free path efficient enough nor are vacuum conditions achievable. [26]

3.4.6.19 Excitation

Excitation of matter by radiation can be differed in direct excitation (primary excitation) and indirect excitation (secondary, tertiary etc. excitation). Direct excitation is the excitation of X-rays (respectively radiation at all) emitted by primary sources such as radionuclides or X-ray tubes. Have emitted primary fluorescence photons sufficient energy to excite further atoms, then this is called indirect excitation. Depending on the level of excitation, further classification is done to secondary, tertiary etc. In general, the extent of excitation is dependent on the energy, mean free path, sample composition etc. Indirect excitation is of high importance at transition elements such as chromium, iron and nickel. Secondary excitation is in particular strong for elements differing by two in the atomic number. Stainless steel is a typical example. Ni leads to a secondary excitation of Fe and to a tertiary excitation of Cr and furthermore Fe leads to a secondary excitation of Cr. This means Cr is beside regular excitation additionally excited by secondary excitation of Fe and tertiary excitation of Ni, and Fe by secondary excitation of Ni. This leads to a significant stronger excitation of Cr and Fe. Contribution amounts up to 30 % from secondary excitation and up to 2.5 % from tertiary excitation. Since this effect is well known, it can be considered with certain factors.

3.4.6.20 Standardization

A well done standardization is the key for reliable detection and identification as well as efficient separation. As explained in Chapter 3.4.1, standardization is the correlation of detected energies at principle lines with internal Bin-numbers. This is done by detection of molybdenum (composite of the alloy underneath detection unit) with its Kα principle line of 17.48 keV. This energy is then correlated to a Bin-number of 435. Hence, every single energy value has its correlated Bin-number and can be identified. This process is done separately for every detector. In general, a variation of 1-2 % from detector to detector is common but basically every variation needs to be avoided as good as possible. Adjustments for poor standardizations can be done by an in- or decrease of the gain-parameter.

3.4.6.21 Calibration

Despite standardization the calibration is another important step. Every element to be detected needs to be calibrated first. The calibration is done by detection of strong representative principle lines of desired elements. During calibration each element count rate is measured and correlated to its characteristic peak with specific energy used for detection. These peaks are not only at different energies but also ensure various count rates and hence various peak heights (compare Figure 33). Furthermore, the background needs to be measured and calibrated. This is done with the empty belt and a certain energy range. For now two different ranges are used either 20.5-22.5 keV or 30-40 keV. For element

calibration, sheets with pure element plates with a size of 1 cm² (0.156 in²) are positioned below detection area.

Important for a reliable calibration is the usage of pure samples. Depending on physical properties either pure foil or pure plates or a powder can be used. Calibration of hazardous or rare elements or, furthermore, elements that are difficult to handle is at the moment not possible. Examples for such elements would be mercury or uranium. One possibility is the use of a principle line of a different element. Bromine and mercury have principle lines differing with 0.1 keV and in additional, arsenic and lead have principle lines with a difference of only 0.01 keV (Compare 3.4.6.12). Even though principle lines are very same, is the detection of elements using another principle line not recommendable. As mentioned in previous Chapters, principle lines for the same element have different probabilities resulting in only a very few likely ones. Lβ principle line of mercury is not as likely as Kα or Kβ. This may result in an insufficient detection.

4 Practical Application

An overview about the area of applications of REDWAVE XRF is given in Chapter 4. At first, an example of a commercial use is given and some fields with high potential of possible future market are presented. Furthermore, this Chapter gives a brief description about glass sorting, a commercial use of REDWAVE XRF. Finally follows a detailed description of a sorting test with scrap metal.

4.1 Area of Application

In general, all solid materials that contain a specific and characteristic element above detection limit can be analyzed and separated with REDWAVE XRF. The technology of X-ray fluorescence is therefore not limited to one material class or application but can be used in a wide variety of fields. At the moment the system is commercially used only for glass sorting. Further fields are certainly possible but require further developments. Areas of application for the REDWAVE XRF include:

- **Glass**: Separation of leaded glass and glass ceramics, flint glass etc.
- **Metals**: Sorting of stainless steel (e.g. 1.4571 and 1.4301), non-ferrous metal (e.g. brass, bronze, Cu, Zn), discarded metal etc.
- **Ores**: Sorting of ores with different content of metals, separation of ores polluted with objectionable inclusions (e.g. mercury) etc.
- **Minerals**: Sorting of different minerals according to purity grade
- **Plastics**: Color independent separation of PVC
- **Electronic scrap**: Separation of electronic scrap coated with bromine and/or cadmium from shredded electronic scrap etc.
- **Quality control**: REDWAVE XRF is also applicable as online quality control in above mentioned areas as well as where a characteristic element is existent. According to requirements, different elements as search key can be adjusted. These elements are continuously identified and evaluated then recorded, giving assurance of a quality material.

4.2 Glass-Sorting

As mentioned above the area of application for REDWAVE XRF is versatile. An already commercial use is glass-sorting, more precisely the separation of leaded glass and heat resistant glass (glass ceramics) out of recyclable material stream of recovered glass. Glass, one of the oldest materials used by human beings, is a mass product of our society. Since the seventies of the last century, glass is collected and recycled in many countries worldwide. Hence, the consumption of quartz sand, the primary resource in glass production, can be reduced and furthermore and this is certainly of higher importance, the high energy consumption at the glass production process can be reduced. Depending on the color of the glass, between 60 % (flint) and 90 % (green) recovered glass cullet are being blended during

the production process. Glass recycling is known as prime example of modern cleaner production. Since neither collection is reliable, a treatment of collected waste glass is essential. Impurities in collected glass may be wrong colors, metals, organics as well as the so called CSP (ceramic, stone and porcelain) but also various glasses, which are not supposed to be in the glass container. This for instance, can be special-purpose glass, laboratory glass or heat resistance glass (out of microwaves, ovens etc.), but also glass containing additives such as lead.

State of the art in glass-sorting is the use of crusher/sieves, magnetic separator and sensor-based sorting technologies as Infrared-Transmission and Line Scan Cameras. Due to upcoming issues with heat resistant glass (glass ceramic) and leaded glass, the separation of both became necessary. Heat resistant glass leads to inclusions during the glass production process resulting in container unusable due to tensions and finally cracks. Lead is toxic and hazardous to the environment and therefore according to the precautionary principle by the EU regulated to a content of 200 ppm (parts per million). The use of X-ray fluorescence implemented at REDWAVE XRF makes a reliable separation of heat resistant glass and leaded glass possible. For detection of heat resistant glass the elements zinc and zirconium and for leaded glass lead are used as sorting criterion. In Table 8 the chemical composition of different glass types measured with portable XRF analyzer Alpha-2000is listed, whereby Figure 43 shows samples of analyzed glass cullet, leaded glass and heat resistant glass.

Table 8 Chemical composition of different glass cullet [m%]

			"Normal Glass"			Leaded Glass				Heat Resistant Glass					Ceramics			TV	Opal
#	Element		Flint	Green	Amber	1	2	3	4	1	2	3	4	5	1	2	3	5	A
22	Titanium	Ti								0,56	0,44	0,34	3,49	3,81					
24	Chromium	Cr		0,101	0,068														
25	Manganese	Mn			-											1,48			
26	Ferrum	Fe	0,206	0,462	0,42										0,2	3,34	0,25		0,19
27	Cobalt	Co															0,09		
29	Copper	Cu														0,09			
30	Zinc	Zn					2,94				1,78	5,28	4,58	3,96		8,02	1,39		1,63
33	Arsenic	As							1,61	0,55	0,91	0,73							
38	Strontium	Sr	0,044	0,039	0,126	0,04		0,31						0,08	0,04	0,04	0,06	8,27	0,59
40	Zirconium	Zr	0,162	0,164	0,168			0,33		2,99	2,39	2,69	2,29	1,84	0,62	0,17	6,33	0,62	0,29
50	Tin	Sn													0,83		0,21		
51	Antimony	Sb											1,92						
56	Barium	Ba										0,26						0,94	
82	Lead	Bp	0,009	0,027	0,024	31,5	30,3	25,5	22,6			0,01	0,19		22,9	0,02	8,77	1,16	
			0,421	0,793	0,806	31,5	33,2	26,1	24,2	4,1	5,52	9,31	12,5	9,67	24,6	13,2	17,1	11	2,7
	Light Elements		99,58	99,21	99,19	68,5	66,8	73,9	75,8	95,9	94,5	90,7	87,5	90,3	75,4	86,8	82,9	89	97,3

Figure 43 Samples, “normal culets”(left), leaded glass (middle), heat resistant glass (right)

The detection of heat resistant glass and leaded glass out of the recovered glass stream is done by simultaneous detection of zinc, zirconium and lead. For a detailed description of the operation sequence see Chapter 3.4.3. Therefore, the ejection follows the principle of negative-sorting. Negative-sorting is the separation of impurities out of the in-feed material. The main focus of attention is a high throughout. In contrary, positive-sorting is the targeted ejection of the product by a main focus of attention of high purity.

With REDWAVE XRF cullets down to a particle size of 8 mm (0.32 in) can be separated. At a particle size of > 16 mm (0.63 in) the efficiency amounts > 98 % at a capacity of 16 Mg/h. A spectrum containing all three elements and the background can be seen in Figure 44.

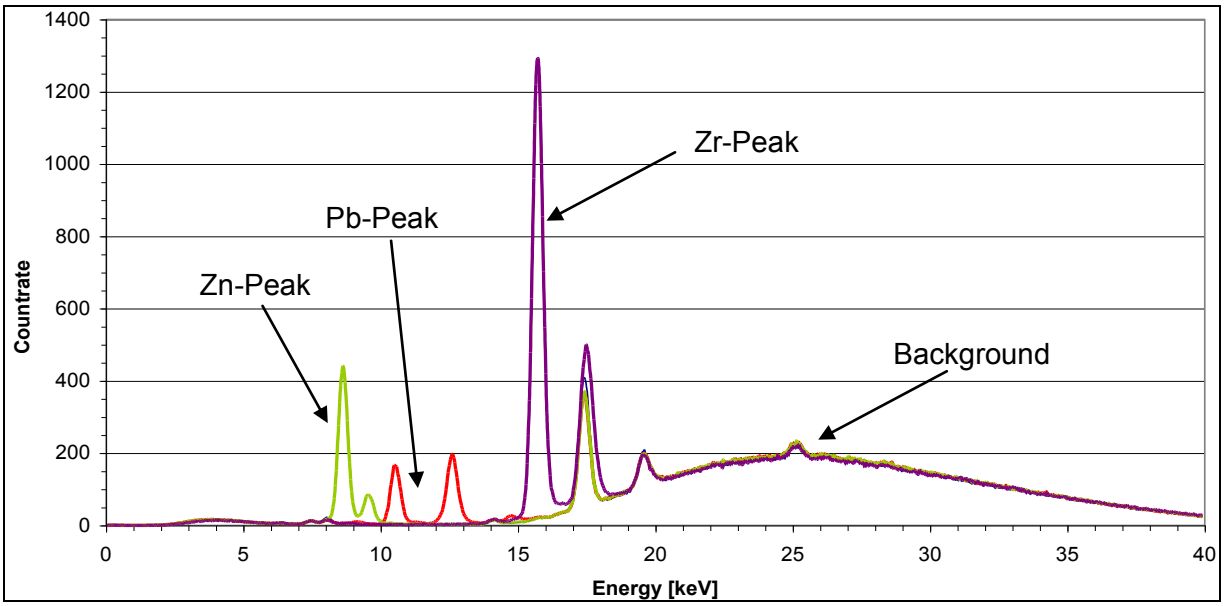

Figure 44 Spectrum in glass sorting

4.3 Metal Sorting

Apart from glass sorting REDWAVE XRF is for now not used commercially in another area of application. An interesting field is scrap metal, more precisely the separation of CRES (Corrosion-Resistant Steel) and non-ferrous metal (copper and brass in the first place) out of various output streams. These output streams can be residues of eddy currents, waste

incineration plants or heavy-media separator as well as further residues and outputs of various waste separations. Following shows a sorting test with enhanced analysis and mass evaluation of each stream.

4.3.1 Assignment of Task

The assignment of task for this experiment was the sorting of CRES, Cu and brass out of two different fractions, fraction 1 “small heavy metals” and fraction 2 “small heavy metals including iron”. The aim of Fraction 1 was the separation of CRES as well as Cu and brass. This was done by a three step sorting. For Fraction 2 the aim was the separation of CRES.

4.3.2 Test Set-up

All tests were done with a REDWAVE XRF-system with a sorting width of 762 mm (three X-ray tubes and 20 detectors). The in-feed material was dumped with a plastic tray onto the feed hopper of a vibratory feeder. By using a certain frequency of the vibratory feeder and speed of the conveyer belt, the material samples were accelerated, separated and transferred towards detection area. These materials are ejected by air blasts into the ejection chute. A further and more detailed description of the feeding and detection process is given in Chapter 3. A photograph of the used demo system can be seen in Figure 45.

All tests for Fraction 1 and Fraction 2 were done with positive-sorting, the targeted separation of the product. In general, positive-sorting is used for high purity. A negative-sorting was in this case due to nonexistent objet recognition not possible.

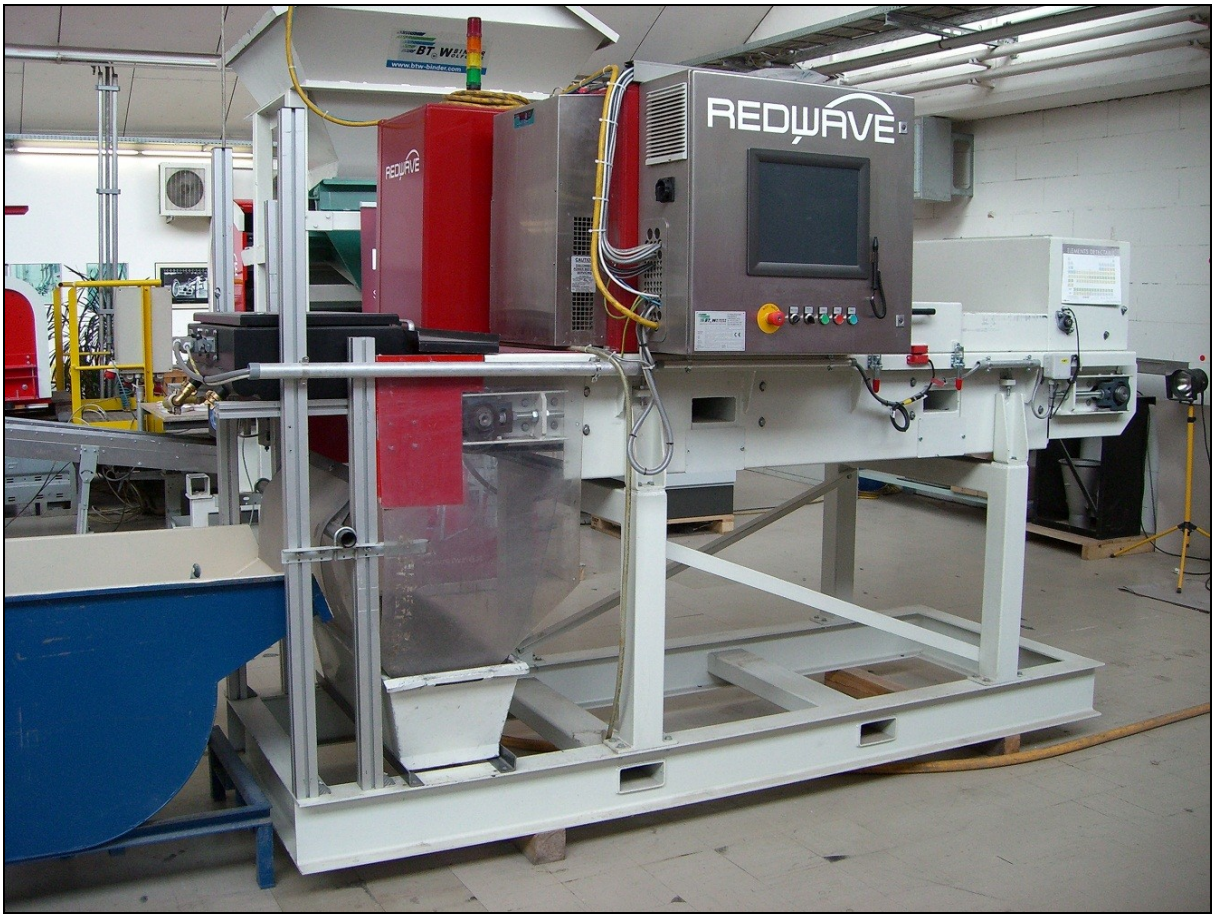

Figure 45 Demo system (without vibratory feeder)

4.3.3 Test Procedure

4.3.3.1 Appliances

The detailed quantitative and qualitative analysis of ejections and throughputs was done by using following appliances and methods:

- Visual inspection
- Handheld Alpha-2000 – Portable XRF Analyzer, Innov-X Systems
- Magnet
- Further sorting/ testing with REDWAVE XRF-system under same or different circumstances

Alpha-2000 is a portable XRF Analyzer manufactured by Innov-X Systems. Excitation source is an X-ray tube with silver-anode providing an energy range of 0-40 kV and 0-100 µA. As detector a Si PIN diode detector is used. The measurement occurs similar as at REDWAVE XRF but measurement time at Handheld is variable and in order to get reliable results at least a few seconds. The accuracy of the result is though highly dependent on the measurement time (compare Figure 8). A longer measurement time gives more accurate

results. Furthermore, Alpha-2000 is able of detecting not only qualities but also quantities in ppm-range. The instrument is calibrated with certified standards. Depending on the element to be analyzed this standards contain only the pure element (e.g. for alloy) or the pure element in matrices as SiO_2 (e.g. for soil, plastics). After that, there is a quality check procedure using certified standards containing a different amount of the element. The real core of the technology is a fundamental parameter algorithm that calculates the raw signals from the detector into a quantitative analysis, taking into account inter-elemental and matrix effects (compare Chapter 2.4). This fundamental parameter algorithm assumes a visibility of the sample of 100 % and then extrapolates all quantities to a total of 100 %. In case of lighter elements this algorithm cannot be used since 100 % are not visible. Hence, a different calculation accounting for light elements is used, and furthermore, by doing the quality check with certified standards a factor can be set for each element. The Handheld allows analysis up to the range of a few ppm (e.g. for V, Cr, Mn, Fr etc.). The first detectable element of the periodic table of elements is Mg with a detection limit of < 1 % in air (compare Appendix III). Ti, Va, Cr etc. have detection limits in the range of 10-100 ppm. By using the Handheld only a small oval shaped spot (12 x 13 mm (0.47 x 0.51 in) of the materials surface is being analyzed. Hence, any result represents only this spot and not the whole material. This is in particular a problem if the material is polluted or of strong composition. Furthermore, coatings or paintings (e.g. zinc) may distort the result since the deepness of detection is limited. For alloys, depending on the material composition the measurement depth is between 10 nm and 150 µm. In general the heavier the element, the higher the measurement depth will be. This can for heavy elements in light matrices be up to 1.5 mm (0.06 in). This is because emitted photons as secondary fluorescence radiation of light elements are only able of travelling such small distances. [20], [23], [31]

Table 9 Accuracy of Alpha-2000 (Metals) [20]

	Precision	
Measurement time	1-100 % concentration range	0.1-1 % concentration range
10 sec	**± 4 %**	**± 6 %**
30 sec	**± 3 %**	**± 5 %**

Note: Precision can only be specified relative to the concentration level (± in %) and not absolute

REDWAVE XRF by contrast uses online measurement within the range of milliseconds, which then results in a measurement limit of approximately 0.5-1.0 %. This is only a rough value since the measurement limit depends on several factors such as materials size, content of detectable elements, matrix, distance etc. In order to give accurate values the measurement limit has to be found out separately for each application. For Gap_Max (detection length amounts in average 62.5 mm) and a belt speed of 50 Hz (1.65 mm/ms) detection time amounts 37.8 ms. Detection limit at settings described in this thesis (conveyer belt speed, Si-PIN-Detector etc.) is vanadium. Light elements are not detectable, but elements below vanadium in the periodic table of elements have higher energies of their

principle lines, which results in a more likely detection. Furthermore, the system is only capable of qualitative analysis but not of reliable quantitative analysis. Firstly, no calibration standards as for the Handheld are used for calibration (compare Chapter 3.4.2 for further description about calibration). Secondly, evaluation of analysis is only based on the detected count rate of the particular element. The detected count rate its turn is dependent on material size and content of detected element. A small object with high content of element x and a big object with low content of element x have in relation to the count rate the same content of element x. A reliable quantitative analysis for the existing system is only possible for material having the same particle size. By combination of the existing detection based on X-ray fluorescence with object recognition, and furthermore, the implementation of a calculation algorithm that correlates the material size to the elemental content, quantitative analysis would also be possible for REDWAVE XRF (see Chapter 5).

A comparison of Handheld and REDWAVE XRF is given in Table 10

For getting rid of above mentioned problems with heterogeneity or surface pollution always at least two measurements of each material piece at different spots were taken. By a given deviation of both measurements of more than 5 %, a third measurement was taken. A fourth measurement was never necessary. Values in tables are always mean values of all measurements. Furthermore, the detected area was cleaned (if necessary).

Table 10 Comparison of Handheld vs. REDWAVE XRF [29], [30], [31]

	Handheld	REDWAVE XRF
Principle	X-ray fluorescence analysis	X-ray fluorescence analysis
Type of Measurement	Static measurement	Online measurement
Measurement Time	10 sec up to a few minutes	approx. 30 ms (depending on the belt speed)
X-ray Tube		Varian VF 50J
Voltage	< 40 kV	< 50 kV
Current	< 50 µA	< 3000µA
Anode	Silver	Tungsten
Detector		Amptek XR-100CR
Detector Type	Si-PIN diode	Si-PIN diode
Specifications	< 230 ev FWHM at 5.95 keV Mn K-alpha line	190-230 eV FWHM at 5.95 keVw Peaking time 32 µs Size 25 mm² Silicon Thickness 500 µm Be-window 100 µm (4 mil)
Element Limit	Mg	Cr (lightest element practically proofed)
Detection Limit	low ppm-range (depending on element, measurement time etc.)	low %-range (depending on conveyer belt speed, gap, element etc.
Detection Area	156 mm² (spot of 12 x 13 mm)	2750 mm² (spot of 55 x 50 mm; Gap_Min) adjustable
Analysis		
Qualitative	possible	possible
Quantitative	possible	not possible (no object recognition)
Application	Various analysis for RoHs, WEEE, toxic metals in plastics, alloy identification (PMI), on-site environmental testing etc.	Separation of glass ceramics and leaded glass

4.3.3.2 Fraction 1

Characteristics for Fraction 1 are given in Table 11. In order to get reliable and comparable results the material was sorted in three sequenced separations. In the first step the separation of CRES took place. The ejection (CRES) of step 1 (Test 4) was fractionated and analyzed (quantitative and qualitative), whereby the throughput of this step was equal to the input-material of the following step. Step two (Test 4a) the separation of brass was handled in the same way. After separation the ejected material was fractionated and analyzed and its throughput was the input of step three (Test 4b). The aim of the final step was the separation of copper. Its ejection (Cu) was after fractionation quantitative and qualitative analyzed. The

throughput of the third step was the remaining residue and the material not to be sorted including a few losses. A flow sheet of the separation of Fraction 1 including all fractionated ejected masses and throughput masses is given in Figure 48. Following shows specification used for Fraction 1:

- Gap Setting: Gap_Max
- Tube Voltage: 30 kV
- Tube Current: 1200 µA
- Belt Speed: 50 Hz (approximately 1.65 m/s)
- Pressure for Reject: 8 bar
- Blow Out Time: 50 ms
- Threshold Settings: Step 1: Cr = 0.5
  Step 2: Cu = 0.5 and ratio brass Cu/Zn = 0.8 – 2.0
  Step 3: Cu = 0.9
- Duration of Test: 10-15 s
- Filter for X-rays: none

Table 11 Characteristics Fraction 1 and Fraction 2

	Fraction 1	Fraction 2
Identification	small heavy metals	small heavy metals including iron
Particle size	< 100 mm (3.94 in)	< 100 mm (3.94 in)
Particle description	mainly flat samples with different shape and width, few elongate round objects, different wire	mainly flat samples with different shape and width, few elongate round objects, few wire
Origin	residue of heavy-media separator	residue of heavy-media separator
Goal of sorting	1 step: separation of CRES 2 step: separation of Cu 3 step: separation of brass	Separation of CRES
Total mass (sorting)	6436 g	approx. 5250 g
Composition	Cu wire- insulated, Cu-wire- non insulated, wire, pieces of Cu, CRES, Zn, brass etc. , stones, slag, miscellaneous etc.	CRES-wire, few Cu-wire- insulated, pieces of CRES and Fe, stones, slag, miscellaneous etc.

4.3.3.3 Fraction 2

The aim of Fraction 2 was the separation of CRES out of a mixed metal fraction. This was done in one step. Characteristics for Fraction 2 are given in Table 11. Altogether three tests (Test 1, Test 2, Test 3) under same circumstances and with same material were done. Following shows specifications used for Fraction 2:

- Gap Setting: Gap_Max
- Tube Voltage: 30 kV

- Tube Current: 1200 µA
- Belt Speed: 50 Hz (approximately 1.65 m/s)
- Pressure for reject: 8 bar
- Blow Out Time: 50 ms
- Threshold Settings: Cr = 0.5
- Duration of Test: 10-15 s
- Filter for X-rays: none

4.3.4 Results and Interpretations

4.3.4.1 Fraction 2, Test 1 – 3

The separation of CRES out of a mixed metal fraction including iron results with consideration of all three tests in an average efficiency of 97.2 % by an average purity of CRES of 92.1 % (compare Table 12). As sorting criterion only a certain threshold for Chromium was used (further explanation given in Chapter 4.3.5).

Table 12 Results Fraction 2

Mass [g]	Ejection		Throughput		CRES total	Total	Efficiency	Purity
	CRES	Impurity	CRES	Residue				
Test 1	1940	170	30	3210	1970	5350	98,5%	91,9%
Test 2	1960	170	40	3070	2000	5240	98,0%	92,0%
Test 3	1950	160	100	2960	2050	5170	95,1%	92,4%
						Average	97,2%	92,1%

Decrease of total mass due to losses during tests

A certain amount of impurity in ejection is never avoidable and has to be accepted. On the one hand these impurities are wires and pieces of fabrics or further material not heavy enough following the trajectory parabola. Hence, it drops into ejection chute instead of passing chute, where it was supposed to be. Another explanation for impurities is agglomerates at which foreign objects are tied with CRES respectively the ejected material. All objects immediately next to eject material are being captured by the air blast as well (compare Figure 46 bottom). Furthermore, all objects having a round or roundish shape are problematic since those are addicted to moving on the belt. If this happens after detection it causes a different delay time and leads to a miss shot of the detected object. Hence, it explains CRES-objects in throughout as can be seen in Figure 47 bottom. The detected count rate is highly dependent on the gap between conveyer belt and detection unit and on content of detectable element and size of material. Furthermore, some CRES-objects in throughput are very small (compare Chapter 3). Those facts explain miss detection of very small objects. For images of Test 2 see Appendix VIII Figure 58 and Appendix VIII Figure 59 for Test 3.

In concluding, all tests had same and comparable results with a maximum deviation of only 2.2 % from mean for efficiency, whereby deviation for purity amounts 0.3 %. The reason for lower efficiency for Test 3 is due to a “heavy” CRES-tube (compare Figure 59 right-bottom). The efficiency is satisfying with an average of 97.2 %. However, the purity has with an average of 92 % not turned out satisfactory. A further explanation and critical analysis is given in Chapter 4.3.5.

Figure 46 Photographs of Test 1- Ejection, CRES (top), Impurity (bottom)

Figure 47 Photograph of Test 1- Throughput, Remain (top), CRES (bottom)

4.3.4.2 Fraction 1

The separation of CRES, brass and copper was done in three sequenced tests. Due to huge effort of qualitative and quantitative analysis of different fractions only one total test (all three steps) was done. Step 1 (Test 4) the separation of CRES resulted in an efficiency of 93.2 % and a purity of CRES of 91.8 %. The throughput of Test 4 was also the input of Test 4a. At an efficiency of 95.4 % the purity of Test 4a amounted 94.3 %. These two values include the implication of objects with high Zn-content. The final step Test 4b the separation of copper has reached a purity of copper of 95.4 % by an efficiency of 95.4 %. Figure 48 shows a flow sheet of all done tests with Fraction 1. Furthermore, a detailed description of all three steps including masses and explanations is given in Table 13. All photographs of each single fraction can be seen in Figure 49 to Figure 57.

Table 13 Results Fraction 1

04.08.2010		Fraction	Mass [g]	Description
Versuch 4/ Test 4 VA-sorting		Input	6436	Heavy metals
	AW/ E	CRES_pure	2900	Pure CRES-fraction
		Cu-pieces	20	Mainly small wires; one short Cu-tube
		Miscellaneous pieces	183	Detailed composition ist given in Appendix
		Wires	55	Miscellaneous wire with isolation
		Total	3158	
	DL/ TP	Total	3278	
		thereof CRES	210	Thin, elongate wires; miscellaneous round objects
		Purity	91,8%	
		Efficiency	93,2%	
Versuch 4a/ Test 4a Brass-sorting		Input	3278	Throughput Test 4
	AW/ E	Brass_pure	508	Pure brass-fraction
		Zn-pieces	117	Various pieces with high Zn-content
		Wires	38	Miscellaneous wires with isolation
		Cu/Zn-pieces	6	One piece with low Cu/Zn-content
		Total	669	
	DL/ TP	Total	2609	
		thereof brass	32	Three small partly round objects
		Purity I	75,9%	Exclusive objects with high Zn-content
		Purity II	94,3%	Inclusive objects with high Zn-content
		Efficiency I	94,1%	Exclusive objects with high Zn-content
		Efficiency II	95,4%	Inclusive objects with high Zn-content
Versuch 4b/ Test 4b Cu-sorting		Input	2609	Throughput Test 4a
	AW/ E	Cu_pure	653	Pure Cu-fraction (Cu-content > 90)
		Cu-pieces	130	Cu-fraction (Cu < 90 %) Detailed composition is given Appendix
		Wire	42	Miscellaneous wire with isolation
		Cr-pieces	8	Two thin wires
		Zn-pieces	23	Three small pieces
		Total	856	
	DL/ TP	Cu-loss	40	Mainly small wires; furthermore one small but heavy piece
		Remain	1700	Miscellaneous (stones, slag, various metals, wire etc.)
		Purity II	95,4%	Inclusive objects with high Cu-content
		Efficiency II	95,4%	Inclusive objects with high Cu-content

For analysis of composition of miscellaneous pieces (Test 4 E) see Appendix VII Table 14 and for Cu-pieces and Cu_pure (Test 4b E) see Appendix VII Table 15.

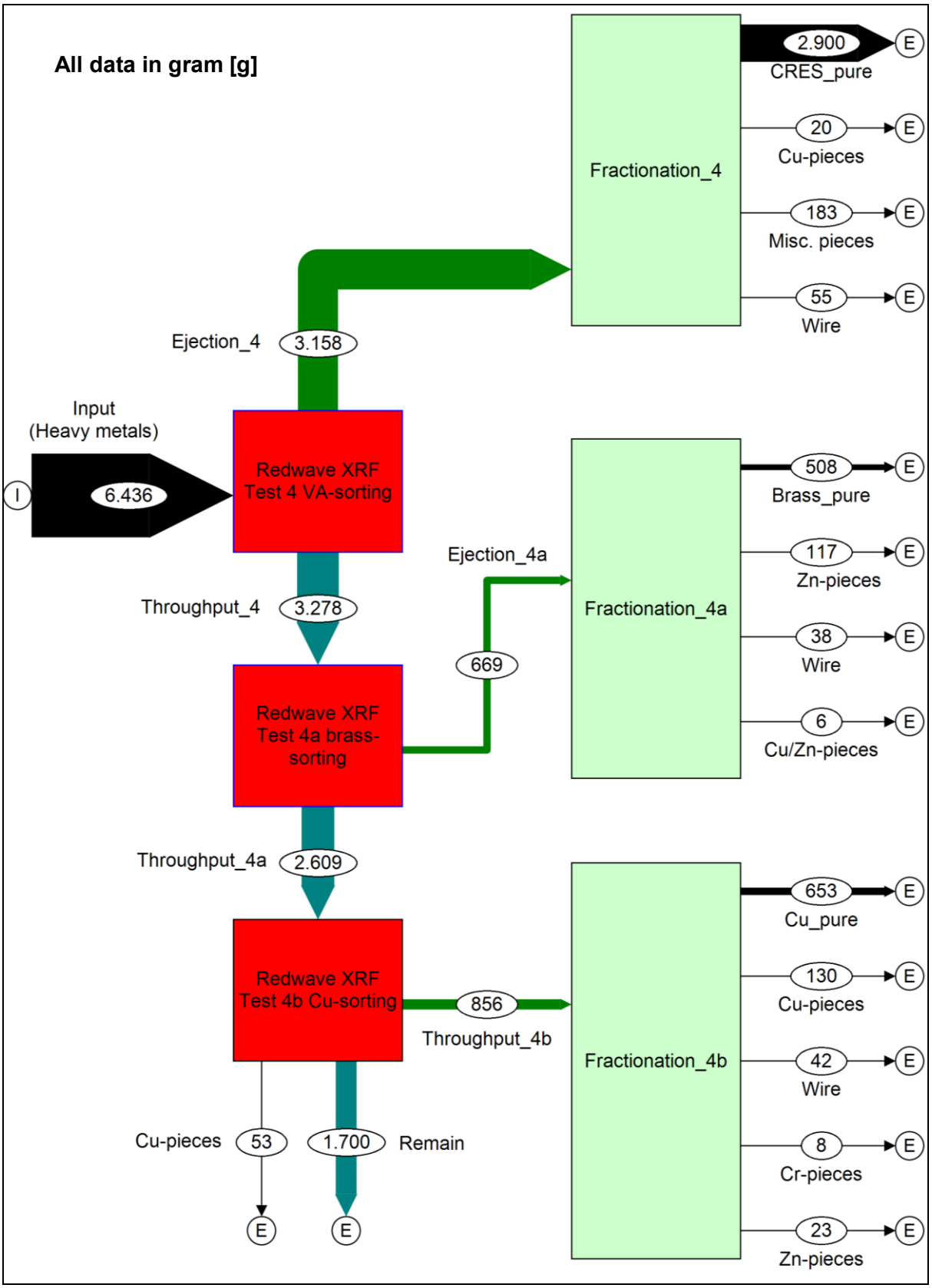

Figure 48 Flow sheet Fraction 1

Test 4, Separation of CRES

The input-fraction of Test 4 was small heavy metals with a total mass of 6436 g. Figure 49 and Figure 51 show the ejected fraction of this Test 4. The wanted CRES (Figure 49) amounted 2900 g by impurities (Figure 51) of 258 g. This led to an efficiency of 93.2 % and a purity of 91.8 %. The impurities were analyzed and separated in following further fractions, Cu-pieces, miscellaneous pieces and wires. The remaining mass of the throughput amounted 3278 g.

Wire and insulated wire (compare Figure 51 left and right) are always problematic and never avoidable at all. First, wires are addicted to agglomerate with material (in this case ejected material, CRES). Secondly, wires may be little and light, do not follow the trajectory parabola and collide with the divider edge or don´t even reach the divider and drop directly into the ejection chute. This case is often likely if the input-material is in average heavy but also includes light material. Then, the divider is adjusted in relation to the trajectory parabola of heavy materials, which means the dividers angle is higher and a collision of light material gets more likely. Thirdly, and this may be an explanation for every impurity, all objects at the moment of detection respectively blow out immediately next to detected material are being captured by the air blast as well.

For fraction miscellaneous pieces (compare Figure 51 middle) a detailed analysis can be seen in Table 14. A few pieces (five out of 16) have a low content (between 1 and 9 %) of zinc, iron and/or copper and another one (# 9) is a brass-piece with a chrome-coating on one side. Eight pieces have a Zn-content between 60 and 70 %. One possible explanation is certainly the capture by an air blast of detected materials. Further and more detailed explanation cannot be given at the moment since the reason for ejection is unknown (compare discussion Chapter 4.3.5).

Table 14 Miscellaneous pieces Test 4 E

Sample	Zn	Fe	Cu	LE	Annotation
1	0,0	3,9	0,0	96,1	
2	0,8	6,5	3,8	88,9	
3	1,1	4,7	2,8	91,4	
4	1,3	6,3	2,1	90,3	
5	1,8	5,0	3,2	90,0	
6	66,0	0,0	0,0	34,0	Zn-pieces
7	61,0	3,0	0,0	36,0	Zn-pieces
8	62,0	4,0	0,0	34,0	Zn-pieces
9	29,0	0,0	55,0	16,0	brass-piece
10	64,0	2,0	0,0	34,0	Zn-pieces
11	65,0	2,6	0,0	32,4	Zn-pieces
12	2,3	8,8	2,7	86,2	Cu/Zn-piece with low content
13	67,5	3,7	0,0	28,8	Zn-pieces
14	60,6	3,9	0,0	35,5	Zn-pieces
15	69,1	0,0	0,9	30,0	Zn-pieces

Note: Detected elements lower 0.5 % were not considered and are part of LE, compare with photographs of numbered samples

The throughput of Test 4 is shown in Figure 50. Parts in the bucket represent missed CRES-pieces. As can be seen objects are either of round/ roundish shape or wires. Material with round or roundish shape is always problematic in detection respectively ejection due to the addiction to moving. When an object moves while or after detection, the delay time gets incorrect, which then mostly (depending on the blow out time) results in a miss shot. Wires cause both problems at throughput but also ejection. The remaining part of missed objects is wires. Wires have compared to round or rectangular shaped objects indeed a higher ratio of surface/volume. This effect normally is of advance due to higher extent of detection, but furthermore since the ratio of surface/length respectively surface/width is very small for wires related to objects of round/roundish or rectangular shape the effect of bigger surface is being relativized. Also the higher specific surface of wires is above a given point disadvantageous due to decreasing detection.

Test 4a, Separation of Brass

For Test 4a the input was the throughput of Test 4 (compare Figure 50). This means the composition of the input was equal to beginning of Test 4 beside ejected CRES-pieces (apart from missed ones). The mass of the input amounted 3278 g, of which 669 g were ejected (throughput 2609 g). With the ejection a separation in four different fractions was done, the wanted brass (Figure 52 left image) with 508 g as well as three different impurities (Figure 52 right image), Zn-pieces (117 g), wire (38 g) and one Cu/Zn-piece (6 g). In this test an efficiency of 95.4 % including Zn-pieces and an efficiency of 94.1 % without Zn-pieces was reached. The purity amounted 94.3 % respectively 75.9 %. The assumption of Zn-pieces to be non-troublesome in the ejection is done due to present Zn in brass. It can be assumed that Zn- pieces in brass fraction do not bother at a certain percentage.

Wire (insulated and non-insulated) as seen in Figure 52 right-bowl are for certain above mentioned reasons always a problem for every sensor based sorting system. Agglomerates, light weight and special shape and accidentally ejections with detected objects are perpetual reasons for wire to be in ejection.

The biggest part of impurities was Zn-pieces (compare Figure 52 right-top) with an amount of 117 g. This is with 17.5 % of the total throughput high. One possible explanation of impurities is always the capture by an air blast of detected objects. Another and in this case more likely reason for ejection is detection and calculation issues. The sorting criterion for brass is a ratio of Cu/Zn and a single threshold for copper. The additional Cu-content-rule is necessary since a ratio of Cu/Zn at this ratio is very likely. Detection of photons at this energy range constantly takes place even though certainly at a low extent. After analysis with Handheld alpha-2000 of different brass-samples taken out of the scrap material an average ratio Cu/Zn of 0.8 to 2.0 was set as sorting criterion. This means everything in between this range was defined as brass but everything above or below not. On closer inspection most pieces had a contaminated surface due to impurities, adherences or oxide formation. After analysis of Zn-pieces with contaminated surface with the Portable XRF Analyzer all pieces had a Zn-content of > 80 % but also various contents of Pb, Ti, Fe and Cu in the range of a few percent. After sanding of the surface the Zn-content amounted > 90 % by a significant degrease of the Cu-content, which results in a significant higher Cu-detection at Zn-pieces due to surface contamination. This fact could have caused miss detections and may be another explanation for the relative high proportion of Zn-pieces in the brass fraction.

In throughput (compare Figure 53) with a total mass of 2609 g were three brass-pieces having a mass of 32 g, which is a reliable separation rate. The shape of all three objects was partly roundish which could have caused the miss shot. An in this case more likely explanation was due to software and internal calculation issues with the Cu/Zn-ratio. The presence of further objects (e.g. pure zinc, pure copper) while detection as well as coatings or surface contaminations (dirt, different material etc.) distorts the measurement. Hence, the detected ratio is below or above set ratio. The throughput of Test 4a equaled the input of test 4b.

Test 4b, Separation of Copper

The input of Test 4b was small heavy metals excluding already ejected CRES and brass and amounted 2609 g. The separation of copper reached an efficiency of 95.4 % by same purity of 95.4 %. Copper in throughput was defined as Cu-pure-fraction plus Cu-pieces (compare Figure 54 and Table 15) and assumed 90 % of wire-fraction (Figure 55 left). All wires in wire-fraction are beside two thin CRES-wires insulated/non-insulated Cu-wires. Hence, wires but also Cu-pieces can be seen as resource. Altogether, the mass of ejected Cu amounted 821 g. Impurities (see Figure 55) in throughput were mentioned two Cr-wires (8 g) and three Zn-pieces (23 g). The throughput amounted 1753 g including a Cu-loss of 53 g. In Figure 56 fraction Cu-loss and in Figure 57 remain-fraction can be seen.

As already mentioned above, wires always cause problems at every sorting. The impurity in ejection is beside wires Zn-pieces with 23 g. Wires are constituent in wire-fraction (two CRES-wires) and Cr-pieces-fraction (8 g). Apart from above mentioned explanations, another possible reason was “contaminant” with copper.

After the last separation step, a throughput of 1753 g remained. The Cu-loss amounted 53 g. Despite one big, heavy piece, the fraction was composed of wires different length and shape. The heavy Cu-piece was of rectangular shape but had a big hole (compare Figure 56). Depending on the position at the moment of the air blast the hole could have caused the miss shot. The fraction Remain with 1700 g had miscellaneous composition (see Figure 57):

- CRES with mostly thin wires but also some objects with complicated shape (knife, knob etc.); difficult to sort
- Wires insulated
- Insulation (without wire)
- Zn-pieces
- Slag-pieces
- Various metal
- Various plastic-pieces
- Stones
- Agglomerates
- Miscellaneous etc.

The separation of copper was the final separation step of the input-fraction Fraction 2. After all three steps (separation of CRES Test a, separation of brass- Test 4a and separation of Cu-Test 4b) a mass of 4683 g was ejected by an input of 6436 g and an output (Remain-fraction plus Cu-loss) of 1753 g. This results in an ejection rate of 73 % of the input.

Table 15 Cu-pieces Test 4b E [m%]

Sample	Cu	Ni	Zn	Fe	Sn	Pb	LE	Annotation
Cu-pieces								
1	55,5	25,7	4,3	0,5			14,0	zinc-plated
2	79,9		4,5	0,7	1,8		13,0	
3	21,9		54,0	3,9			20,0	
4	30,2	26,8	32,6	2,5			7,7	brass-piece from Test 4a, zinc-plated
5	85,7		0,5	1,8	3,5		7,8	
6	53,3	1,3	30,0				13,2	brass-piece from Test 4a
7	72,7		7,1	1,7		3,7	14,8	
8	80,3		4,2	0,5	1,4		13,4	
9	56,6		24,0	2,4		1,6	15,1	
10	63,3		9,1	1,9		8,3	16,3	
11	77,5		1,3	1,2		8,3	11,4	
12	57,7		0,3	2,2		1,3	38,4	Agglomerate with Cu-wire
Cu_pure								
13	88,5			0,9			10,5	
14	87,9		0,3	1,9			9,6	
15	97,9						1,7	
16	91,0						9,0	

Figure 49 Photograph of Test 4- Ejection, CRES_pure

Figure 50 Photograph of Test 4- Throughput/ Input Test 4a

Figure 51 Photographs of Test 4- Ejection, wire (left), miscellaneous pieces (middle), Cu-pieces (right)

Figure 52 Photographs of Test 4a- Ejection, brass_pure (left), Zn-pieces (right-top), wire (right-bowl), Cu/Zn-piece (right-left)

Figure 53 Photograph of Test 4a- Throughput/ Input Test 4b

Figure 54 Photographs of Test 4b- Ejection, Cu_pure (left), Cu-pieces (right)

Figure 55 Photographs of Test 4b- Ejection, wire (left), Cr-pieces (left-bottom), Zn-pieces (left-top)

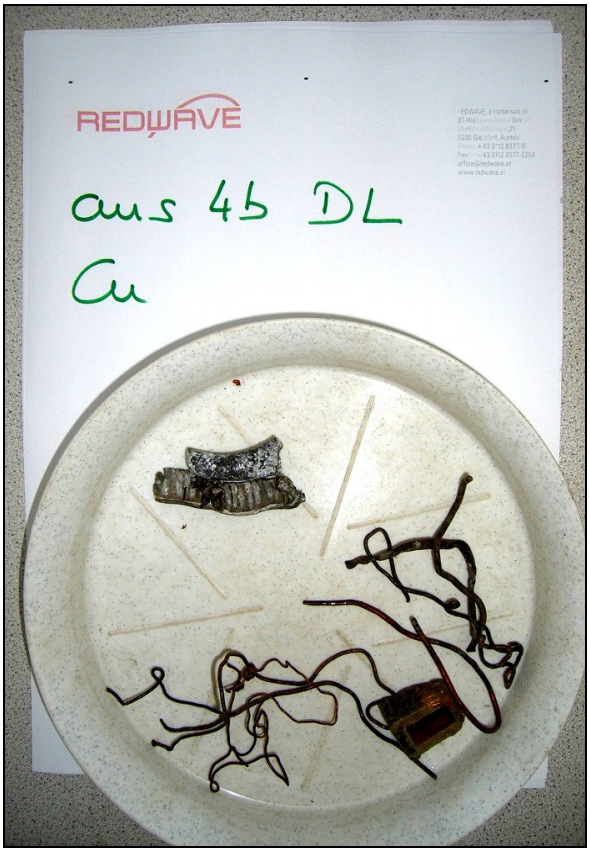

Figure 56 Photograph of Test 4b- Throughput, Cu-pieces

Figure 57 Photograph of Test 4b Throughput, Remain

4.3.5 Discussion and Comments

4.3.5.1 Test Results

Both, Fraction 2 with Test 1-3 and Fraction 1 with Test 4-4b were done with a material amount of 5350 g respectively 6436 g and a duration of 10-15 seconds per test. Hence, estimation regarding the capacity in the range of several double-digit tons per hour cannot be done based on these tests. This implies further testing at larger scale.

Fraction 2, Test 1-3

In concluding, both tests were satisfying. At Fraction 2 all three tests had same and comparable results (deviation 2.2 % for efficiency and 0.3 % for purity). An efficiency of 97.2 % for a one step separation is terrific but in contrary the purity of 92 % for all three tests has not turned out satisfactory and needs to be improved. As already mentioned wires are always problematic and never entirely avoidable. Despite wires also a certain amount of rectangular shaped objects were ejected. Explanations for these miss shots may be agglomerations, a heterogeneous composition (existence of detectable elements), a capture by the air blast of detected objects (due to a too long blow out time) or a non-reaching of the divider due to too heavy weight. Furthermore, software issues in calculation may have caused miss detections. But since these explanations are only assumptive, a further improvement and testing is necessary and essential to get a higher purity.

Fraction 1, Test 4

The separation of CRES out of Fraction 1 at Test 4 reached an efficiency of 93.2 %. The efficiency is satisfactory, CRES-pieces in throughput were mainly of round shape or wires. Both are for already mentioned reasons always difficult to eject. The purity with 91.8 % is similar to the purity of Fraction 2 and not really satisfactory. For Fraction 1 Test 4 apply same conditions as for Fraction 2. Furthermore, the cause of miscellaneous pieces to be in ejection chute is still unknown and requires further and more detailed research.

Fraction 1, Test 4a

For a discussion of Test 4a, the separation of brass out of the throughput of Test 4, further information regarding the assignment of task needs to be known. Whether certain proportions of Zn-pieces in the Cu-fraction bother or not is unknown and depends on the customer respectively the further treatment. The assumption Zn-pieces to be non-troublesome in the Cu-fraction was done due to present Zn-content in brass but is arbitrary supposition. The efficiency is with 95.4 % (inclusive Zn-pieces) respectively 94.1 % (exclusive Zn-pieces) in both cases terrific since the Cu-part in throughput only consisted of three pieces with roundish shape. The purity was with 94.3 % including the Zn-pieces good but has still room for improvement. A poor result had the purity by consideration of only the brass pieces to be allowed in the ejection. With 75.9 % only three out of four pieces were

brass. The most reliable explanation for the bad purity is detection and software issues due to the Cu/Zn-ratio as explained in the previous chapter. Furthermore, agglomerates, too little mass, complicated shape, accidentally ejections etc. are always possible reasons.

Fraction 1, Test 4b

The separation of copper (Test 4b) was the final separation step of Fraction 2 and reached an efficiency of 95.4 % by a purity of 95.4 % as well. Since the wire-fraction contains beside two CRES-wires only insulated/non-insulated Cu-wires, assumed 90 % of the mass were counted to the Cu-fraction. Additionally, all Cu-objects above a Cu-content of 50 % were defined as copper. For an accurate interpretation detailed assignment of task of the customer is obligatory. By implication of mentioned assumption, an efficiency of 95.4 % can be seen as excellent. Most of Cu-pieces of the input were of round/roundish shape respectively wires which are as above mentioned always problematic to eject. Additionally, the Cu-part of the throughput consisted of only wires (beside one object having rectangular shape and a big hole). Hence, also the purity with 95.4 % is good under given circumstances.

After all three steps (separation of CRES Test a, separation of brass- Test 4a and separation of Cu-Test 4b) a mass of 4683 g was ejected by an input of 6436 g and an output (Remain-fraction plus Cu-loss) of 1753 g. This results in an ejection rate of 73 % of the input. The Remain-fraction can be subdivided in two main parts, one containing all remaining resources with shapes difficult to eject and a second including all “useless material” (insulation without wire, various plastic-pieces, stones, slag-pieces, various metal, agglomerates, miscellaneous etc.). A further treatment of the Remaining-fraction seems to be not economical.

4.3.5.2 Test Specifications

Ratio vs. Single Threshold

For sorting criterion of **CRES-separation** only a threshold of chromium was used. This is due to weak detection of nickel relative to chromium. As described in Chapter 2.5 indirect excitation (secondary as well as tertiary excitation) is particularly strong for elements differing by two in the atomic number. Hence, nickel leads to a secondary excitation of iron and to a tertiary excitation of chromium and furthermore iron leads to a secondary excitation of chromium. This means chromium is beside regular excitation additionally excited by a secondary excitation of iron and a tertiary excitation of nickel, and iron by a secondary excitation of nickel. This leads to a significant stronger excitation of chromium. Contribution amounts up to 30 % from secondary excitation and up to 2.5 % from tertiary excitation. As the extent of this effect in real was unknown and no testing was done either, only a threshold for chromium was used instead of a ratio Cr/Ni. In principle this has no negative effect on separation but chromium-plated material was then also defined as CRES.

For **brass-separation** a ratio as well as a Cu-threshold was used for detection. The Cu-threshold is needed since a ratio of Cu/Zn as set with 0.8-2.0 is always likely. Detection of photons at this energy respectively at every energy range constantly takes place even

though certainly at a low extent. Brass with its constituents copper and zinc has negligible indirect excitation effects. Hence, both a ratio and a single threshold were used as sorting criterion.

The single threshold as used for CRES- and Cu-separation was the lowest possible and estimated by running the system with empty belt for a time of > 5 min and no false detection occurring.

Distance to Detection Unit

The **distance Gap_Max** for Fraction 1 and Fraction 2 was chosen due to particle size. Even though the material was sieved, some objects (mainly of round shape) had a size extending the distance between detection unit and conveyer belt. Such objects could have caused irreparable damages of the bottom side of the detection unit. Experiences in glass-sorting show that especially the Kapton-window is susceptible for damage. The loss of intensity due to greater distance was taken deliberately (compare Chapter 2.2).

Pressure

Both fractions were tested at pressure for ejection valves of 8 bars. This pressure was chosen for ensuring a reliable ejection of detected material. In general, the material size composition was relatively homogenous and the material was sieved before separation. Nevertheless, a few especially round objects were of longer shape and heavier than the average. To ensure also a reliable ejection of these objects a pressure higher than probably needed was used. Higher pressure consumption leads to a higher energy use and is furthermore cost intensive. Therefore, the minimum needed pressure should be evaluated in further tests to have the economical facts optimized

Blow Out Time

For all tests the blow out time was set 50 ms. The parameter blow out time sets the minimal time interval each valve respectively its correlated nozzles open for the compressed air blow. If the material size, however, exceeds 50 ms (at a conveyer belt speed of 1.65 m/s this would be > 82.5 mm, 3.25 in), then the valve is open as long as the threshold is exceeded and a signal is triggered (compare 3.4.6.15). In general, the adjusted blow out time should approximately be equal the minimal average material length. In order to get reliable separation, the blow out time was set slightly higher than the minimal average material length of Fraction 1 and Fraction 2. A too long blow out time certainly causes more ejection of unwanted objects. This is a reason for some impurities in the ejection chute and the lower purity at some tests.

Tube Voltage

For all tests the tubes voltage was set 30 kV. As explained in Chapter 3.4.6.1 a rule of thumb regarding tube voltage is to a set the voltage roughly three times the energy of the principle line of the element to be detected. The energy of principle lines for chromium, copper and zinc is between 5.41 keV (Cr-Kα) and 8.64 keV (Zn-Kα). Hence, the used voltage of 30 kV is reasonable and by knowledge for now the best value for an application likes this. In general having applications with several elements deciding principle line is whose with the higher energy (Zn-Kα with 8.64 keV).

Tube Current

The current is linear correlated to the intensity respectively the count rate. An increased current leads to higher count rates. The limit of count rate based to used detectors needs to be considered in order to avoid an increase of dead time. For all tests a current of 1200 µA was used. This is an empiric value of previous tests and can be seen as adequate for metal scrap (compare Chapter 3.4.6.2).

5 Results and Discussion

In the last decades an enormous developing process in waste management took place. Starting with the separated collection of some recyclables, nowadays a lot of different fractions are collected separately. Waste management leads to recycling economy and cleaner production and away from landfill and unnecessary disposal of (secondary) resources. Even though, waste collection has reached a high standard, an after-treatment of every single waste fraction is still obligatory and will be more and more necessary in the future. Not only extinguish primary resources that can be (partly) replaced by secondary resources out of waste, or rising prices for raw materials as well as for energy in general will appear, but also more and more laws and regulations such as landfill prohibitions or recycling rates are adopted. The separation of waste will get more and more economic and ecologic in the next time. Furthermore, more and more waste fractions not treated now will be treated in the future due to reason of resource recovery, regulations etc.

REDWAVE XRF is a sensor-based sorting system with detection based on X-ray fluorescence. This technique is independent on color and most surface impurities of the material to be sorted. It identifies the elemental composition of each object and separates those that meet adjusted sorting criteria. Problems may cause strong impurities of the surface since X-ray radiation only reaches a certain depth. REDWAVE XRF is already in commercial use in the field of glass-sorting, more precisely the separation of glass ceramic (CSP) and leaded glass. Lead is a typical example of upcoming regulations of the EU. Recently the lead content has been limited to 200 ppm for glass containers. Apart from mentioned glass-sorting, there are a few promising areas of applications for REDWAVE XRF. First, the resource recovery from material such as scrap metal or electronic boards. Already done sorting tests show budding results. In general, with this system various kinds of metals can be identified, but in this case especially CRES, brass and copper are of interest. Iron or aluminum can easily be separated by magnets or eddy currents. Secondly, the sorting of minerals and ores show high potential. In mining the exploration of wanted minerals and ores always goes along with unwanted rocks such as gangue. Furthermore, minerals and ores may have contaminating inclusions (e.g. mercury, plutonium) that can be separated. Another promising area of application is quality control. REDWAVE XRF is also applicable as online quality control in various fields of applications either via the analysis of a bypass-stream or the whole product-stream. According to requirements, different elements as search key can be adjusted. These elements can be continuously identified and evaluated then recorded, giving assurance of a quality material.

For the use in further area of applications respectively for enhancing the system, different modifications and extensions could be done. On the one hand a combination of X-ray fluorescence with camera provides object recognition. With object recognition, allocation of every single object is achievable. This would make negative-sorting and positive-sorting in every field possible since beside detectable objects also not detectable objects (light matrix with no distinguishing element) would be visible. Furthermore, quality control not only by measuring the count rate but also by a real quantitative analysis was feasible. Hence,

reliable quantitative analysis could be done. This is certainly tough, since calculation algorithms that correlate the content of elements to materials size, needs to be estimated. Despite from object recognition, another interesting modification would be calibration without pure elements. By doing so, the allocation of principle lines with certain energies to elements was done by the software itself. Hence, every single element in the periodic table of elements that is identifiable could be easily implemented without the need of the pure elements as a reference (hazardous elements or compounds). On the other hand a new "waterfall-principle" would improve detection and ejection. The material is then detected in free fall. This eliminates disturbing background noise (no conveyer belt needed) which then results in an increased detection limit. Furthermore, it reduces the required air pressure for ejection since material to be ejected needs deflection at a lower extent compared to above described design. Additionally, with a waterfall-principle it is possible to getting rid of miss shots caused by round/roundish objects and the sorting of in-feed material having a wider particle size gets easier. Despite already mentioned enhancements, improved technical devices as more sensible detectors, new upgraded electronic tools (e.g. DCM) or enhanced detectors would also lead to an improved system. Especially the use of SDD detectors is seen to be a huge step forward. SDD have decreased noise, shorter shaping times and faster counting than the used Si-PIN detectors.

In conclusion, the system is capable of sorting different materials in various areas of application. In glass-sorting REDWAVE XRF is already in commercial use, but also tests in other fields show promising results. In contrary, the system is only the right choice if no (cheaper) alternatives are capable of fulfilling the assignment of task. If (cheaper) alternatives are available and have similar sorting results as this system, then in general, the decision would be made based on economic facts for the alternative (several cost-effective devices such as X-ray tubes, detectors etc.). Above mentioned improvements would definitely result in a more efficient system and lead to a more technically mature system. By realizing such extensions and modifications, REDWAVE XRF would definitely become a stronger alternative for various areas of applications.

6 Conclusion

In the recent decades waste management developed away from throwaway society towards recycling, waste recovery and waste treatment. This development is a result of extinguishing primary resources, rising energy prices and increasing prices for raw materials, but also due to stricter getting laws as landfill prohibitions or recycling rates. Even though waste collection is at a high standard nowadays, an after treatment of most waste streams is obligatory. Sensor-based sorting systems using different physical principle for detection such as “Near Infrared Spectroscopy”, “Infrared-Transmission” and “Line Scan Cameras” have taken over the recycling market. A new sensor-based sorting system, named REDWAVE XRF, based on X-ray fluorescence analysis was developed by BT-Wolfgang Binder GmbH in collaboration with Innov-X Systems.

X-rays were discovered by W. C. Röntgen in 1885 in his laboratory at the Julius-Maximilians University in Würzburg, Bavaria. They are high energy, electromagnetic waves with a wavelength range of 0.001 nm to 80 nm (between UV-light and Gamma-rays) corresponding to energies between 1.2 MeV and 15 eV. When X-rays strike matter different interactions take place, diversion into heat, different scattering processes and emission of photons. In REDWAVE XRF X-ray tubes providing a maximum voltage of 50 kV are used as X-ray source. Scattering can be separated in Rayleigh scattering and Compton scattering. Compton scattering is the interaction of photons with weakly bounded electrons of the outer orbital and results in a transfer of energy. The wavelength of the scattered photon is thus longer (has less energy). At Rayleigh scattering no energy transfer takes place and the incident photon and the scattered photon have the same wavelength and energy. Rayleigh scattering is the interaction of radiation with strongly bounded inner orbital electrons. The emission of photons also referred to as Photoelectric effect takes place if the energy of the incident radiation exceeds the bond energy of electrons on the orbital. The quantity of absorbed energy is equal to the bond energy of the emitted electrons. Is an inner electron removed from its orbital, a vacancy occurs and the atom gets ionized. This vacancy is being replaced by an electron transition from an outer orbital within picoseconds. Photoelectric effect is most effective for energies just above the absorption edge of the interacting element (respectively the interacting electron transition). Since the bond energy of outer orbital electrons is always higher than inner ones, energy is obtained during the electron transition. This energy can either be emitted as secondary fluorescence radiation or as Auger-electron. Which mechanism is more likely to take place, is governed by quantum-mechanical selection rules and depends on the atomic number and the electron transition. In general, the fraction of fluorescence radiation increases with rising atomic number. Both, secondary fluorescence radiation and Auger electrons are characteristic for each element and its electron transition making quantitative and qualitative analysis possible. Auger electrons have very low energies and are thus not of importance for REDWAVE XRF. X-ray fluorescence is the emission of characteristic secondary X-rays (photons) from atoms that have been excited by X-rays. By measuring this radiation with detectors, it is possible to determine the elemental composition of the targeted object material. REDWAVE XRF uses energy dispersive X-ray fluorescence analysis as sorting criterion. Generally, a lot different electron transitions can

origin but only a few are of likelihood high enough to be used as sorting criterion. These are the strong K and L-lines.

REDWAVE XRF is assembled as all sensor-based sorting system and consists in general of four main assemblies, vibratory feeder and conveyer belt, detection system, control and evaluation unit and ejection unit. Sorting material is constantly fed onto a conveyer belt by a vibratory feeder. The conveyer belt accelerates, separates and transfers the material towards detection area where it is excited by X-rays. Detectors capture secondary X-ray radiation emitted by the sample material. The detector signal is constantly evaluated by the control and evaluation unit and if it meets the set sorting criteria a further signal is sent to the ejection unit. High speed valves and air jets operated by compressed air then reject those materials. Depending on the sorting width, a different number of X-ray tubes and detectors are implemented. The detection is based on comparison of the steadily detected photons with a calibrated value and whether it meets a certain adjustable threshold. Before any measurement can take place standardization is required. At standardization the energy is correlated to an internal Bin-number. It can be done by any element having strong principle lines. The peak energy is known and then correlated to its Bin-number, giving all energies its correlated Bin-number. The system is able to detect signals within the energy rage of 0 to 40 keV. After that, a calibration of all elements of desired detection is needed. This is done by detection of strong principle lines and pure element plates. Measurement time is about 30 ms. Hence, only qualitative analysis is possible.

A reliable detection and separation is dependent on various different **factors of influence**. First, the X-ray tube influences the detection in several ways. Set parameters such as tube voltage, tube current and filament current are of importance. Besides that, the choice of the anode material is of high interest as well. Secondly, used filters positioned between X-ray tube and sample and the distance effect the intensity of radiation. While filters are implemented deliberately to avoid unwanted detections, is the attenuation due to the distance between X-ray tube, material and detectors always crucial, since the intensity of radiation is described by the inverse-square law. The adjusted distance is always a compromise between required gap due to material size and intensity loss. Thirdly, various influences due to physics effect the detection including the choice of the principle line and its similarities in energy and possible overlapping with other principle lines, interactions of X-rays with matter (Compton and Rayleigh scattering as well as Auger effect) and the excitation of atoms due to secondary excitation. Fourthly, the conveyer belt speed and the measurement time but also the set blow out time and the background material as well as the composition of the conveyer belt effect the detection. Fifthly, the material to be sorted more precisely the material size, content of detectable element, the matrix and surface contaminations determine the level of possible detection. Finally, a well done standardization and calibration is certainly required as well.

The **areas of applications** for REDWAVE XRF are versatile. In general, all solid materials which contain a specific and characteristic element above detection limit can be analyzed and separated. Possible areas of applications include the material classes glass (separation

of leaded glass and glass ceramics, etc.), metals (separation of stainless steel, non-ferrous metals such as brass, bronze, copper, zinc etc. out of metal scrap), ores and minerals (sorting of ores and minerals according to purity grade, separation of polluted inclusions etc.), plastics (color independent separation of PVC) and electronic scrap (separation of electronic scrap coated with bromine and cadmium from shredded electronic scrap). Furthermore, the system is also applicable as online quality control in mentioned areas. Different adjustable elements are continuously identified and evaluated then recorded, giving assurance of a quality material. The separation of leaded glass and glass ceramics is a commercial use. Test with other materials show promising results. A detailed sorting test with scrap metal description is included in this work.

The system is independent on color and most surface impurities and is capable of sorting different materials in various areas of application. For the use in other areas respectively for enhancing the system different modifications and extensions could be done. The combination of the existing detection system with camera would provide object recognition and allocation of every single object of the input. The calibration with allocation of the principle lines by the software and without pure elements can avoid troubles with hazardous materials and make the calibration a lot easier. Furthermore, a new principle of sorting, the “waterfall-principle” will improve detection and ejection. Since the material is detected in free fall this eliminates disturbing background noise. Additionally, the waterfall principle reduces the required air pressure, eliminates miss shots of round/roundish objects and makes the sorting of material with a wider particle size easier. Despite mentioned enhancements, improved technical devices such as the use of SDD (silicon drift detector) and upgraded electronic boards (DCM, LPM etc.) will also lead to an improved system.

7 Appendices

7.1 Bibliography

[1] Beckhoff B. et al: Handbook of Practical X-Ray Fluorescence Analysis, Springer-Verlag Berlin Heidelberg, Berlin, 2006, ISBN-10 3-540-28603-9

[2] Winklmair D.: RFA- Röntgenfluoreszenzanalyse, Download: http://www.winklmair.de/ianSS09/Texte/RFA.pdf, Date: 20.09.2010

[3] Laboratory for Atmospheric and Space Physics- University of Colorado: Electromagnetic Spectra, Download: http://lasp.colorado.edu/cassini/images/Electromagnetic%20Spectrum_noUVIS.pdf, Date: 10.11.2010

[4] Spektrum- Akademischer Verlag (Editor): Lexikon der Physik

[5] Pichl E. et al: Skriptum Strahlenschutzausbildung für nichtmedizinische Anlagen, WIFI Österreich, Graz, 2009

[6] Pahlke A. et al: Versuchsanleitung Fortgeschrittenenpraktikum: Röntgen-fluoreszenzanalyse mit einem Silizium-Driftdetektor, Halbleiterlabor der Max-Planck-Institute für Physik und für extraterrestrische Physik, München, 2002, Download: http://www.hll.mpg.de/07_publication/2002/praktikum.pdf, Date: 20.09.2010

[7] SII NanoTechnology Inc., X-Ray tube, Download: http://www.siint.com/en/images/technology/XRF_e_figure03.jpg, Date: 10.11.2010

[8] InnovX Systems: Periodic Table of the Elements- Elements detectable

[9] Hippert F. et al: Neutron and X-ray spectroscopy, Springer, Dordrecht, 2006, ISBN-10 1-4020-3336-2 (HB)

[10] Meirer F.: Integration eines Silizium-Drift-Detektors in einen vollautomatischen Totalreflexions-Röntgenfluoreszenz-Waferanalysator, Technische Universität Wien-Atominstitut der Österreichischen Universitäten, Wien, 2005

[11] A. Thompson et al: X-Ray Data Booklet, University of Carolina- Lawrence Berkely National Laboratory, Berkely, 2009

[12] Tsuji K. et al: X-ray spectrometry: recent technological advances, John Wiley & Sons Ltd, Chichester, 2004, ISBN 0-471-48640-X

[13] Winklmair D.: Röntgenspektrometrie, Download: http://www.winklmair.de/ianSS09/Folien/Roentgenspektrometrie.pdf, Stand 18.10.2010.

[14] Mantler M.: Der Kaskadeneffekt in der Röntgenfluoreszenzanalyse, Technische Universität Wien- Institut für Festkörperphysik, Wien, 2007

[15] International Centre of Diffraction: Advances in X-ray Analysis, 2002, Download: http://www.icdd.com/resources/axa/vol45/V45_79.pdf, Date: 07.03.2011

[16] Jenkins R. et al: Nomenclature System for X-ray Spectroscopy, IUPAC- International Union for Pure and Applied Chemistry, Great Britain, 1991, Download: http://www.iupac.org/publications/pac/1991/pdf/6305x0735.pdf, Date: 22.1.2010

[17] Hyper Physics- George State University: Rayleigh Scattering, Download: http://hyperphysics.phy-astr.gsu.edu/hbase/atmos/blusky.html#c2, Date: 15.11.2010

[18] Machinery Lubrication: XRF A Powerful Oil Analysis Tool, Download: http://www.machinerylubrication.com/Read/602/xrf-oil-analysis, Date: 07.04.2011

[19] Stöcker H.: Fortgeschrittenenpraktikum RS- Röntgenspektren, Technische Universität Dresden- ISP Institut für Strukturphysik, Dresden, 2009

[20] E-Mail, Jansen T., Innov-X Systems, Date: 28.03.2011

[21] E-Mail, Hubbard-Nelson B., Innov-X Systems, Date: 12.04.2011

[22] Jansen T et al, Detection of Bromine Contamination in Goodyear Rubber Samples using the X-Stream Glass Sorter, Innox-X Systems, 2010

[23] E-Mail, Jansen T., InnovX- Systems, Date: 01.04.2011

[24] Phone call, Hubbard-Nelson B., Innov-X Systems, Date: 01.04.2011

[25] Cartz L.: Nondestructive Testing- Radiography- Ultrasonics- Liquid Penetrant- Magnetic Particle- Eddy Current, ASM International, USA, 1999

[26] Chourasia A.R. et al: Auger Electron Spectroscopy, Texas A&M University- Commerce Department of Physics, Texas

[27] E-Mail, Hubbard-Nelson B., Innov-X Systems, Date: 19.05.2011

[28] Innov-X Systems, Elements Detectable, Download: http://www.innovx.com/system/files/Handheld_Periodic%20Table%20of%20Elements-LOD%20sheet_104-3.11_1.pdf, Date: 15.11.2010

[29] Varian Medical Systems, Datasheet X-ray tube VF 50j , Download: http://www.varian.com/media/xray/products/pdf/vf50j.pdf, Date: 28.03.2011

[30] Amptek, Datasheet Si-PIN Detector XR-100 CR, Download: http://www.amptek.com/pdf/xr100cr.pdf, Date: 28.03.2011

[31] Innov-X Systems, Datasheet Alpha-2000 Portable XRF Analyzer, Download: http://www.innovx.com/products/alpha, Date: 28.03.2011

7.2 List of Abbreviations

µA	Micro Amperes
µs	Micro Seconds
Be	Beryllium
CCD	Charge-Couple Device
Cr	Chromium
CRES	Corrosion-Resistant Steel
CSP	Ceramic, stone, porcelain
Cu	Copper
DCM	Diverter Channel Module
EDX	Energy dispersive Spectrometer
EDXRF	Energy Dispersive X-ray Fluorescence Analysis
EU	European Union
eV	Electronvolt
Fe	Iron
FEL	Free Electron Laser
FWHM	Full width half maximum
G	Giga
GeV	Giga Electronvolts
H	Hydrogen
He	Helium
ICR	Input Count Rate
in	Inch
IUPAC	International Union for Pure and Applied Chemistry
KCl	Potassium chloride
kV	Kilo Volts
kW	Kilo Watts

Li	Lithium
LPM	Local Processor Module
M	Mega
MBq	Mega Becquerel
MCA	Multichannel Analyzer
Mev	Mega Electronvolts
Mg	Manganese
Mn	Magnesium
Mo	Molybdenum
NaCl	Sodium chloride
Nb	Niobium
Ni	Nickel
Nm	namometer
OCR	Output Count Rate
PLC	Programmable Logic Controller
PMI	Positive Material Identification
ppm	Parts per Million
Ps	Picosecond
Pu	Plutonium
Rh	Ruthenium
RoHS	Restriction of Hazardous Substandes
RTM	Rhenium-Tungsten-Molybdenum
SDD	Silicon-Drift-Detector
Si-PIN	Silicon-Positive Intrinsic Negative
SR	Synchrotron Radiation
Ti	Titanium
UI	User Interface
UV	Ultra violet
V	Vanadium
WDX	Wavelength Dispersive Spectrometer
WDXRF	Wavelength Dispersive X-ray Fluorescence Analysis
WEEE	Waste Electrical and Electronic Equipment Directive
XRF	X-ray fluorescence
Z	Atomic number
Zr	Zirconium

7.3 List of Tables

7.4 List of Figures

Appendix

I. Electron Binding Energies [11 p. 1-2 – 1-7]

The energies are given in [eV].

"*", "†" and "b" mean the taken reference;
"a" One-particle approximation not valid owing to short ore-hole lifetime

Element	K 1s	L_1 2s	L_2 $2p_{1/2}$	L_3 $2p_{3/2}$	M_1 3s	M_2 $3p_{1/2}$	M_3 $3p_{3/2}$	M_4 $3d_{3/2}$	M_5 $3d_{5/2}$	N_1 4s	N_2 $4p_{1/2}$	N_3 $4p_{3/2}$
1 H	13.6											
2 He	24.6*											
3 Li	54.7*											
4 Be	111.5*											
5 B	188*											
6 C	284.2*											
7 N	409.9*	37.3*										
8 O	543.1*	41.6*										
9 F	696.7*											
10 Ne	870.2*	48.5*	21.7*	21.6*								
11 Na	1070.8†	63.5†	30.65	30.81								
12 Mg	1303.0†	88.7	49.78	49.50								
13 Al	1559.6	117.8	72.95	72.55								
14 Si	1839	149.7*b	99.82	99.42								
15 P	2145.5	189*	136*	135*								
16 S	2472	230.9	163.6*	162.5*								
17 Cl	2822.4	270*	202*	200*								
18 Ar	3205.9*	326.3*	250.6†	248.4*	29.3*	15.9*	15.7*					
19 K	3608.4*	378.6*	297.3*	294.6*	34.8*	18.3*	18.3*					
20 Ca	4038.5*	438.4†	349.7†	346.2†	44.3 †	25.4†	25.4†					
21 Sc	4492	498.0*	403.6*	398.7*	51.1*	28.3*	28.3*					
22 Ti	4966	560.9†	460.2†	453.8†	58.7†	32.6†	32.6†					
23 V	5465	626.7†	519.8†	512.1†	66.3†	37.2†	37.2†					
24 Cr	5989	696.0†	583.8†	574.1†	74.1†	42.2†	42.2†					
25 Mn	6539	769.1†	649.9†	638.7†	82.3†	47.2†	47.2†					
26 Fe	7112	844.6†	719.9†	706.8†	91.3†	52.7†	52.7†					
27 Co	7709	925.1†	793.2†	778.1†	101.0†	58.9†	59.9†					
28 Ni	8333	1008.6†	870.0†	852.7†	110.8†	68.0†	66.2†					
29 Cu	8979	1096.7†	952.3†	932.7	122.5†	77.3†	75.1†					
30 Zn	9659	1196.2*	1044.9*	1021.8*	139.8*	91.4*	88.6*	10.2*	10.1*			
31 Ga	10367	1299.0*b	1143.2†	1116.4†	159.5†	103.5†	100.0†	18.7†	18.7†			
32 Ge	11103	1414.6*b	1248.1*b	1217.0*b	180.1*	124.9*	120.8*	29.8	29.2			
33 As	11867	1527.0*b	1359.1*b	1323.6*b	204.7*	146.2*	141.2*	41.7*	41.7*			
34 Se	12658	1652.0*b	1474.3*b	1433.9*b	229.6*	166.5*	160.7*	55.5*	54.6*			
35 Br	13474	1782*	1596*	1550*	257*	189*	182*	70*	69*			
36 Kr	14326	1921	1730.9*	1678.4*	292.8*	222.2*	214.4	95.0*	93.8*	27.5*	14.1*	14.1*
37 Rb	15200	2065	1864	1804	326.7*	248.7*	239.1*	113.0*	112*	30.5*	16.3*	15.3 *
38 Sr	16105	2216	2007	1940	358.7†	280.3†	270.0†	136.0†	134.2†	38.9†	21.3	20.1†
39 Y	17038	2373	2156	2080	392.0*b	310.6*	298.8*	157.7†	155.8†	43.8*	24.4*	23.1*
40 Zr	17998	2532	2307	2223	430.3†	343.5†	329.8†	181.1†	178.8†	50.6†	28.5†	27.1†
41 Nb	18986	2698	2465	2371	466.6†	376.1†	360.6†	205.0†	202.3†	56.4†	32.6†	30.8†
42 Mo	20000	2866	2625	2520	506.3†	411.6†	394.0†	231.1†	227.9†	63.2†	37.6†	35.5†
43 Tc	21044	3043	2793	2677	544*	447.6	417.7	257.6	253.9*	69.5*	42.3*	39.9*
44 Ru	22117	3224	2967	2838	586.1*	483.5†	461.4†	284.2†	280.0†	75.0†	46.3†	43.2†
45 Rh	23220	3412	3146	3004	628.1†	521.3†	496.5†	311.9†	307.2†	81.4*b	50.5†	47.3†
46 Pd	24350	3604	3330	3173	671.6†	559.9†	532.3†	340.5†	335.2†	87.1*b	55.7†a	50.9†
47 Ag	25514	3806	3524	3351	719.0†	603.8†	573.0†	374.0†	368.3	97.0†	63.7†	58.3†

Element	N_4 $4d_{3/2}$	N_5 $4d_{5/2}$	N_6 $4f_{5/2}$	N_7 $4f_{7/2}$	O_1 5s	O_2 $5p_{1/2}$	O_3 $5p_{3/2}$	O_4 $5d_{3/2}$	O_5 $5d_{5/2}$	P_1 6s	P_2 $6p_{1/2}$	P_3 $6p_{3/2}$
48 Cd	11.7†	10.7†										
49 In	17.7†	16.9†										
50 Sn	24.9†	23.9†										
51 Sb	33.3†	32.1†										
52 Te	41.9†	40.4†										
53 I	50.6	48.9										
54 Xe	69.5*	67.5*	—	—	23.3*	13.4*	12.1*					
55 Cs	79.8*	77.5*	—	—	22.7	14.2*	12.1*					
56 Ba	92.6†	89.9†	—	—	30.3†	17.0†	14.8†					
57 La	105.3*	102.5*	—	—	34.3*	19.3*	16.8*					
58 Ce	109*	—	0.1	0.1	37.8	19.8*	17.0*					
59 Pr	115.1*	115.1*	2.0	2.0	37.4	22.3	22.3					
60 Nd	120.5*	120.5*	1.5	1.5	37.5	21.1	21.1					
61 Pm	120	120	—	—	—	—	—					
62 Sm	129	129	5.2	5.2	37.4	21.3	21.3					
63 Eu	133	127.7*	0	0	32	22	22					
64 Gd	—	142.6*	8.6*	8.6*	36	28	21					
65 Tb	150.5*	150.5*	7.7*	2.4*	45.6*	28.7*	22.6*					
66 Dy	153.6*	153.6*	8.0*	4.3*	49.9*	26.3	26.3					
67 Ho	160*	160*	8.6*	5.2*	49.3*	30.8*	24.1*					
68 Er	167.6*	167.6*	—	4.7*	50.6*	31.4*	24.7*					
69 Tm	175.5*	175.5*	—	4.6	54.7*	31.8*	25.0*					
70 Yb	191.2*	182.4*	2.5*	1.3*	52.0*	30.3*	24.1*					

Element	K 1s	L_1 2s	L_2 $2p_{1/2}$	L_3 $2p_{3/2}$	M_1 3s	M_2 $3p_{1/2}$	M_3 $3p_{3/2}$	M_4 $3d_{3/2}$	M_5 $3d_{5/2}$	N_1 4s	N_2 $4p_{1/2}$	N_3 $4p_{3/2}$
71 Lu	63314	10870	10349	9244	2491	2264	2024	1639	1589	506.8*	412.4*	359.2*
72 Hf	65351	11271	10739	9561	2601	2365	2108	1716	1662	538*	438.2†	380.7†
73 Ta	67416	11682	11136	9881	2708	2469	2194	1793	1735	563.4†	463.4†	400.9†
74 W	69525	12100	11544	10207	2820	2575	2281	1872	1809	594.1†	490.4†	423.6†
75 Re	71676	12527	11959	10535	2932	2682	2367	1949	1883	625.4†	518.7†	446.8†
76 Os	73871	12968	12385	10871	3049	2792	2457	2031	1960	658.2†	549.1†	470.7†
77 Ir	76111	13419	12824	11215	3174	2909	2551	2116	2040	691.1†	577.8†	495.8†
78 Pt	78395	13880	13273	11564	3296	3027	2645	2202	2122	725.4†	609.1†	519.4†
79 Au	80725	14353	13734	11919	3425	3148	2743	2291	2206	762.1†	642.7†	546.3†
80 Hg	83102	14839	14209	12284	3562	3279	2847	2385	2295	802.2†	680.2†	576.6†
81 Tl	85530	15347	14698	12658	3704	3416	2957	2485	2389	846.2†	720.5†	609.5†
82 Pb	88005	15861	15200	13035	3851	3554	3066	2586	2484	891.8†	761.9†	643.5†
83 Bi	90524	16388	15711	13419	3999	3696	3177	2688	2580	939†	805.2†	678.8†
84 Po	93105	16939	16244	13814	4149	3854	3302	2798	2683	995*	851*	705*
85 At	95730	17493	16785	14214	4317	4008	3426	2909	2787	1042*	886*	740*
86 Rn	98404	18049	17337	14619	4482	4159	3538	3022	2892	1097*	929*	768*
87 Fr	101137	18639	17907	15031	4652	4327	3663	3136	3000	1153*	980*	810*
88 Ra	103922	19237	18484	15444	4822	4490	3792	3248	3105	1208*	1058	879*
89 Ac	106755	19840	19083	15871	5002	4656	3909	3370	3219	1269*	1080*	890*
90 Th	109651	20472	19693	16300	5182	4830	4046	3491	3332	1330*	1168*	966.4†
91 Pa	112601	21105	20314	16733	5367	5001	4174	3611	3442	1387*	1224*	1007*
92 U	115606	21757	20948	17166	5548	5182	4303	3728	3552	1439*b	1271*b	1043†

Element	N_4 $4d_{3/2}$	N_5 $4d_{5/2}$	N_6 $4f_{5/2}$	N_7 $4f_{7/2}$	O_1 5s	O_2 $5p_{1/2}$	O_3 $5p_{3/2}$	O_4 $5d_{3/2}$	O_5 $5d_{5/2}$	P_1 6s	P_2 $6p_{1/2}$	P_3 $6p_{3/2}$
71 Lu	206.1*	196.3*	8.9*	7.5*	57.3*	33.6*	26.7*					
72 Hf	220.0†	211.5†	15.9†	14.2†	64.2†	38*	29.9†					
73 Ta	237.9†	226.4†	23.5†	21.6†	69.7†	42.2*	32.7†					
74 W	255.9†	243.5†	33.6*	31.4†	75.6†	45.3*b	36.8†					
75 Re	273.9†	260.5†	42.9*	40.5*	83†	45.6*	34.6*b					
76 Os	293.1†	278.5†	53.4†	50.7†	84*	58*	44.5†					
77 Ir	311.9†	296.3†	63.8†	60.8†	95.2*b	63.0*b	48.0†					
78 Pt	331.6†	314.6†	74.5†	71.2†	101.7*b	65.3*b	51.7†					
79 Au	353.2†	335.1†	87.6†	84.0	107.2*b	74.2†	57.2†					
80 Hg	378.2†	358.8†	104.0†	99.9†	127†	83.1†	64.5†	9.6†	7.8†			
81 Tl	405.7†	385.0†	122.2†	117.8†	136.0*b	94.6†	73.5†	14.7†	12.5†			
82 Pb	434.3†	412.2†	141.7†	136.9†	147*b	106.4†	83.3†	20.7†	18.1†			
83 Bi	464.0†	440.1†	162.3†	157.0†	159.3*b	119.0†	92.6†	26.9†	23.8†			
84 Po	500*	473*	184*	184*	177*	132*	104*	31*	31*			
85 At	533*	507	210*	210*	195*	148*	115*	40*	40*			
86 Rn	567*	541*	238*	238*	214*	164*	127*	48*	48*	26		
87 Fr	603*	577*	268*	268*	234*	182*	140*	58*	58*	34	15	15
88 Ra	636*	603*	299*	299*	254*	200*	153*	68*	68*	44	19	19
89 Ac	675*	639*	319*	319*	272*	215*	167*	80*	80*	—	—	—
90 Th	712.1†	675.2†	342.4†	333.1†	290*a	229*a	182*a	92.5†	85.4†	41.4†	24.5†	16.6†
91 Pa	743*	708*	371*	360*	310*	232*	232*	94*	94*	—	—	—
92 U	778.3†	736.2†	388.2*	377.4†	321*ab	257*ab	192*ab	102.8†	94.2†	43.9†	26.8†	16.8†

II. X-ray Emission Energies [11 p. 1-9 – 1-13]

This table gives characteristic X-ray line energies [eV] for K, L and M-orbital and elements with 3 ≤ Z ≤ 95. Only the strongest lines are included: Kα1, Kα2, Kα3, Lα1, Lα2, Lβ1, Lβ2, Lγ1 and Mα1 but in general a lot more electron transition are possible even though certainly at different possibilities (compare Figure 14).

Element	$K\alpha_1$	$K\alpha_2$	$K\beta_1$	$L\alpha_1$	$L\alpha_2$	$L\beta_1$	$L\beta_2$	$L\gamma_1$	$M\alpha_1$
3 Li	54.3								
4 Be	108.5								
5 B	183.3								
6 C	277								
7 N	392.4								
8 O	524.9								
9 F	676.8								
10 Ne	848.6	848.6							
11 Na	1,040.98	1,040.98	1,071.1						
12 Mg	1,253.60	1,253.60	1,302.2						
13 Al	1,486.70	1,486.27	1,557.45						
14 Si	1,739.98	1,739.38	1,835.94						
15 P	2,013.7	2,012.7	2,139.1						
16 S	2,307.84	2,306.64	2,464.04						
17 Cl	2,622.39	2,620.78	2,815.6						
18 Ar	2,957.70	2,955.63	3,190.5						
19 K	3,313.8	3,311.1	3,589.6						
20 Ca	3,691.68	3,688.09	4,012.7	341.3	341.3	344.9			
21 Sc	4,090.6	4,086.1	4,460.5	395.4	395.4	399.6			
22 Ti	4,510.84	4,504.86	4,931.81	452.2	452.2	458.4			
23 V	4,952.20	4,944.64	5,427.29	511.3	511.3	519.2			
24 Cr	5,414.72	5,405.509	5,946.71	572.8	572.8	582.8			
25 Mn	5,898.75	5,887.65	6,490.45	637.4	637.4	648.8			
26 Fe	6,403.84	6,390.84	7,057.98	705.0	705.0	718.5			
27 Co	6,930.32	6,915.30	7,649.43	776.2	776.2	791.4			
28 Ni	7,478.15	7,460.89	8,264.66	851.5	851.5	868.8			
29 Cu	8,047.78	8,027.83	8,905.29	929.7	929.7	949.8			
30 Zn	8,638.86	8,615.78	9,572.0	1,011.7	1,011.7	1,034.7			
31 Ga	9,251.74	9,224.82	10,264.2	1,097.92	1,097.92	1,124.8			
32 Ge	9,886.42	9,855.32	10,982.1	1,188.00	1,188.00	1,218.5			
33 As	10,543.72	10,507.99	11,726.2	1,282.0	1,282.0	1,317.0			
34 Se	11,222.4	11,181.4	12,495.9	1,379.10	1,379.10	1,419.23			
35 Br	11,924.2	11,877.6	13,291.4	1,480.43	1,480.43	1,525.90			
36 Kr	12,649	12,598	14,112	1,586.0	1,586.0	1,636.6			
37 Rb	13,395.3	13,335.8	14,961.3	1,694.13	1,692.56	1,752.17			
38 Sr	14,165	14,097.9	15,835.7	1,806.56	1,804.74	1,871.72			
39 Y	14,958.4	14,882.9	16,737.8	1,922.56	1,920.47	1,995.84			
40 Zr	15,775.1	15,690.9	17,667.8	2,042.36	2,039.9	2,124.4	2,219.4	2,302.7	

41	Nb	16,615.1	16,521.0	18,622.5	2,165.89	2,163.0	2,257.4	2,367.0	2,461.8	
42	Mo	17,479.34	17,374.3	19,608.3	2,293.16	2,289.85	2,394.81	2,518.3	2,623.5	
43	Tc	18,367.1	18,250.8	20,619	2,424	2,420	2,538	2,674	2,792	
44	Ru	19,279.2	19,150.4	21,656.8	2,558.55	2,554.31	2,683.23	2,836.0	2,964.5	
45	Rh	20,216.1	20,073.7	22,723.6	2,696.74	2,692.05	2,834.41	3,001.3	3,143.8	
46	Pd	21,177.1	21,020.1	23,818.7	2,838.61	2,833.29	2,990.22	3,171.79	3,328.7	
47	Ag	22,162.92	21,990.3	24,942.4	2,984.31	2,978.21	3,150.94	3,347.81	3,519.59	
48	Cd	23,173.6	22,984.1	26,095.5	3,133.73	3,126.91	3,316.57	3,528.12	3,716.86	
49	In	24,209.7	24,002.0	27,275.9	3,286.94	3,279.29	3,487.21	3,713.81	3,920.81	
50	Sn	25,271.3	25,044.0	28,486.0	3,443.98	3,435.42	3,662.80	3,904.86	4,131.12	
51	Sb	26,359.1	26,110.8	29,725.6	3,604.72	3,595.32	3,843.57	4,100.78	4,347.79	
52	Te	27,472.3	27,201.7	30,995.7	3,769.33	3,758.8	4,029.58	4,301.7	4,570.9	
53	I	28,612.0	28,317.2	32,294.7	3,937.65	3,926.04	4,220.72	4,507.5	4,800.9	
54	Xe	29,779	29,458	33,624	4,109.9	—	—	—	—	
55	Cs	30,972.8	30,625.1	34,986.9	4,286.5	4,272.2	4,619.8	4,935.9	5,280.4	
56	Ba	32,193.6	31,817.1	36,378.2	4,466.26	4,450.90	4,827.53	5,156.5	5,531.1	
57	La	33,441.8	33,034.1	37,801.0	4,650.97	4,634.23	5,042.1	5,383.5	5,788.5	833
58	Ce	34,719.7	34,278.9	39,257.3	4,840.2	4,823.0	5,262.2	5,613.4	6,052	883
59	Pr	36,026.3	35,550.2	40,748.2	5,033.7	5,013.5	5,488.9	5,850	6,322.1	929
60	Nd	37,361.0	36,847.4	42,271.3	5,230.4	5,207.7	5,721.6	6,089.4	6,602.1	978
61	Pm	38,724.7	38,171.2	43,826	5,432.5	5,407.8	5,961	6,339	6,892	—
62	Sm	40,118.1	39,522.4	45,413	5,636.1	5,609.0	6,205.1	6,586	7,178	1,081

Element	Kα_1	Kα_2	Kβ_1	Lα_1	Lα_2	Lβ_1	Lβ_2	Lγ_1	Mα_1
63 Eu	41,542.2	40,901.9	47,037.9	5,845.7	5,816.6	6,456.4	6,843.2	7,480.3	1,131
64 Gd	42,996.2	42,308.9	48,697	6,057.2	6,025.0	6,713.2	7,102.8	7,785.8	1,185
65 Tb	44,481.6	43,744.1	50,382	6,272.8	6,238.0	6,978	7,366.7	8,102	1,240
66 Dy	45,998.4	45,207.8	52,119	6,495.2	6,457.7	7,247.7	7,635.7	8,418.8	1,293
67 Ho	47,546.7	46,699.7	53,877	6,719.8	6,679.5	7,525.3	7,911	8,747	1,348
68 Er	49,127.7	48,221.1	55,681	6,948.7	6,905.0	7,810.9	8,189.0	9,089	1,406
69 Tm	50,741.6	49,772.6	57,517	7,179.9	7,133.1	8,101	8,468	9,426	1,462
70 Yb	52,388.9	51,354.0	59,370	7,415.6	7,367.3	8,401.8	8,758.8	9,780.1	1,521.4
71 Lu	54,069.8	52,965.0	61,283	7,655.5	7,604.9	8,709.0	9,048.9	10,143.4	1,581.3
72 Hf	55,790.2	54,611.4	63,234	7,899.0	7,844.6	9,022.7	9,347.3	10,515.8	1,644.6
73 Ta	57,532	56,277	65,223	8,146.1	8,087.9	9,343.1	9,651.8	10,895.2	1,710
74 W	59,318.24	57,981.7	67,244.3	8,397.6	8,335.2	9,672.35	9,961.5	11,285.9	1,775.4
75 Re	61,140.3	59,717.9	69,310	8,652.5	8,586.2	10,010.0	10,275.2	11,685.4	1,842.5
76 Os	63,000.5	61,486.7	71,413	8,911.7	8,841.0	10,355.3	10,598.5	12,095.3	1,910.2
77 Ir	64,895.6	63,286.7	73,560.8	9,175.1	9,099.5	10,708.3	10,920.3	12,512.6	1,979.9
78 Pt	66,832	65,112	75,748	9,442.3	9,361.8	11,070.7	11,250.5	12,942.0	2,050.5
79 Au	68,803.7	66,989.5	77,984	9,713.3	9,628.0	11,442.3	11,584.7	13,381.7	2,122.9
80 Hg	70,819	68,895	80,253	9,988.8	9,897.6	11,822.6	11,924.1	13,830.1	2,195.3
81 Tl	72,871.5	70,831.9	82,576	10,268.5	10,172.8	12,213.3	12,271.5	14,291.5	2,270.6
82 Pb	74,969.4	72,804.2	84,936	10,551.5	10,449.5	12,613.7	12,622.6	14,764.4	2,345.5
83 Bi	77,107.9	74,814.8	87,343	10,838.8	10,730.91	13,023.5	12,979.9	15,247.7	2,422.6
84 Po	79,290	76,862	89,800	11,130.8	11,015.8	13,447	13,340.4	15,744	—
85 At	81,520	78,950	92,300	11,426.8	11,304.8	13,876	—	16,251	—
86 Rn	83,780	81,070	94,870	11,727.0	11,597.9	14,316	—	16,770	—
87 Fr	86,100	83,230	97,470	12,031.3	11,895.0	14,770	14,450	17,303	—
88 Ra	88,470	85,430	100,130	12,339.7	12,196.2	15,235.8	14,841.4	17,849	—
89 Ac	90,884	87,670	102,850	12,652.0	12,500.8	15,713	—	18,408	—
90 Th	93,350	89,953	105,609	12,968.7	12,809.6	16,202.2	15,623.7	18,982.5	2,996.1
91 Pa	95,868	92,287	108,427	13,290.7	13,122.2	16,702	16,024	19,568	3,082.3
92 U	98,439	94,665	111,300	13,614.7	13,438.8	17,220.0	16,428.3	20,167.1	3,170.8
93 Np	—	—	—	13,944.1	13,759.7	17,750.2	16,840.0	20,784.8	—
94 Pu	—	—	—	14,278.6	14,084.2	18,293.7	17,255.3	21,417.3	—
95 Am	—	—	—	14,617.2	14,411.9	18,852.0	17,676.5	22,065.2	—

III. Elements Detectable [28]

Following periodic table of the elements shows XRF detectable elements based by Innov-X Systems Handheld XRF Analyzers. For the use in stationary sorting machines using XRF these detection limits cannot be abided since several factors (e.g. very short measuring time, background noise, matrix effect, material composition etc.) negatively affect the detection limit. Nevertheless this table represents a good reference including the most important electron transition energies that are used as sorting criterion.

ELEMENTS DETECTABLE

BY INNOV-X SYSTEMS HANDHELD XRF ANALYZERS

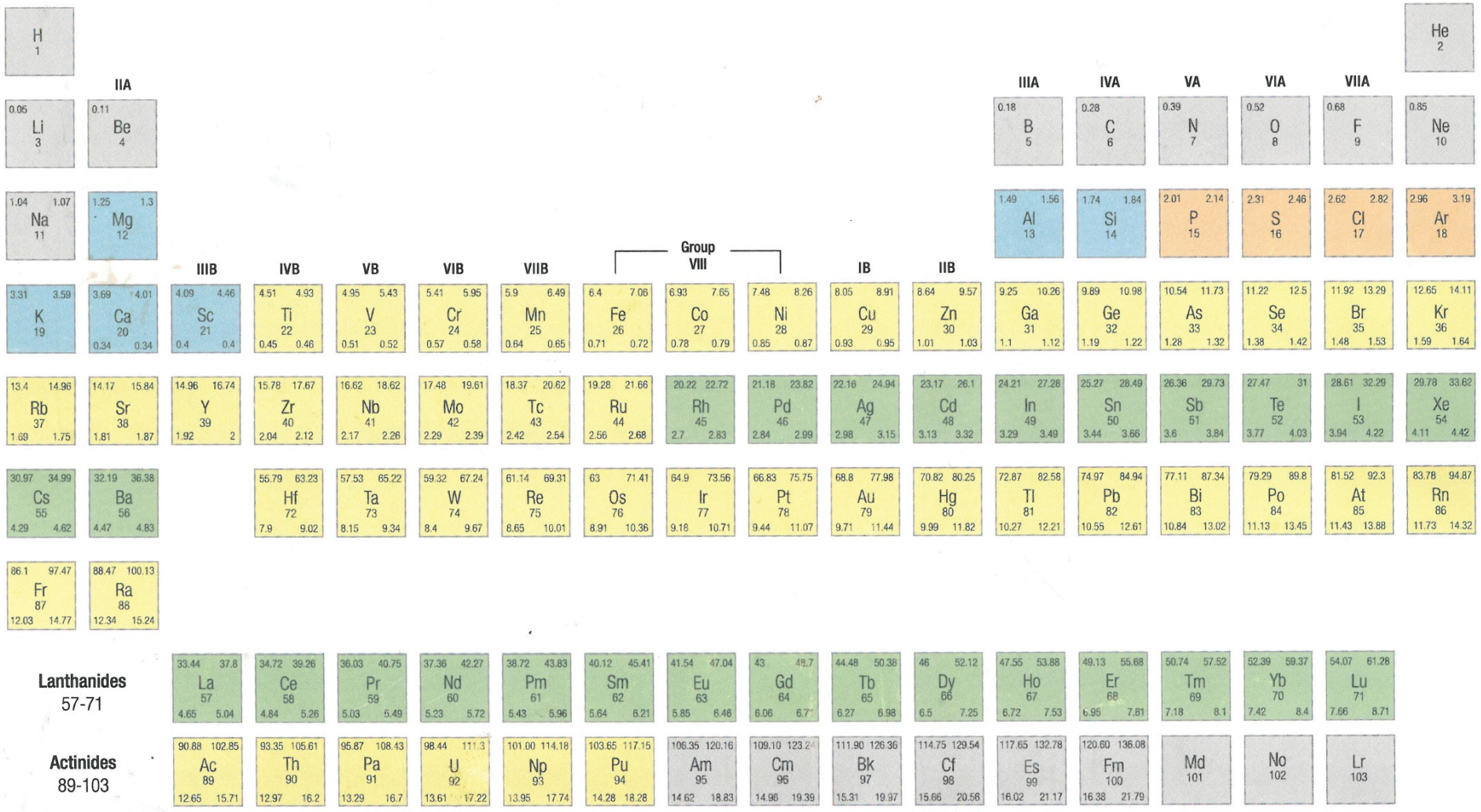

Alloy Elements and Detection Limit Guidelines:

Elements Detected Magnesium (Mg, Z=12) through Silicon (Si, Z=14) and Titanium (Ti, Z=22) through Plutonium (Pu, Z=94) typically 0.1% - some elements as low as 0.01%

Low-Density Sample Types (Soils, powders, liquids)

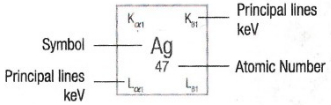

LOD 1% - 5% | 250 - 2,500 ppm | 10 - 100 ppm | 50 - 150 ppm | Not Measured

Detection limits are a function of testing time, sample matrix and presence of interfering elements.
Detection limits are estimates based on 1-2 minutes test times and detection confidence of 3σ (99.7% confidence).
Interference-free detection limits are intended as guidelines: please contact Innov-X Systems to discuss your specific application.

INNOV-X SYSTEMS

PHOTON ENERGIES, IN ELECTRON VOLTS, OF PRINCIPAL K- AND L-SHELL EMISSION LINES

Element	Symbol	Atomic #	$K_{\alpha 1}$	$K_{\beta 1}$	$L_{\alpha 1}$	$L_{\beta 1}$
Actinium	Ac	89	90.88	102.85	12.65	15.71
Aluminum	Al	13	1.49	1.56	0	0
Antimony	Sb	51	26.36	29.73	3.6	3.84
Argon	Ar	18	2.96	3.19	0	0
Arsenic	As	33	10.54	11.73	1.28	1.32
Astatine	At	85	81.52	92.3	11.43	13.88
Barium	Ba	56	32.19	36.38	4.47	4.83
Beryllium	Be	4	0.11	0	0	0
Bismuth	Bi	83	77.11	87.34	10.84	13.02
Boron	B	5	0.18	0	0	0
Bromine	Br	35	11.92	13.29	1.48	1.53
Cadmium	Cd	48	23.17	26.1	3.13	3.32
Calcium	Ca	20	3.69	4.01	0.34	0.34
Carbon	C	6	0.28	0	0	0
Cerium	Ce	58	34.72	39.26	4.84	5.26
Cesium	Cs	55	30.97	34.99	4.29	4.62
Chlorine	Cl	17	2.62	2.82	0	0
Chromium	Cr	24	5.41	5.95	0.57	0.58
Cobalt	Co	27	6.93	7.65	0.78	0.79
Copper	Cu	29	8.05	8.91	0.93	0.95
Dysprosium	Dy	66	46	52.12	6.5	7.25
Erbium	Er	68	49.13	55.68	6.95	7.81
Europium	Eu	63	41.54	47.04	5.85	6.46
Fluorine	F	9	0.68	0	0	0
Francium	Fr	87	86.1	97.47	12.03	14.77
Gadolinium	Gd	64	43	48.7	6.06	6.71
Gallium	Ga	31	9.25	10.26	1.1	1.12
Germanium	Ge	32	9.89	10.98	1.19	1.22
Gold	Au	79	68.8	77.98	9.71	11.44
Hafnium	Hf	72	55.79	63.23	7.9	9.02
Holmium	Ho	67	47.55	53.88	6.72	7.53
Indium	In	49	24.21	27.28	3.29	3.49
Iodine	I	53	28.61	32.29	3.94	4.22
Iridium	Ir	77	64.9	73.56	9.18	10.71
Iron	Fe	26	6.4	7.06	0.71	0.72
Krypton	Kr	36	12.65	14.11	1.59	1.64
Lanthanum	La	57	33.44	37.8	4.65	5.04
Lead	Pb	82	74.97	84.94	10.55	12.61
Lithium	Li	3	0.05	0	0	0
Lutetium	Lu	71	54.07	61.28	7.66	8.71
Magnesium	Mg	12	1.25	1.3	0	0
Manganese	Mn	25	5.9	6.49	0.64	0.65
Mercury	Hg	80	70.82	80.25	9.99	11.82
Molybdenum	Mo	42	17.48	19.61	2.29	2.39
Neodymium	Nd	60	37.36	42.27	5.23	5.72
Neon	Ne	10	0.85	0	0	0
Nickel	Ni	28	7.48	8.26	0.85	0.87
Niobium	Nb	41	16.62	18.62	2.17	2.26
Nitrogen	N	7	0.39	0	0	0
Osmium	Os	76	63	71.41	8.91	10.36
Oxygen	O	8	0.52	0	0	0
Palladium	Pd	46	21.18	23.82	2.84	2.99
Phosphorus	P	15	2.01	2.14	0	0
Platinum	Pt	78	66.83	75.75	9.44	11.07
Polonium	Po	84	79.29	89.8	11.13	13.45
Potassium	K	19	3.31	3.59	0	0
Praseodymium	Pr	59	36.03	40.75	5.03	5.49
Promethium	Pm	61	38.72	43.83	5.43	5.96
Protactinium	Pa	91	95.87	108.43	13.29	16.7
Radium	Ra	88	88.47	100.13	12.34	15.24
Radon	Rn	86	83.78	94.87	11.73	14.32
Rhenium	Re	75	61.14	69.31	8.65	10.01
Rhodium	Rh	45	20.22	22.72	2.7	2.83
Rubidium	Rb	37	13.4	14.96	1.69	1.75
Ruthenium	Ru	44	19.28	21.66	2.56	2.68
Samarium	Sm	62	40.12	45.41	5.64	6.21
Scandium	Sc	21	4.09	4.46	0.4	0.4
Selenium	Se	34	11.22	12.5	1.38	1.42
Silicon	Si	14	1.74	1.84	0	0
Silver	Ag	47	22.16	24.94	2.98	3.15
Sodium	Na	11	1.04	1.07	0	0
Strontium	Sr	38	14.17	15.84	1.81	1.87
Sulfur	S	16	2.31	2.46	0	0
Tantalum	Ta	73	57.53	65.22	8.15	9.34
Technetium	Tc	43	18.37	20.62	2.42	2.54
Tellurium	Te	52	27.47	31	3.77	4.03
Terbium	Tb	65	44.48	50.38	6.27	6.98
Thallium	Tl	81	72.87	82.58	10.27	12.21
Thorium	Th	90	93.35	105.61	12.97	16.2
Thulium	Tm	69	50.74	57.52	7.18	8.1
Tin	Sn	50	25.27	28.49	3.44	3.66
Titanium	Ti	22	4.51	4.93	0.45	0.46
Tungsten	W	74	59.32	67.24	8.4	9.67
Uranium	U	92	98.44	111.3	13.61	17.22
Vanadium	V	23	4.95	5.43	0.51	0.52
Xenon	Xe	54	29.78	33.62	4.11	4.42
Ytterbium	Yb	70	52.39	59.37	7.42	8.4
Yttrium	Y	39	14.96	16.74	1.92	2
Zinc	Zn	30	8.64	9.57	1.01	1.03
Zirconium	Zr	40	15.78	17.67	2.04	2.12

IV. Varian Industrial X-ray tube VF-50J, Datasheet [29]

VARIAN
medical systems

X-RAY
PRODUCTS

VF-50J
Industrial X-Ray Tube

APPLICATION

The VF-50 series x-ray tube is a beryllium window x-ray tube designed for use as a radiation source for x-ray fluorescence systems.

CONSTRUCTION

The beryllium x-ray window is located at the end of the tube and the beam is projected along the longitudinal axis of the tube. The cathode operates at ground potential and the envelope is ceramic with the high voltage section potted to increase the high voltage stand off.

Specification

Envelope	Ceramic
Be Window	.003" (.076 mm) Thick
Anode	Copper body with the target material attached
Standard Target Materials	Rhodium, Palladium, Tungsten, Titanium, Moly, Copper, Silver, Chrome
Target Angle	90° from the central ray
Focal Spot	1 mm x 1 mm square
Maximum Anode Dissipation with 10 cfm forced air cooling	50 Watts Titanium - 20 Watts Chrome - 40 Watts
Filament Characteristics	3.3 Amps and 2.5 Volts maximum
Maximum Anode Potential	50 kVp Maximum D.C. (Titanium - 20 kV)
Maximum Tube Current	Refer to Emission and Rating Chart
Cooling Method	Forced air convection
Weight	2 lbs (1.2 kg)

VF-50 Non-Shielded Cable

NOTES:
1. HV OUTPUT CONNECTOR: AMP LGH-4 COMPATIBLE LEAD ASSY
2. FILAMENT CONNECTOR: PHOENIX CONTACT 300V 10A MAX 28-2 AWG
3. SHIELD MUST BE CONNECTED TO THE GROUND @ M3x0.5H HOLE

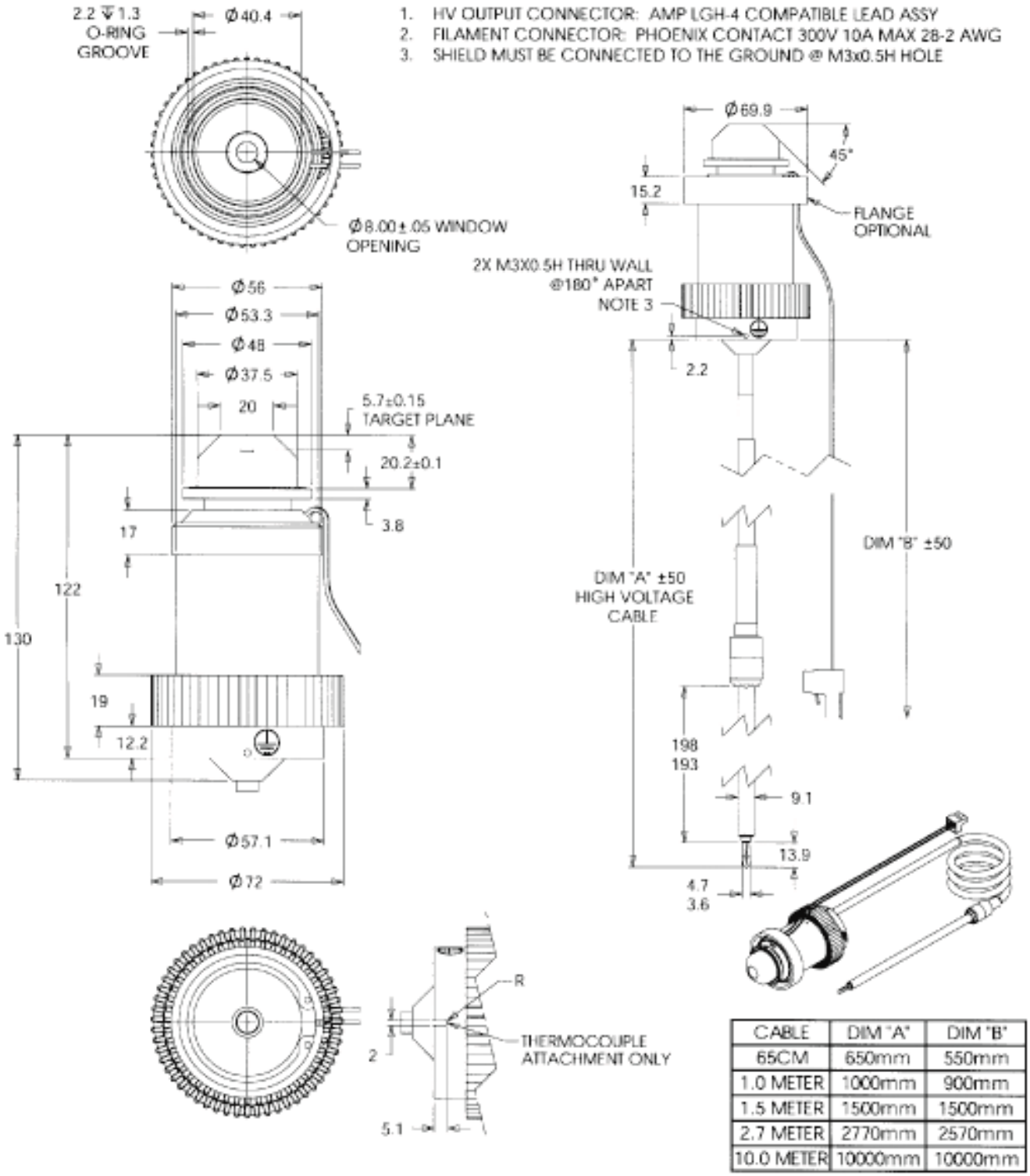

CABLE	DIM "A"	DIM "B"
65CM	650mm	550mm
1.0 METER	1000mm	900mm
1.5 METER	1500mm	1500mm
2.7 METER	2770mm	2570mm
10.0 METER	10000mm	10000mm

VF-50 Shielded Cable

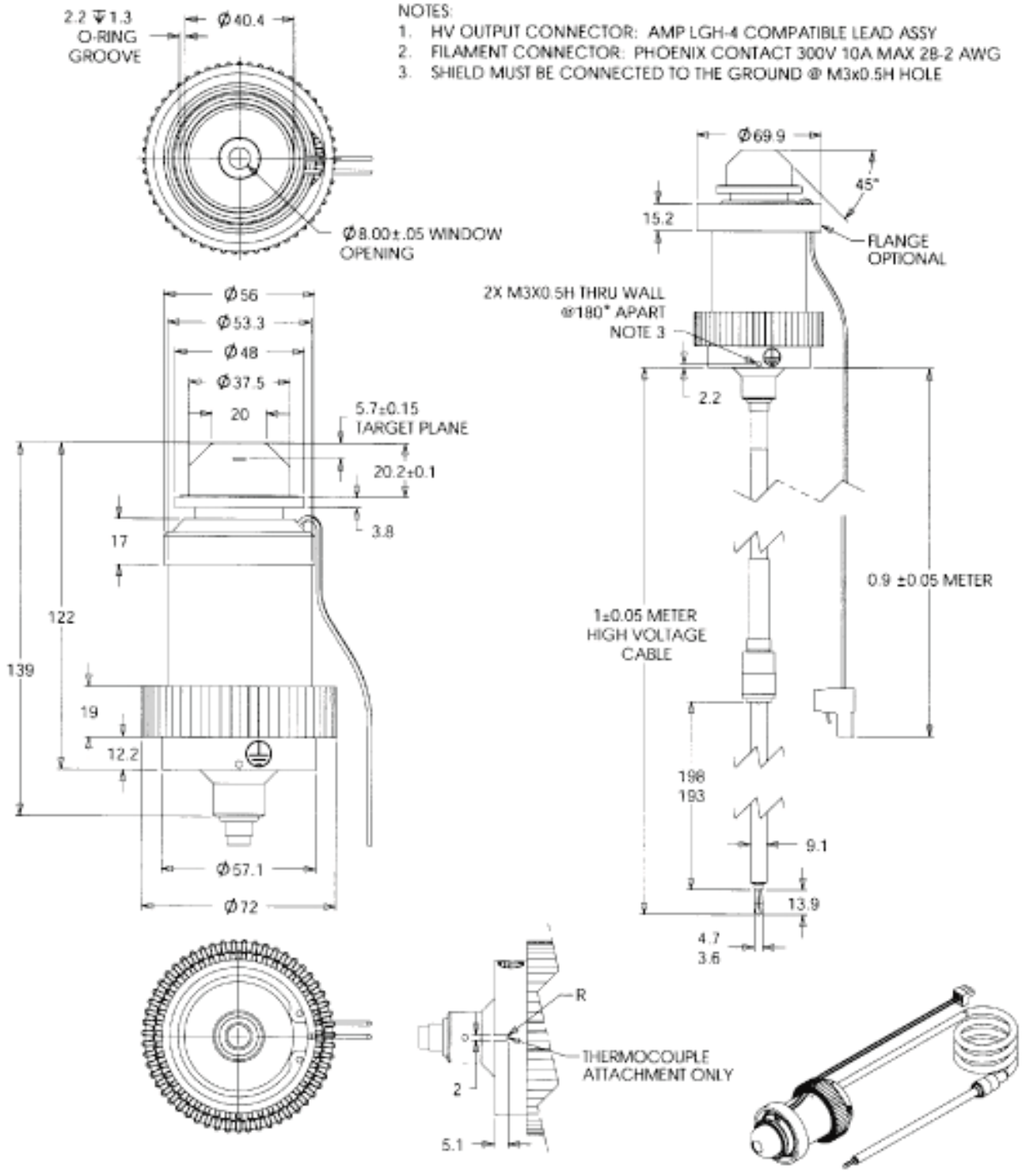

V. Amptek XR-100CR Si-PIN detector, Datasheet [30]

X-RAY DETECTOR

XR-100CR

No Liquid Nitrogen
Solid State Design

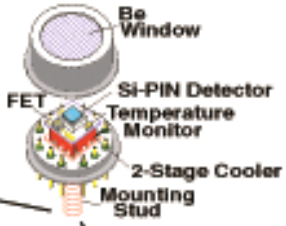

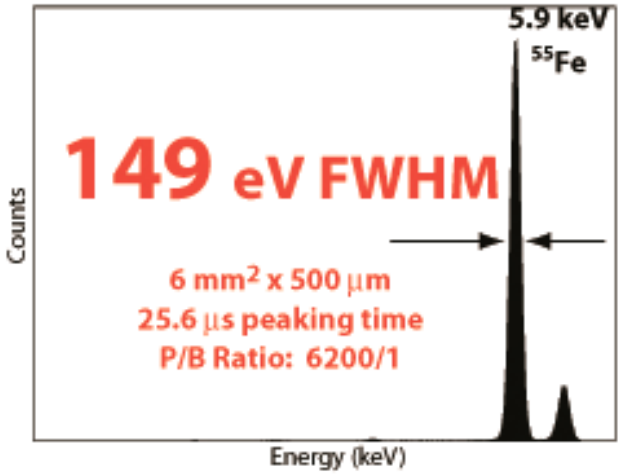

Resolution vs. ICR for Different Peaking Times

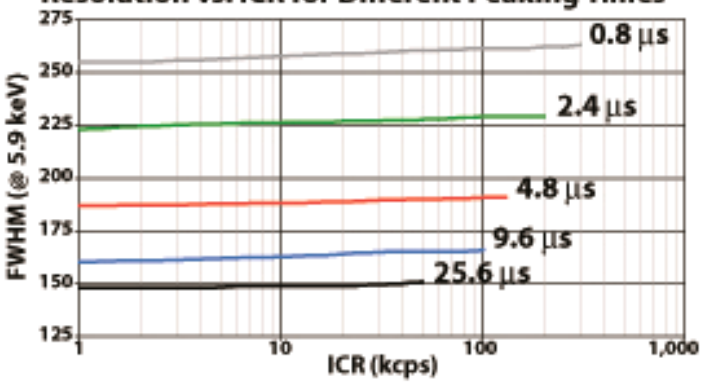

Throughput for Different Peaking Times

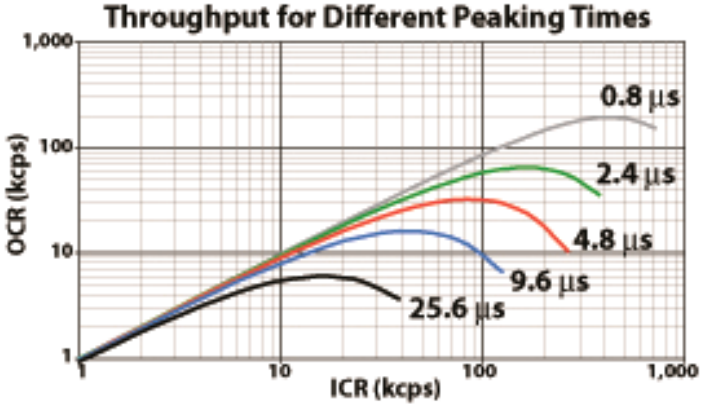

High Performance at Low Cost

FEATURES

- Si-PIN Photodiode
- Thermoelectric Cooler
- Beryllium Window
- Hermetic Package (TO-8)
- Wide Detection Range
- Easy to Operate

APPLICATIONS

- X-Ray Fluorescence
- OEM
- Process Control
- RoHS / WEEE Compliance
- Portable Instruments
- Art & Archaeology
- Teaching & Research
- Lead Detectors
- Space and Astronomy
- Environmental Monitoring
- Nuclear Plant Monitoring
- Heavy Metals in Plastic
- Semiconductor Processing
- Plating Thickness
- Sulfur in Oil & Coal Detection
- Smoke Stack Analysis
- Coal & Mining Operations
- Jewelry Analysis
- Forensic Investigations

Model ***XR-100CR*** is a high performance X-Ray Detector, Pre-amplifier, and Cooler system using a thermoelectrically cooled Si-PIN Photodiode as an X-Ray detector. Also mounted on the 2-stage cooler are the input FET and a novel feedback circuit. These components are kept at approximately -55°C, and are monitored by an internal temperature sensor. The hermetic TO-8 package of the detector has a light tight, vacuum tight thin Beryllium window to enable soft X-Ray detection.

Power to the XR-100CR is provided by either the PX2CR or the PX4. The PX2CR is AC powered and includes a spectroscopy grade Shaping Amplifier with fixed time constant (6 µs, 12 µs, or 20 µs). The PX4 is DC powered by an AC adaptor and provides both a variable Shaping Amplifier (.25 ns to 40 µs) and the MCA function.

The XR-100CR/PX2CR or XR-100CR/PX4 system ensures stable operation in less than one minute from power turn-on.

The resolution for the 5.9 keV peak of ^{55}Fe is 145 eV FWHM to 260 eV FWHM depending on the detector type and shaping time constant (see next page for selection guide).

SPECIFICATIONS

GENERAL	
Detector Type	Si-PIN
Detector Size	5 mm² to 25 mm². See Selection Guide.
Silicon Thickness	300 µm, 500 µm, 680 µm
Energy Resolution @ 5.9 keV, ^{55}Fe	145 eV FWHM to 230 eV FWHM depending on detector type and shaping time constant. See Selection Guide.
Background counts	<3 x 10^{-3} /s, 2 keV to 150 keV for 7 mm² / 300 µm detector
Be Window	1 mil (25 µm), or 0.5 mil (12.5 µm) thick
Charge Sensitive Preamplifier	Amptek custom design with reset though the H.V. connection
Gain Stability	<20 ppm/°C (typical)
Case Size	3.00 x 1.75 x 1.13 in (7.7 x 4.4 x 2.9 cm)
Weight	4.4 ounces (125 g)
Total Power	<1 Watt
Warranty Period	1 year
Typical Lifetime	5 to 10 years, depending on use
Storage Time	10+ years in dry environment
Operation Conditions	0°C to +40°C
UL Certified	Certificate #: CU 72072412 01 Tested to: UL 61010-1: 2004 R7 .05 CAN/CSA-C22.2 61010-1: 2004

OPTIONS
Detector sizes from 5 mm² to 25 mm² (300 µm to 680 µm thick). See Selection Guide.
Other Beryllium window thicknesses are available on special order (0.3 mil - 7.5 µm).
See also XR-100SDD specifications using Silicon Drift Detectors.
See also XR-100T-CdTe specifications using Cadmium Telluride (CdTe) diode detectors for high efficiency and high resolution Gamma Ray detection (<1 keV FWHM @ 122 keV, ^{57}Co).
Collimator Kit for high flux applications.

INPUTS	
Preamp Power	±8 to 9 V @ 15 mA with <50 mV peak-to-peak noise.
Detector Power	+100 to +200 V @ 1 µA depending on detector type; <0.1% variation.
Cooler Power	Current = 350 mA maximum Voltage = 4 V maximum with <100 mV peak-to-peak noise Internal temperature controller

OUTPUTS	
Preamplifier Sensitivity	1 mV/keV typical (may vary for different detectors)
Polarity	Negative Signal Out, 1 kΩ max. load
Feedback	Reset through the detector capacitance
Temperature Monitor Sensitivity	PX2CR: 770 mV = -50 °C PX4: direct reading in K through software

CONNECTORS	
Preamp Output	BNC coaxial connector
Power and Signal	6-Pin LEMO connector
Interconnect Cable	To PX2CR: 6-Pin LEMO 9-Pin D, 5 ft length To PX4: 6-Pin LEMO to 6-Pin LEMO, 5 ft length

6-PIN LEMO CONNECTOR	
Pin 1	Temperature monitor diode
Pin 2	+ H.V. Detector Bias, +100 - 200 V max.
Pin 3	-9 V Preamp Power
Pin 4	+9 V Preamp Power
Pin 5	Cooler Power Return
Pin 6	Cooler Power: 0 to +4 V @ 350 mA
CASE	Ground and Shield

AMPTEK XR-100 Selection Guide

Detector Type Area/Thickness Be Window Thickness Options	Guaranteed Energy Resolution eV FWHM @ 5.9 keV* Peak to Background Ratio**
The following detectors are fully depleted and contain a Multilayer (ML) Internal Collimator.	
Si-PIN 6 mm² / 500 µm 0.5 or 1.0 mil Be	145 - 170 eV 32 µs Peaking Time P/B Ratio: 6200/1
Si-PIN 13 mm² / 500 µm 1.0 mil Be	180 - 210 eV 32 µs Peaking Time P/B Ratio: 4100/1
Si-PIN 25 mm² / 500 µm 1.0 mil Be	190 - 230 eV 32 µs Peaking Time P/B Ratio: 2000/1
Super SDD 25 mm² / 500 µm 0.5 mil Be	127 - 140 eV 11.2 µs Peaking Time P/B Ratio: 8000/1
The following detectors are partially depleted and contain no internal collimator. Recommended for use between 1.5 and 8 keV	
Si-PIN 7 mm² / 300 µm 1.0 mil Be	165 - 185 eV 44.8 µs Peaking Time P/B Ratio: 250/1 (5000/1 with external collimator)
Si-PIN 13 mm² / 300 µm 1.0 mil Be	200 - 220 eV 44.8 µs Peaking Time P/B Ratio: 550/1 (4000/1 with external collimator)

*Peaking Time is approximately 2.4x shaping time.
**The Peak to Background (P/B) Ratio is the ratio of the counts at the 5.9 keV to 2 keV.

For full system specifications, please see http://www.amptek.com/xr100cr.html

VI. Innov-X Systems Alpha-2000 Portable XRF Analyzer, Datasheet [31]

Alpha Series

analyzers provide on-site RoHS & WEEE compliance verification.

For plastics and solder analysis – without radioactivity – Innov-X offers the smallest, fastest and most versatile handheld XRF analyzer available anywhere.

The Innov-X tube-based Alpha Series is isotope free and delivers instant, accurate readings. It features a miniature X-ray tube and high-resolution detector. Engineered around the HP iPAQ pocket PC, the Alpha Series is user-friendly, flexible, upgradeable and has a bright color display for easy viewing in all lighting conditions and a rear-facing LCD display. This analyzer provides fast, reliable, non-destructive screening.

XRF is a standard lab technique for metals and plastics. Now it is available in the field!

82	80	48	35	24
2 8 18 32 18 4	2 8 18 32 18 2	2 8 18 18 2		
Pb	Hg	Cd	B	Cr
Lead	Mercury	Cadmium	Bro	Chro
207.2	200.59	112.411	79.	51.9

The Alpha Series identifies toxic metals in waste electronics.

Mercury in Plastics

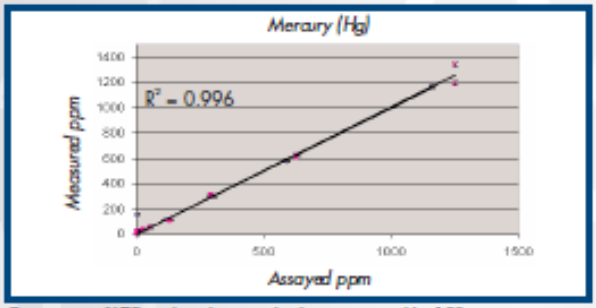

Comparison of XRF results with assayed values containing Hg, 120 sec. measurement

Here's a summary of its capabilities:

- RoHS, WEEE, Prop. 65 compliance verification.
- Toxic metals in plastics – Pb, Hg, Cd. Cr, Br & others.
- Pb-free electronics – new alloys, pure metal substitutes, prevention of Sn whiskering.
- FASTSORT of PVC & Br- or Sb-based flame retardants.
- Versatile PDA platform.
- Easy-to-read displays.

INNOV-X SYSTEMS™

Innovative XRF Technologies

Innov-X Alpha Series

The plastics analyzer for fast, confident and non-destructive compliance screening.

Rely on the Alpha Series for accurate screening of electronic parts, components and assembled products. Monitor toxic metals at ppm levels for compliance verification, on-site QC and documented traceability. The analyzer is applicable to each link in the supply chain: manufacturer, supplier, distributor and end user.

FASTSORT high-speed sorting.

Alpha Series FASTSORT provides fast sorting of PVC and Br-based flame retardants. This tube-based analyzer quickly delivers reliable quantitative analysis of lead in solder for Pb-free electronics requirements. It also fast sorts pure metal and alloy substitutes such as, Sn, Ag, Cu, Zn, Bi, In, Sb and Cd. In addition, it can even measure P, a typical component of a flame retardant substitute for Br.

Typical Plastics Performance.

Cd	30 ppm
Pb, Hg	10 ppm
Br	5 ppm
Cr	40 ppm
Sb	45 ppm

Software for a variety of plastics.

- Automatically determine plastic type with a single calibration for elements of interest.
- Accuracy of results is independent of specific plastic matrices.

Cutting edge PDA technology.

The Alpha Series is driven by the HP iPAQ pocket PC. Data entry is instant. Reports are generated on the spot. Upgrades are possible over the lifetime of the analyzer.

Custom holster lets you take alpha series anywhere.

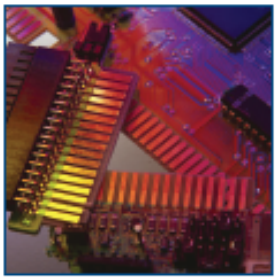

Use Alpha Series to analyze for Pb-free compliance.

Basic Specifications.

Weight: 2.625 lbs. (base wt.) 3.375 lbs. (1.6 kg.) with batteries.
Excitation Source: X-ray tube, W anode, 10-40 kV, 10–50 µA, up to 6 wheel positions and 5 filters.
LEAP: Delivers industry-leading detection limits on critical elements Cr, Cl, P.
Detector: Si PIN diode detector, < 230 eV FWHM at 5.95 keV Mn K-alpha line. Temperature Range: -10°C to +50°C.
Operation: Trigger or Start/Stop Icon. One-touch trigger or "deadman" trigger option. Optional control from external PC.
Power: Li-ion batteries, rechargeable (charger included). Powers analyzer and iPAQ simultaneously. AC Adapter optional.
Battery life: 8 hours (typical duty cycle), 4 hrs continuous (tube on) operation.
Number of Elements: Standard package includes 20 elements.
Standard Elements: Pb, Cr, Hg, Br, Cd, Sb, Cl, P, Ti, Mn, Fe, Ni, Cu, Zn, Bi, Sn, Ag.
Display Screen: Color, high resolution touchscreen. Variable brightness provides easy viewing in all ambient lighting conditions.
Data Display: Concentrations in ppm, spectra and/or peak intensities (count rate) or user-specified units, depending on software mode selected.
Memory, Data storage: Minimum 20,000 test results with spectra, upgradeable to >100,000 test results with upgrade to 1 Gb flash card. 128 Mb standard memory.
Processor: Intel 400 MHz StrongArm processor.
Operating System: Microsoft Windows CE (portable system) or Windows (PC-based). Software Modes: Quantitative for accurate chemical analysis, FASTSORT for high speed sorting (2 sec tests) of PVC or Brominated plastics.

Specifications subject to change without notice.

INNOV-X SYSTEMS™

Innovative XRF Technologies

Innov-X Systems, Inc., Worldwide Headquarters, Woburn, MA USA (781) 938-5005 (866) 4-Innov-X www.Innov-Xsys.com

VII. Tables

Table 16 Data_width_gap_min

Count rate * 1000	Detektor										
	1	2	3	4	5	6	7	8	9	10	11
40	0,0										
45	0,7										
50	7,8										
55	16,3										
60	19,5										
65	21,8										
70	23,0										
75	23,8										
80	24,5	0,0									
85	25,3	4,5									
90	25,5	12,8									
95	25,8	19,0									
100	24,2	21,0									
105	16,0	22,5									
110	3,0	23,5									
115	0,0	23,5	0,0								
120		24,3	0,8								
125		24,3	7,8								
130		24,3	15,0								
135		23,5	18,5								
140		21,0	19,5								
145		10,5	20,5								
150		4,8	21,0	0,0							
155		0,0	21,0	0,0							
160			21,5	1,8							
165			20,5	10,0							
170			20,5	16,8							
175			19,0	18,0							
180			14,5	18,5							
185			4,8	18,7							
190			0,0	18,7							
195				18,5	0,0						
200				18,5	5,2						
205				18,0	14,8						
210				17,5	19,3						
215				16,2	20,5						
220				9,8	20,5						
225				2,3	20,5						
230				0,0	20,5	0,0					
235					20,0	1,8					
240					20,0	11,5					
245					19,0	19,0					
250					18,3	22,0					
255					15,8	22,0					
260					6,3	22,3					
265					0,8	21,0	0,0				
270					0,0	21,0	0,5				
275						20,0	4,3				
280						20,5	13,8				
285						20,5	21,0				
290						20,2	26,3				
295						15,5	28,3				
300						3,8	28,0				
305						0,0	26,8	0,0			
310							24,5	0,8			
315							22,0	8,3			
320							21,0	17,5			
325							20,0	22,0			
330							16,3	23,8			
335							7,0	23,8			
340							0,8	24,0			
345							0,0	24,0	0,0		
350								24,7	2,4		
355								24,7	18,3		
360								24,5	21,0		
365								24,2	21,5		
370								19,0	22,1		
375								6,7	22,7		
380								0,5	23,0		
385								0,0	23,5	0,0	
390									24,0	7,0	
395									24,2	12,4	
400									24,0	19,0	
405									23,5	24,5	
410									14,8	25,8	
415									2,5	26,5	
420									0,0	26,8	0,0
425										26,8	1,2
430										26,8	8,0
435										26,8	17,5
440										24,3	20,8
445										21,5	21,5
450										12,8	22,0
455										2,0	21,5
460										0,0	21,8

Distance from beginning of detection unit [mm]

Table 17 Data_width_gap_max

Count rate * 1000		Detector										
		1	2	3	4	5	6	7	8	9	10	11
Distance from left edge [mm]	35	0,5										
	45	7,50										
	55	13,50										
	65	15,00										
	75	16,00	0									
	85	17,00	9,25									
	95	17,50	13,50									
	105	17,00	15,00	0								
	115	8,25	16,00	2,5								
	125	0,00	16,50	11								
	135		16,50	13,5								
	145		15,50	14,25	0							
	155		5,00	14,75	3,75							
	165		0,00	14,75	12							
	175			14,75	13,5	0						
	185			12	14	7,25						
	195			2	14	14						
	205			0	13,5	15						
	215				12,5	14,5	0					
	225				9,5	14,25	0,75					
	235				1,5	13,5	8,25					
	245				0	12,5	13,25					
	255					7,25	13,5	0				
	265					0	15	1,5				
	275						16	12,75				
	285						15,25	18				
	295						7,25	18,25	0			
	305						0	17	3,75			
	315							15	17			
	325							11,5	17,5			
	335							7	17	0		
	345							3	16,5	4		
	355							0	16,25	14		
	365								16	16,5		
	375								13,5	17,5	0	
	385								2,5	18	4,25	
	395								0	18	14,5	
	405									18	17,25	
	415									15,5	18	0
	425									1,25	18,5	9
	435									0	18,5	15
	445										16,75	15,75
	455										12	16
	465										0,75	16

Table 18 Data_tube test

Count rate *1000		distance to detector axis [mm]	tube 1	tube 2	tube 3
Dekector	1	77	54,0	0,2	0,0
	2	115	40,0	0,4	0,0
	3	153	29,0	0,5	0,0
	4	191	25,8	0,5	0,1
	5	229	30,3	0,3	0,1
	6	268	41,3	39,5	0,1
	7	306	63,0	65,0	0,2
	8	344	28,5	56,0	0,3
	9	382	0,4	45,0	0,4
	10	420	0,4	41,5	0,6
	11	458	0,6	32,5	0,5
	12	496	0,4	40,0	0,6
	13	534	0,2	51,0	58,0
	14	572	0,2	60,0	56,0
	15	610	0,1	37,5	43,5
	16	649	0,1	0,3	33,5
	17	687	0,1	0,5	30,0
	18	725	0,0	0,5	31,0
	19	763	0,0	0,4	45,5
	20	801	0,0	0,3	58,5

Table 19 Data_area of detection- length

Count rate [Tsd]		Max		Min	
		Detector 4	Detector 7	Detector 4	Detector 7
distance left edge [mm]		191	305	191	305
depth from detection unit[mm]	190	0,0	0,0	0,0	0,0
	195	0,5	0,5	0,0	0,0
	200	4,8	2,3	0,5	0,0
	205	10,8	8,5	4,9	1,8
	210	13,8	15,0	14,3	7,3
	215	14,0	17,8	19,3	17,5
	220	14,0	17,8	18,9	23,5
	225	14,0	17,5	18,8	24,8
	230	13,5	17,0	18,0	23,3
	235	12,8	16,5	17,3	22,0
	240	12,3	15,5	15,5	21,3
	245	11,5	15,0	14,3	19,8
	250	10,8	14,0	12,8	17,8
	255	10,3	13,5	11,5	16,5
	260	9,5	12,8	10,1	14,3
	265	8,3	11,3	4,8	12,5
	270	5,0	8,3	3,0	8,6
	275	1,5	4,3	0,4	3,8
	280	0,5	1,3	0,0	0,7
	285	0,0	0,0	0,0	0,0

VIII. Images

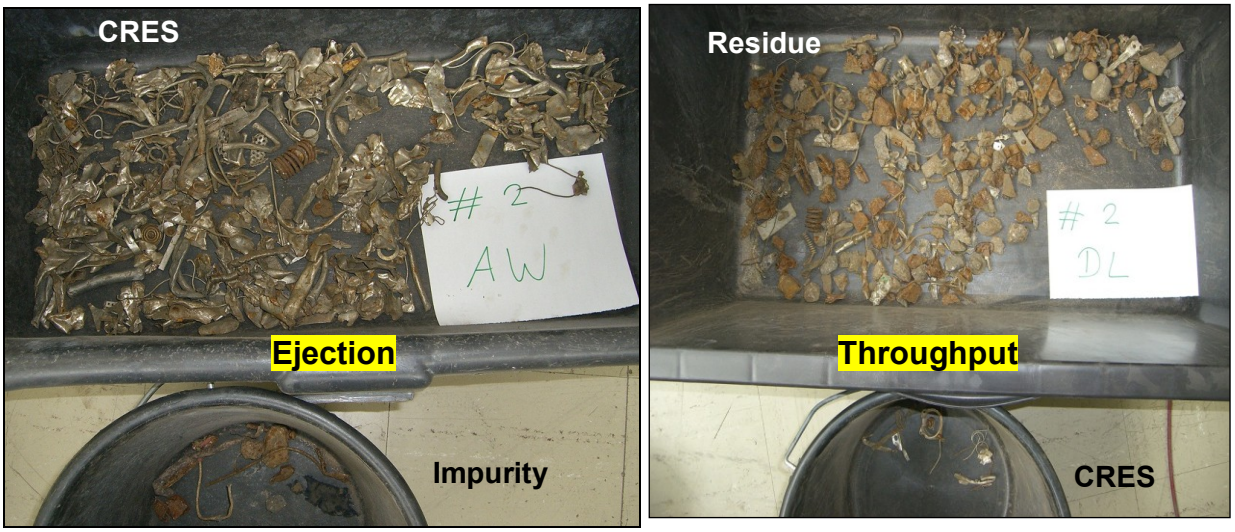

Figure 58 Photographs Test 2

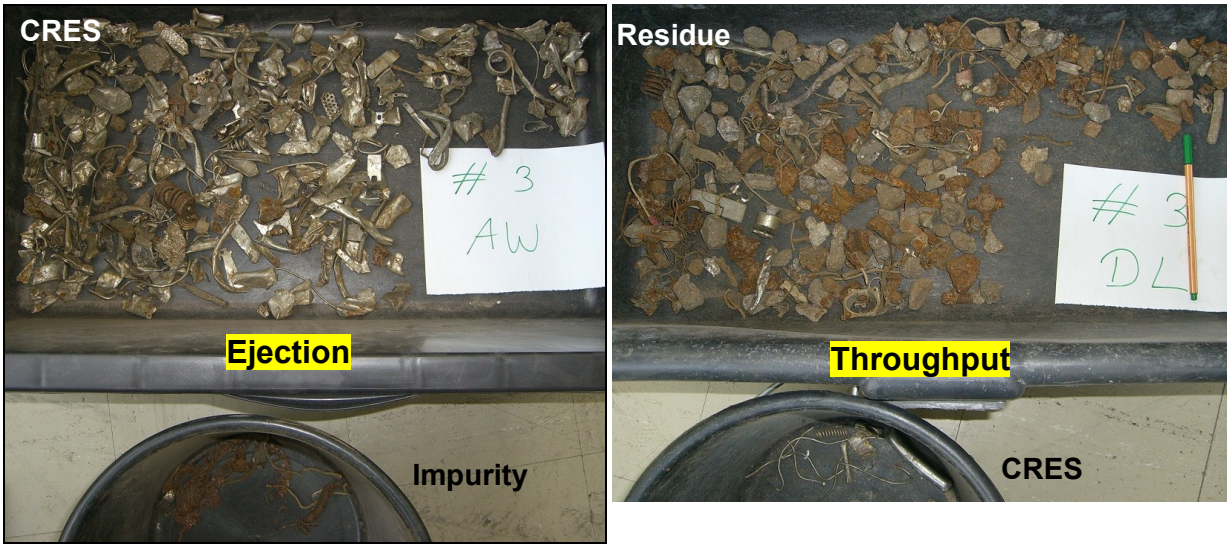

Figure 59 Photographs Test 3